PhD Thesis

Correlations in spontaneous activity states in the brain

Memoria de tesis doctoral presentada por

D. Jesús Manrique Gómez

para optar al grado de
Doctor en Ciencias Físicas

Universidad Autónoma de Madrid
Facultad de Ciencias
Departamento de Física Teórica

Madrid, mayo de 2014

Director: Dr. Néstor Parga. Universidad Autónoma de Madrid

Contents

Acknowledegements

I would like to express my thanks to my advisor Professor N. Parga for his priceless help during these years. The same applies to my collaborators Jaime, Alfonso, M. Victoria and Álvaro. Thanks also to Professor. C. Stevens for his very useful comments on this manuscript. I would also want to show my gratitute towards the people in the Department, from the secretaries to the technical staff, including professors and other students (my especial thanks to J. Larrea's unconditional help). I also want to have a word of thanks to my office mates that provided a nice stay during these five years: Jesús, Rubén, Fede, Miguel, Anaely, Marina, Aura and to other people whom I am lucky to have met here: Marta, Javier, Stefania, Daniel, Iván ...

A deep thanks to my family and friends. I want to be especially thankful to my parents and sisters for all the patience and care. It would not be fair not to mention my gratitude to my friends Eduardo, Javi and Miguel for their constant support during these years. I am particularly in debt to my former housemate Eduardo for listening to my very long complaints (and to put up with my infinite mess). This debt should be paid off when we account Ercilla's receipts. And, of course, I cannot forget to mention Pablo, Álvaro, Álex, Pilar, Natascha, Irene, Yasmina, Sancho, Cristina, Nabstars, my aunt, uncle, cousins, grandparents and in-law family for the good moments shared during these years.

To finish, I would like to show my very deep gratitude to my wife and my son. To Yihwa, because not only has she read this manuscript and correct my English countless times, but also has been able to understand and sacrifice a lot of things. To Chemin, thank you for the little *help* during this last year. To both of you, I would like to promise a life full of money and a good inheritance but I know that my love and a drawing are enough for you.

Agradecimentos

Me gustaría expresar mi agradecimiento a mi director de tesis N. Parga por su inestimable ayuda durante estos años. Por las mismas razones quiero agradecer también a mis colaboradores Jaime, Alfonso, M. Victoria and Álvaro. Muchas gracias también a C. Stevens por sus muy útiles comentarios sobre este manuscrito. Querría mostrar mi gratitud hacia las personas del Departamento, desde las secretarias hasta todo el personal técnico, incluyendo profesores y otros estudiantes (en especial quiero agradecer a J. Larrea su ayuda incondicional). Quiero también dedicar unas palabras de reconocimiento a mis compañeros de despacho que me proporcionaron una agradable estancia durante estos cinco años: Jesús, Rubén, Fede, Miguel, Anaely, Marina, Aura y a otras personas a las que he tenido la suerte de conocer aquí: Marta, Javier, Stefania, Daniel, Iván ...

Muchísimas gracias a mi familia y amigos. Quiero agradecer especialmente a mis padres y hermanas por toda su paciencia y cuidados. No sería justo tampoco dejar de nombrar a mis amigos Eduardo, Javi y Miguel por su apoyo constante durante estos años. Como antiguo compañero de piso, estoy particularmente en deuda con Eduardo por escuchar mis interminables quejas (y aguantar mi infinito desorden). Espero saldar esta deuda cuando hagamos las cuentas de Ercilla. Y, por supuesto, no me olvido de Pablo, Álvaro, Álex, Pilar, Natascha, Irene, Yasmina, Sancho, Cristina, Nabstars, mis tíos, primos, abuelos (los que están y los que no) y familia política, por los buenos momentos compartidos estos años.

Para terminar, quiero mostrar mi más profundo agradecimiento a mi mujer y a mi hijo. A Yihwa porque, además de corregir el inglés de este manuscrito un número incontable de veces, ha sabido comprender y sacrificar muchas cosas. A Chemin debo agradecerle el *empujoncito* final durante este último año. A los dos me gustaría prometeros una vida llena de dinero y una buena herencia, pero sé que con mi amor y un dibujo tenéis más que suficiente.

Abstract

Studying neural activity correlations is essential for understanding how information is processed in the brain. Traditionally, it was believed that the activities of neighbouring neurons were necessarily correlated, due to the large amount of common afferents [Shadlen and Newsome, 1998]. However, recent studies have found that this is not always the case [Renart et al., 2010, Ecker et al., 2010].

The main topic of this thesis is the study of decorrelation in *balanced* recurrent networks of *densely* connected neurons with *strong* interactions. Our main contribution is the development of a theory that generalizes and extends the previously found results in binary neurons [Renart et al., 2010] to different kinds of neuron models, with special emphasis on biologically realistic ones.

We show that most of the features of the *asynchronous* state, if it *exists*, do not depend on the neuron model. *Asynchronous* states are equivalent to a dynamical phenomenon that consists in the precise tracking of excitatory fluctuations by inhibition. In such states, balance equations that relate spike train auto- and cross-covariance functions *necessarily* have to be accomplished. Although both spike train and total current cross-covariance functions are small, the *asynchronous* state is characterized by finite values of cross-covariances between the current components, i.e., the part of the incoming current that arrives from a given population (Excitatory, Inhibitory, External) in agreement with experimental data [Graupner and Reyes, 2013].

We analytically show that the *asynchronous* state in networks of leaky-integrate-and-fire (LIF) neurons *exists*. Two approximations are employed. We use the linear response [Brunel and Hakim, 1999, Lindner and Schimansky-Geier, 2001] and the adiabatic approximations [Moreno-Bote and Parga, 2004] that account for the effect of incoming currents on the activity of the neuron and allow one to find self-consistent equations for spike train cross-covariance functions. Analytical and numerical results are in agreement for networks whose sizes are biologically relevant. We also show how

the balance equations for spike train cross-covariance functions allow one to calculate auto-covariance functions of macroscopic magnitudes, such as the multi-unit activity (MUA).

In the last chapter of this thesis we study the generation of slow oscillations using a model where adaptation and slow inhibition ($GABA_B$) are present [Parga and Abbott, 2007]. The model reproduces experimental data in slices of ferrets and explains the role of the slow inhibition in the durations of the Up/Down cycles and their variability. We find that the degree by which the tracking of excitation by inhibition is accomplished also has an impact on these magitudes.

Resumen

El estudio de correlaciones en la actividad neuronal resulta fundamental para entender cómo la informacion se procesa en el cerebro. Tradicionalmente se ha pensado que la actividad de neuronas próximas necesariamente debía de estar correlacionada debido a que, presumiblemente, comparten un gran numero de entradas [Shadlen and Newsome, 1998]. Sin embargo, estudios recientes han mostrado que esto no es siempre así [Renart et al., 2010, Ecker et al., 2010].

El tema principal de esta tesis es el estudio de los mecanismos que originan esta falta de correlación en redes *balanceadas* de neuronas *densamente* conectadas y que interactúan *fuertemente*. Nuestra principal aportación es el desarrollo de una teoría que generaliza y extiende los resultados previamente encontrados en neuronas binarias [Renart et al., 2010] a diferentes tipos de modelos biológicamente más realistas.

Mostramos analíticamente que la mayoría de características del estado asíncrono, de existir, no dependen del modelo de neurona estudiado. El estado asíncrono es equivalente a un feómeno dinámico por el cual las fluctuaciones excitadoras son rápidamente seguidas por fluctuaciones inhibidoras. En este estado, ecuaciones de balance que relacionan las funciones de covarianza cruzadas y auto-covarianzas de trenes de espigas *necesariamente* han de cumplirse. Aunque tanto las funciones de covarianzas cruzada de trenes de espigas como las de corrientes aferentes totales son pequeñas, el estado *asíncrono* se caracteriza por el hecho de que las correlaciones entre las componentes de la corriente (excitadora, inhibidora) son grandes, en consonancia con estudios experimentales [Graupner and Reyes, 2013].

Para el modelo de neurona de integración y disparo se demuestra analíticamente que el estado asíncrono existe. Para estudiar este caso, utilizamos dos aproximaciones distintas que relacionan el efecto de las corrientes aferentes con la actividad de las neuronas. Estas aproximaciones son respuesta lineal [Brunel and Hakim, 1999, Lindner and Schimansky-Geier, 2001] y una aproximación adiabática [Moreno-Bote and Parga,

2004]. Las predicciones de la teoría y las simulaciones están de acuerdo para redes de un tamaño biológico. También mostramos cómo las ecuaciones de balance de las funciones de covarianza cruzada de trenes de espigas permiten calcular funciones de auto-covarianza de señales macroscópicas como el MUA.

En el último capítulo de esta tesis se estudia la generación de oscilaciones lentas usando un modelo con adaptación y receptores de $GABA_B$ [Parga and Abbott, 2007]. El modelo reproduce datos experimentales y nos ayuda a entender el rol de la inhibición lenta en la duración de los ciclos Up/Down y su variabilidad. Encontramos que la precisión con que la inhibición sigue a la excitación repercute en estas magnitudes.

Chapter 1

Introduction

The main objective of this thesis is to study different brain dynamics, with a especial focus on the neural activity correlations caused by shared input. In the first part of this thesis (chapters 2, 3 and 4), we will explore uncorrelated neural states in balanced networks of *densely* connected neurons with *strong* interactions. We first characterize the *asynchronous* state (chapter 2) and show that it exists in networks of leaky-integrate-and-fire neurons (chapter 3 and chapter 4). To do this, we employ both computer simulations and analytical methods. In the second part of this thesis (chapter 5) we will focus on slow oscillations in spontaneous activity states. We use computer simulations to study some of their relevant features.

In the next sections we briefly describe spontaneous activity states, present examples of correlated and uncorrelated activity states and discuss the sources of neural correlations and their importance. We also present the definition of balanced networks. Finally, a summary of the main analytical techniques is also given.

1.1 Spontaneous activity in the brain

Spontaneous activity is defined as the activity of neurons in the brain in the absence of stimulation. Such states are the ones that consume the most energy, comprising around 60 to 80% of the metabolic energy consumption in the brain [Raichle and Mintun, 2006]. Spontaneous neural activity has been observed during development in many species [Nakayama et al., 1999, Wong and Oakley, 1996, Wong et al., Demas et al., 2003] and it is thought to be fundamental in the creation of the primitive synaptic circuitry [Katz and Shatz, 1996, O'Donovan, 1999]. Although it has been shown to be informative of the mental state of the animal, such as the level of alertness [Sadaghiani et al., 2010], its functional role and mechanisms in adult brain are not well

understood yet.

Spontaneous activity can manifest in states in which neurons cooperate giving rise to oscillatory waves [Steriade et al., 1993c, Contreras et al., 1996]. Scenarios in which the activity of the neurons is very uncorrelated have also been described [Renart et al., 2010].

1.2 Correlated brain activity

Neuronal population oscillations are common examples of correlated activity. In chapter 5 we will focus on a particular example of this kind of activity: slow (< 1 Hz) oscillations characterized by the spontaneous transitions of neuronal firing patterns between periods of activity (Up states) and silence (Down states) [Steriade et al., 1993a,b,c, Lampl et al., 1999, Sanchez-Vives and McCormick, 2000]. These oscillations appear during slow wave sleep [Steriade et al., 1993a,c,b] but also in anesthetized animals [Lampl et al., 1999] and can be evoked in brain slices *in vitro* [Sanchez-Vives and McCormick, 2000].

Experimental studies have shown that intrinsic features of individual neurons [Crunelli et al., 2005, Mao et al., 2001, Sanchez-Vives and McCormick, 2000] and/or the synaptic dynamics generated in the network they are embedded in [Cossart et al., 2003, Metherate and Ashe, 1993, Sanchez-Vives and McCormick, 2000, Seamans et al., 2003, Wilson and Kawaguchi, 1996] are important in the generation of slow oscillations. Computational models as the one in Parga and Abbott, 2007, for example, incorporate both kind of properties. There, the dynamics of synaptic receptors and adaptation currents together with nonlinear membrane currents were responsible for the emergence of slow oscillations characterized by a bimodal distribution of neuron's membrane potentials. Adaptation of excitatory activity [Sanchez-Vives and McCormick, 2000, Compte et al., 2003] and short-term synaptic depression [Timofeev et al., 2000, Melamed et al., 2008] have been also suggested as candidates to explain these kinds of rhythms. Finally, the impact of neuron's intrinsic excitability on the generation of Up/Down cycles is studied in Bazhenov et al., 2002.

1.3 Uncorrelated brain activity

Recordings of ensembles of neighboring neurons have shown that their activity can, under some circumstances, be asynchronous. In Renart et al., 2010, activity correla-

tions are measured in somatosensory and auditory cortices of urethane anesthetized rats. During periods of tonic activity, neurons spiking patterns are uncorrelated. Interestingly, during slow oscillations the correlation in spiking activity in the periods of high activity (Up states) is also very low. Paradoxically, correlated patterns as neural oscillations give rise to asynchronous firing events. There, it is shown that in random recurrent networks of binary neurons, the correlation vanishes provided the inhibition is fast enough.

Uncorrelated activity has also been observed in the presence of stimulation. Working with multielectrode arrays implanted in macaques, Ecker et al., 2010 show that neighboring neurons in primary visual cortex of awake animals can be very little correlated. Since these two works appeared, some others have reported very small values of activity correlation, e.g., Miura et al., 2012, Hansen et al., 2012, Middleton et al., 2012, Graupner and Reyes, 2013.

Previous studies in cortex pointed out higher values of spike-count cross-correlation coefficients (around 0.1-0.3) of pairs of neighboring cells [Gawne and Richmond, 1993, Zohary et al., 1994, Bair et al., 2001, Kohn and Smith, 2005]. Such high values had been traditionally attributed to the fact that these neurons should share many inputs. In Ecker et al., 2010 and Cohen and Kohn, 2011 some reasons are given on why low spike-count cross-correlation coefficients had not been reported previously. For example, an almost negligible common rate modulation originated from uncontrollable cognitive states could give rise to spike-count cross-correlation coefficients of the same order as the ones previously found. Supporting this idea, experimental studies, have reported that noise correlations are modulated by behavior or the level of attention [Noda and Adey, 1970, Poulet and Petersen, 2008, Cohen and Maunsell, 2009, Mitchell et al., 2009, Herrero et al., 2013], while, in a perceptual decision-making task, it was shown that noise correlations vary according to the stage of the decision process [Carnevale et al., 2012] . The extremely sensitive experimental setup or the difficulty to isolate and recognize spikes arriving from different cells are also proposed as plausible reasons that could have led to misestimations of spike-count cross-correlation coefficients. Measurements of correlations may vary according to some other variables, such as the distance between neurons [Constantinidis and Goldman-Rakic, 2002, Smith and Kohn, 2008, Ecker et al., 2010, Komiyama et al., 2010], their firing rate [de la Rocha et al., 2007], or the presence/absence of anesthesia [Ecker et al., 2014], which explains the very different values of spike-count cross-correlation coefficients found in the literature.

These recent findings cast some doubts on the previously accepted idea of the common input as an unavoidable source of correlations, suggesting either that neighboring neurons do not share so many inputs as thought or that an active decorrelation mechanism such as the one suggested in Renart et al., 2010 takes place.

1.4 Importance of correlations in the brain

In this section, we will give some representative examples that show the importance of neural activities correlations in brain computations, specifically in the coding of signals.

Covariations of neural responses can be of two types. Covariations of neural responses when changing the stimulus are referred to as *signal* correlations. Covariations of neural activity independently of the stimulus (or in absence of it) are referred to as *noise* correlations. Hereby, when not specified, 'correlations' refers to noise correlations. In the coding processes, correlations can be important both at encoding and decoding stages.

As an example of the importance of correlations in the decoding state let us consider the experiment described in Britten et al., 1992. In this experiment, a monkey has to determine the direction in which most of the points on a screen move. Interestingly, the decision the animal makes and the level of success can be accurately predicted by the firing rate of just one neuron. An explanation to this phenomenon is given in Zohary et al., 1994: if the response of neurons is correlated, the effect of adding the response of many neurons does not contribute to reduce the noise and thus the failure ratio is similar for one neuron and for a population of cells.

Correlations are also important at the encoding stage. Several studies have shown that correlations can enlarge or reduce the amount of encoded information [Oram et al., 1998, Johnson, 1980, Panzeri et al., 1999, Averbeck et al., 2006]. The effects reported in the experiments for a pair of neurons are quite small [Golledge et al., 2003]. However, in Zohary et al., 1994, Salinas and Sejnowski, 2000, it is shown how a small degree of correlation in each pair of neurons of a network can have a strong impact in the firing rate and variability of the spike trains when the network is large enough.

1.5 Correlation sources and decorrelation mechanisms

Given the fact that neural activity correlations can be relevant one can ask how these correlations appear. Typically three causes seem to be the most relevant.

1. The effect of shared input.
Neurons that share a large amount of inputs are supposed to fire in a more correlated way [Shadlen and Newsome, 1998].

2. The effect of direct connections.
Two neurons that are synaptically connected are expected to be correlated because the activity of the pre-synaptic cell necessarily affects the behavior of the post-synaptic one.

3. The effect of correlated inputs.
This effect is similar to the one of common input previously described, but it does not assume any common source for the input but just the fact that it is correlated, no matter the reason.

In Ostojic et al., 2009 the first two sources of correlations are studied in detail with LIF neurons. Cross-correlations of pairs of neurons are studied using the linear response approximation [Brunel and Hakim, 1999, Lindner and Schimansky-Geier, 2001, Lindner et al., 2005] in different feedforward architectures. It is convenient to notice that this model does not take into account network effects: the whole effect of a network where neurons are embedded in has been fully replaced by a white noise [1]. Similarly, in de la Rocha et al., 2007, a study of pairs of neurons receiving cross-correlated white noise revealed a relationship between firing rates and the correlation of the activities of the neurons. In Moreno-Bote and Parga, 2006, cross-covariance and auto-covariance functions of spike trains were computed for a pair of LIF neurons with current based synapses receiving common input when the synaptic kinetics is slower than the one of the membrane potential using the *adiabatic* approximation. The use of such temporal constants and of this analytical approximation is justified because membrane time constants are effectively reduced when the neuron is receiving a large number of inputs [Bernarder et al., 1991, Destexhe et al., 1999, 2001, Kuhn et al., 2004, Moreno-Bote and Parga, 2005, Léger et al., 2005]. The adiabatic approximation will be explained in

[1] A very simple recurrent network is also studied in this work. This network consists of two mutually connected neurons that receive white noise.

detail in chapter 4.

Simulations of recurrent networks of LIF neurons have shown that the firing activity of cells can be decorrelated even if the amount of common inputs is not negligible [Amit and Brunel, 1997b] which explains why some predictions of mean field theories that do not take correlations into account, such as firing rates, are accurate[Amit and Brunel, 1997a]. As mentioned before, this contradicts the assumption that the common input is an unavoidable source of correlations [Shadlen and Newsome, 1998]. Recent theoretical works have put effort on elucidating the effect of the network recurrency on correlations. In Pernice et al., 2011, Trousdale et al., 2012, it is shown that under certain circumstances, one can decompose the random networks into *motifs*, which are defined as the subnetworks connecting two neurons through a number of intermediate cells. A perturbation method is proposed that consists in adding the effect of the subsequent higher order *motifs*, characterized by the increasing number of intermediate cells. The hypothesis lying beneath this scheme is the fact that two neurons that are topologically further away tend to be less correlated than neurons that are closer. The method described works well, provided that the synaptic strength is not big, but it is less accurate for stronger coupling.

A different perturbation approach is found in Renart et al., 2010. In this work, the very small spike-count cross-correlation coefficients were explained by a recurrent network model of binary excitatory and inhibitory neurons in the *balanced* regime (see next section). In that network, the components of the synaptic currents (defined as the part of the current originated from a given population of neurons) were high due to the presence of common inputs and a strong coupling between neurons. Nevertheless, a cancellation of the total current correlation occurs by means of a dynamical network phenomenon by which inhibitory currents follow excitatory ones with a short time delay (actually, a vanishing time delay in the case of infinite size networks). A previous work [Ginzburg and Sompolinsky, 1994] studied also correlations in binary networks and reported that a very weak degree of correlation can occur if the neurons are weakly coupled. In this theoretical work, both the components and the total pre-synaptic current correlations are small. In Okun and Lampl, 2008, the correlation of the different components of the current afferent to a pair of neurons was experimentally measured. To do this, they hyperpolarized (depolarized) the membrane of neurons to the reversal potential of inhibitory (excitatory) current in order to study the correlations of the excitatory (inhibitory) current components. They found that the correlation between current components was large. Besides, they reported that inhibitory current lags be-

hind the excitatory one by some milliseconds. More recently, Graupner and Reyes, 2013 has explicitly shown with similar experiments that the highly correlated current components can combine in a way that they decorrelate membrane potentials, suggesting that the situation described by Renart et al., 2010 takes place.

Some other theoretical studies have also focused on the role of inhibition in the decorrelation of neuronal activity in recurrent networks. In Helias et al., 2014, finite size networks of binary neurons are studied and the importance of inhibition for decorrelation is also pointed out. Employing a model of LIF and finite size random homogeneous networks [2], Tetzlaff et al., 2012, Helias et al., 2013 also show that the effect of the inhibitory recurrent loop is to diminish the correlation originated by the common input. Recently, a calculation using a firing rate model has reported similar results [Bernacchia and Wang, 2013]. Notice, however, that these works focus on very specific and unrealistic network connectivities or are not based on biophysical models. Although not centered on the decorrelation mechanisms, a recent study has shown that the strength of inhibition determines two types of *asynchronous* activity [Ostojic, 2014]. Strong inhibition favors bursting activity while weak inhibition produces more tonic firing.

A simulation study on high-conductance states [Hertz, 2010] confirms the importance of inhibition and specifically its capability to respond to excitatory inputs in short time scales as a mechanism that contributes to decorrelation. Cancellation of correlations and its dependence on network architecture was studied by means of a computational model in Hansen et al., 2012. They found that when the range of excitatory connections is narrower than the one of inhibitory ones, the balance of correlations described in Renart et al., 2010 cannot be sustained. This could explain the different correlations observed in supra- and infragranular layers (high correlation, shorter range of excitatory connections) and granular layers (low correlation, similar range of excitatory and inhibitory connections) of monkeys.

Finally, other mechanisms have been suggested as responsible for neural decorrelation. In Kriener et al., 2008, it is shown that if synapses do not follow Dale's principle , activity correlations can be reduced. A recent study has pointed out the relevance of feedforward inhibition and neuron's non-linearities as mechanisms that reduce the

[2]Homogeneous networks are those in which all neurons' parameters and pre-synaptic currents are statistically indistinguishable, no matter the inhibitory or excitatory character of the post-synaptic neurons. As we will see in chapter 3 (Appendix 3-A5), the differences between homogeneous networks and more general networks are not trivial.

correlation [Middleton et al., 2012]. Synaptic depression can also contribute to neural decorrelation in recurrent binary networks [Igarashi et al., 2012].

1.6 Balanced networks

A well established feature of neurons in the cortex is that their firing patterns are highly irregular, with coefficients of variation of inter-spike intervals close to Poissonian values [Softy and Koch, 1993]. Cortical neurons receive inputs from thousands of neurons. If all of them were excitatory and fire independently this would produce an almost constant depolarizing current that will lead post-synaptic neurons to fire periodically. A solution to this apparent conflict can be found by incorporating inhibitory neurons. If the amount of inhibition is large enough, it can counteract the strength of the excitatory drive and the membrane potential of post-synaptic cells would remain below their spiking threshold most of the time, crossing it at random times. These kind of networks are referred to as *balanced* networks [Shadlen and Newsome, 1994, 1998].

The way balanced networks of excitation and inhibition are defined varies depending on the author. In modeling works, it is usually accepted that balanced networks consist of systems in which the mean incoming current is zero or at least much smaller than the current needed to increase neurons' membrane potentials from their resting to their spiking threshold values [Vogels and Abbott, 2005]. A more mathematically precise definition can be found in van Vreeswijk and Sompolinsky, 1996. In that work, it is shown that in a recurrent network of sparsely connected excitatory and inhibitory units, a balance among the mean firing rates of external, excitatory and inhibitory cells has to be established in order for the mean current not to be arbitrarily large or small and, consequently, for the neurons not to reach neither a saturated nor a quiescent state. This definition of balanced states does not impose a precise value of incoming currents and, thus, does not require a fine tuning of the parameters, provided some relations of the synaptic couplings are satisfied. These constraints are some inequalities among the synaptic efficacies that can be summarized as the need for a strong enough inhibition. The condition of sparse coupling can be relaxed and a regime with the same first moment statistics of activity can be obtained in the case of densely connected networks [Renart et al., 2010]. This regime also assures that the balance of inhibition and excitation is not only achieved in terms of the temporal-averaged currents but also instantaneously, with a vanishing delay of inhibition with respect to excitation as the

number of inputs increase.

1.7 Methods employed in this thesis

Although this section does not intend to be an exhaustive description of the methods employed in this work (to this aim, we have explained them in each of the chapters that compose this volume), a quick overview of some of the analytical tools employed could be relevant for a better understanding on the types of questions our investigation can answer and the conclusions that could be derived from our work.

1.7.1 About the scaling approach

Most of the analytical work on this thesis is based on a scaling approach. Scaling methods have been widely used in Physics. The idea of these methods is the following. Many-body problems are, in general, difficult to solve and can be more easily dealt with by assuming the number of particles involved is infinite. The way to go from one state with a finite number of particles to one with infinite number of them requires the renormalization of some of the parameters of the system, in order to obtain physically plausible states. The scaling of these parameters depends on which characteristics of the finite particle number problem are aimed to be preserved.

In a scaling scheme, magnitudes are evaluated asymptotically as the number of particles increases. Because of the fact that biological systems, as the brain, have a defined number of cells, a direct comparison between theory and experiments is not always straightforward. Even so, these formulations can be useful when looking for magnitudes whose values are not dependent on precise values of network sizes and when describing qualitative aspects of some phenomena.

1.7.2 Scaling brains

Examples of scaling methods in theoretical neuroscience can be found in works such as Ginzburg and Sompolinsky, 1994, van Vreeswijk and Sompolinsky, 1996, Brunel and Hakim, 1999 and Renart et al., 2010. As mentioned before, one deals with a network of N neurons and makes N tend to infinity. In order for the input current not to be unrealisticaly large, same scaling hypothesis need to be made. In van Vreeswijk and Sompolinsky, 1996, for example, the perspective adopted is to keep constant the

number of pre-synaptic neurons to a given neuron. By doing so, the probability of connection decreases as $1/N$. Networks with this property are referred to as *sparse* networks. In this kind of networks, neuronal activities are uncorrelated by construction and standard mean-field approximations are often used. On the other hand, *dense* networks are those in which the connection probability does not scale with network size [Renart et al., 2010]. As the ratio of common input shared by neurons does not depend on the network size, these networks offer the possibility of studying magnitudes that depend on the amount of shared connections.

Another scaling hypothesis deals with the normalization of synaptic weights. By *weakly* coupled networks one ususally refers to networks in which the synaptic weights are $O(1/K)$, K being the average number of pre-synaptic neurons. By *strongly* coupled networks one refers to networks in which synaptic efficacies are larger than $O(1/K)$ and especially to the case they are $O(1/\sqrt{K})$ [van Vreeswijk and Sompolinsky, 1996]. The reason for these names, are the typical number of excitatory inputs that the neuron has to receive to fire. Notice that, in the case of a $O(1/\sqrt{K})$ scaling of the synaptic strengths, if one makes the number of incoming inputs grow as N, which is the case in dense networks [Renart et al., 2010], one could think that the synaptic current that arrives to post-synaptic neurons would grow as $\sqrt{N}$. However, as we have previously mentioned, in the case where inhibitory neurons are present, the networks dynamically arrive to a stable state known as *balanced*, that guarantees reasonable values of the input currents.

1.7.3 Definition of asynchronous states

In the context of scaling approaches a formal definition of asynchronous states can be found in Ginzburg and Sompolinsky, 1994. There, asynchronous states were defined as those in which the average value of the correlation among the activity of the neurons decreases as $1/N$, N being the number of neurons in the network. The same definition was employed in a more recent work [Renart et al., 2010].

In the next chapter, we will propose a definition of asynchronous states in *densely* connected networks of *strongly* interacting neurons compatible with the one in Ginzburg and Sompolinsky, 1994. As we will see, some interesting conclusions can be derived assuming that an asynchronous state exists. In chapters 3 and 4 we will show, for two different networks of leaky-integrate-and-fire neurons, that asynchronous states indeed exist.

Chapter 2

Model-independent features of asynchronous states

2.1 Introduction

As explained in the previous chapter, recent works [Renart et al., 2010, Ecker et al., 2010] have pointed out that correlation in the activity of neighbouring neurons can be much lower than previous studies indicate [Bair et al., 2001, Kohn and Smith, 2005]. Traditionally, it was believed that one of the causes of highly correlated activity could be the large amount of common input the neurons receive [Shadlen and Newsome, 1998]. In Renart et al., 2010, it was shown that, for binary neurons, it is possible to obtain decorrelated states in networks in which the amount of common input is not negligible.

In this chapter we will derive some neuron model-independent features of asynchronous states in *balanced* heterogeneous networks of neurons [1] which are *densely* connected and interact *strongly*.

We start by assuming a definition of the asynchronous state that we will prove to be compatible with the one in Ginzburg and Sompolinsky, 1994, i.e., the cross-correlations of the activity of neurons decay linearly with the number of neurons. We then show that *necessarily* some balance equations arise that relate spike train cross-covariance and auto-covariance functions in a precise way, no matter the neuron model employed. We also show that the existence of asynchronous states is equivalent to the tracking of

[1] By *heterogeneous* networks we refer to networks in which the statistics of the synaptic couplings depend on the type of the post-synaptic neurons (excitatory or inhibitory) in contrast to *homogeneous* networks, in which they are statistically identical. We restrict ourselves to the case of heterogenous networks because they represent the most biologically plausible situation.

excitatory fluctuations by inhibitory neurons.

In the next two chapters, we will analytically prove, using two different approaches, that for networks of leaky-integrate-and-fire neurons an asynchronous state indeed exists, thus, all the results exposed in this chapter apply. However, we want to stress that the conclusions we derive here do not depend on the neuron model, i.e., once one has shown by any means (numerical or analytical) that the network operates in an asynchronous state all the results presented here are valid.

For the sake of generality we will focus on recurrent networks of excitatory and inhibitory neurons randomly connected receiving inputs from an excitatory external population. It is trivial to show that the conclusions are valid if the recurrent network is composed only of inhibitory cells (this architecture will be studied in chapter 4).

Because this chapter can be considered common to chapters 3 and 4 we will introduce the notation for some of the magnitudes that appear in those chapters in the *Methods* section. More specific magnitudes or computations will be described in the corresponding chapters.

2.2 Methods

2.2.1 Model

2.2.1.1 Network model

We consider a recurrent network composed of N_E excitatory (E) and N_I inhibitory (I) neurons. These neurons receive input from an external pool of $N_X = N$ excitatory neurons (X) firing independently and randomly with known statistics. Neurons in the recurrent network are randomly connected with connection probability p. External afferents are connected to cells in the network with the same probability p.

2.2.1.2 Network scaling

The analysis of the network behavior is based on a scaling approach in which the statistical properties of the network are analyzed as a function of its size. We find it

useful to define $\gamma_\alpha \equiv \frac{N}{N_\alpha}$ (α = E,I,X), which is kept constant as N varies. Since we are interested in the study of correlations in *densely* connected networks, the connection probability p stays constant, i.e., the mean number of neurons connected to a given cell increases linearly with N. This guarantees that the mean fraction of common input does not vary with network size. Synaptic couplings $J_{ij}^{\alpha\beta}$ are $O(1/\sqrt{N})$:

$$J_{ij}^{\alpha\beta} = \frac{j_{ij}^{\alpha\beta}}{\sqrt{N}} \tag{2.1}$$

where $j_{ij}^{\alpha\beta} \sim O(1)$. This scaling is referred to as *strong* coupling. Although the average number of inputs is proportional to N, the number of E inputs needed to induce firing is only proportional to $\sqrt{N}$.

The scaling of both p and the synaptic couplings are necessary for the network to be balanced (see Appendix 2.A at the end of the chapter). They also guarantee that the noise of the system does not depend on the network size [Renart et al., 2007].

2.2.1.3 Synaptic currents

The spike train produced by neuron j in population β = E, I, X, (j, β), denoted as $y_j^\beta(t)$, is:

$$y_j^\beta(t) \;=\; \sum_k \delta(t - t_j^{\beta,k}) \tag{2.2}$$

where $t_j^{\beta,k}$ is the spike time of the k-th action potential fired by the neuron.

The total input current afferent to neuron (i, α) is given by the sum of the pre-synaptic spike trains, each weighted with the corresponding synaptic efficacy $J_{ij}^{\alpha\beta}$ and filtered with a synaptic kernel $j_{syn}^{\alpha\beta}(t)$:

$$I_i^\alpha(t) \;=\; \sum_{(j,\beta)} m_{ij}^{\alpha\beta} J_{ij}^{\alpha\beta} (j_{syn}^{\alpha\beta} * y_j^\beta)(t), \tag{2.3}$$

where $m_{ij}^{\alpha\beta}$ is the connectivity matrix and * is the convolution operator.

Synaptic efficacies, $J_{ij}^{\alpha\beta}$, are sampled from random distributions with mean:

$$J^{\alpha\beta} \equiv \frac{j^{\alpha\beta}}{\sqrt{N}} \tag{2.4}$$

where $j^{\alpha\beta} \sim O(1)$. Besides, we find it useful to define:

$$\bar{j}^{\alpha\beta} \equiv \gamma_\beta^{-1} j^{\alpha\beta} \tag{2.5}$$

We denote by $J^{(2)\,\alpha\alpha'}$ the second moment of the distribution of synaptic efficacies

$$J^{(2)\,\alpha\alpha'} \equiv [(J_{ij}^{\alpha\alpha'})^2] \tag{2.6}$$

where $[.]$ denotes an average over pairs. It is easy to show that $J^{(2)\,\alpha\alpha'} \sim O(1/N)$. Thus, we can write:

$$J^{(2)\,\alpha\alpha'} \equiv \frac{j^{(2)\,\alpha\alpha'}}{N} \tag{2.7}$$

where $j^{(2)\,\alpha\alpha'} \sim O(1)$.

2.2.2 Current and spiking statistics

In the following we denote by $< . >$ temporal averages and by $[.]$ averages in population of neurons or neuron pairs.

2.2.2.1 Current statistics

Temporal mean of the pre-synaptic current to neuron (i, α), $< I_i^\alpha(t) >$, is calculated as:

$$< I_i^\alpha(t) > = \frac{1}{S} \int_0^S I_i^\alpha(t) \mathrm{d}t, \tag{2.8}$$

where S stands for the total time in which one computes $< I_i^\alpha(t) >$.

Cross-covariance function between total pre-synaptic currents to neurons (i, α) and (j, β) $(i \neq j)$, $c_{ij}^{\alpha\beta}(\tau)$, is defined and calculated, assuming stationary conditions, as:

$$
\begin{aligned}
c_{ij}^{\alpha\beta}(\tau) &\equiv < \delta I_i^\alpha(t)\delta I_j^\beta(t+\tau) > = \\
&= \frac{1}{\Lambda(\tau)}\int_0^S \delta I_i^\alpha(t)\delta I_j^\beta(t+\tau)\mathrm{d}t, \qquad (2.9)
\end{aligned}
$$

where $\delta Z(t) = Z(t) - < Z >$ and $\Lambda(\tau) = S - |\tau|$. This last factor is added to correct for the finite amount of data [Bair et al., 2001]. We denote by $CC_{I,\,ij}^{\alpha\beta}$ the zero-lag cross-covariance of the two currents $I_i^\alpha(t)$ and $I_j^\beta(t)$:

$$
CC_{I,\,ij}^{\alpha\beta} \equiv c_{ij}^{\alpha\beta}(0). \qquad (2.10)
$$

The cross-correlation coefficient of the total pre-synaptic currents afferent to neurons (i,α) and (j,β), $\overline{CC}_{I,\,ij}^{\alpha\beta}$ $(i \neq j)$, is defined as:

$$
\overline{CC}_{I,\,ij}^{\alpha\beta} \equiv \frac{CC_{I,\,ij}^{\alpha\beta}}{\sigma_{I_i^\alpha}\sigma_{I_j^\beta}}. \qquad (2.11)
$$

where, $\sigma_{I_i^\alpha}$ is the standard deviation of $I_i^\alpha(t)$:

$$
\sigma_{I_i^\alpha} \equiv < (\delta I_i^\alpha(t))^2 > . \qquad (2.12)
$$

We are interested in averaging correlations over populations of neurons. We then define:

$$
\begin{aligned}
c^{\alpha\beta}(\tau) &\equiv [c_{ij}^{\alpha\beta}(\tau)] && (2.13)\\
CC_I^{\alpha\beta} &\equiv [CC_{I,\,ij}^{\alpha\beta}] && (2.14)\\
\overline{CC}_I^{\alpha\beta} &\equiv [\overline{CC}_{I,\,ij}^{\alpha\beta}] && (2.15)
\end{aligned}
$$

Notice that in population-averaged magnitudes, individual neuron indices (Latin characters) disappear, while those that refer to the population over which we compute that average (Greek characters) remain. We find it useful to define the magnitudes $c_{\mathcal{I};\alpha'\beta'}^{\alpha\beta}(\tau)$ and $\bar{c}_{\mathcal{I};\alpha'\beta'}^{\alpha\beta}(\tau)$ that should be interpreted as the population-averaged cross-covariance and cross-correlation functions between components α' and β' of the currents afferent to neurons in populations α and β respectively:

$$
\begin{aligned}
c_{\mathcal{I};\alpha'\beta'}^{\alpha\beta}(\tau) &\equiv [< \mathcal{I}_i^{\alpha\alpha'}(t)\mathcal{I}_j^{\beta\beta'}(t+\tau) >] && (2.16)\\
\bar{c}_{\mathcal{I};\alpha'\beta'}^{\alpha\beta}(\tau) &\equiv [< \frac{\mathcal{I}_i^{\alpha\alpha'}(t)\mathcal{I}_j^{\beta\beta'}(t+\tau)}{\sigma_{\mathcal{I}_i^\alpha}\sigma_{\mathcal{I}_j^\beta}} >]. && (2.17)
\end{aligned}
$$

.

2.2.2.2 Spike train statistics

The stationary firing rate of neuron (i, α) is defined as:

$$\nu_i^\alpha \equiv < y_i^\alpha(t) > . \tag{2.18}$$

Cross- and auto-covariance functions of the spiking activity of a pair of neurons, in the stationary regime, are:

$$r_{ij}^{\alpha\beta}(\tau) \equiv < \delta y_i^\alpha(t) \delta y_j^\beta(t+\tau) > \qquad (i \neq j) \tag{2.19}$$

$$a_i^\alpha(\tau) \equiv < \delta y_i^\alpha(t) \delta y_i^\alpha(t+\tau) > . \tag{2.20}$$

To estimate these functions, some facts must be taken into consideration. Due to the discrete nature of spike trains, we first discretize time in small bins of size dt. Then, for each neuron (i, α), we define a vector $\chi_i^\alpha(t)$, whose components are *one* or *zero* according to whether the neuron has fired or not at the corresponding time bin. The cross- and auto-covariance functions of spike trains are estimated as:

$$r_{ij}^{\alpha\beta}(\tau) = \frac{1}{\Lambda(\tau)\mathrm{d}t^2} \sum_{t=0}^{L} \left(\chi_i^\alpha(t) \chi_j^\beta(t+\tau) - \nu_i^\alpha \nu_j^\beta dt^2 \right) \tag{2.21}$$

$$a_i^\alpha(\tau) = \frac{1}{\Lambda(\tau)\mathrm{d}t^2} \sum_{t=0}^{L} \left(\chi_i^\alpha(t) \chi_i^\alpha(t+\tau) - {\nu_i^\alpha}^2 dt^2 \right), \tag{2.22}$$

here τ is the time lag in units of dt, L is the number of time bins in the whole time interval in which the magnitude is measured ($S = L\mathrm{dt}$). Spike-count cross-covariances ($CC_{sc}(T)$) are normalized by the time window in which they are computed,T, [Renart et al., 2010] and are obtained from cross-covariance functions of spike trains as in [Bair et al., 2001]:

$$\begin{aligned} CC_{sc\,ij}^{\alpha\beta}(T) &\equiv < \delta n_{i;T}^\alpha(t) \delta n_{j;T}^\beta(t) > /T = \\ &= \int_{-T}^{T} r_{ij}^{\alpha\beta}(\tau) \frac{T - |\tau|}{T} \mathrm{d}\tau. \end{aligned} \tag{2.23}$$

where $n_{i;T}^\alpha(t)$ denotes the spike-count of neuron (i, α) in a time window of duration T around the time t. Analogously, spike-count cross-correlation coefficients ($\overline{CC}_{sc}(T)$), are computed as:

$$\begin{aligned}\overline{CC}^{\alpha\beta}_{sc\,ij}(T) &\equiv \frac{<\delta n^{\alpha}_{i;T}(t)\delta n^{\beta}_{j;T}(t)>}{\sigma_{n^{\alpha}_{i;T}}\sigma_{n^{\beta}_{j;T}}} = \\ &= \frac{\int_{-T}^{T} r^{\alpha\beta}_{ij}(\tau)\frac{T-|\tau|}{T}\mathrm{d}\tau}{\sqrt{\int_{-T}^{T} a^{\alpha}_{i}(\tau)\frac{T-|\tau|}{T}\mathrm{d}\tau \int_{-S}^{S} a^{\beta}_{j}(\tau)\frac{T-|\tau|}{T}\mathrm{d}\tau}}. \qquad (2.24)\end{aligned}$$

The population averages of these magnitudes are:

$$\nu^{\alpha} \equiv [\nu^{\alpha}_{i}] \qquad (2.25)$$

$$a^{\alpha}(\tau) \equiv [a^{\alpha}_{i}(\tau)] \qquad (2.26)$$

$$r^{\alpha\beta}(\tau) \equiv [r^{\alpha\beta}_{ij}(\tau)] \qquad (2.27)$$

$$CC^{\alpha\beta}_{sc}(T) \equiv [CC^{\alpha\beta}_{sc\,ij}(T)] \qquad (2.28)$$

$$\overline{CC}^{\alpha\beta}_{sc}(T) \equiv [\overline{CC}^{\alpha\beta}_{sc\,ij}(T)] \qquad (2.29)$$

$$. \qquad (2.30)$$

2.2.2.3 Fourier transform

The Fourier transform of the spike train cross-covariance functions are defined as:

$$\tilde{r}^{\alpha\beta}_{ij}(\omega) \equiv \mathcal{F}\Big(r^{\alpha\beta}_{ij}(\tau)\Big)(\omega) = \int_{-\infty}^{\infty} e^{-i\omega\tau} r^{\alpha\beta}_{ij}(\tau)\mathrm{d}\tau, \qquad (2.31)$$

The population-averaged value of $\tilde{r}^{\alpha\beta}_{ij}(\omega)$ is denoted by $\tilde{r}^{\alpha\beta}(\omega)$:

$$\tilde{r}^{\alpha\beta}(\omega) = [\tilde{r}^{\alpha\beta}_{ij}(\omega)] \qquad (2.32)$$

Analogously the Fourier transform of the spike train auto-covariance function is:

$$\tilde{a}^{\alpha}_{i}(\omega) \equiv \mathcal{F}(a^{\alpha}_{i}(t)) = \int_{-\infty}^{\infty} e^{-i\omega t} a^{\alpha}_{i}(t)\mathrm{d}t, \qquad (2.33)$$

and its population average is denoted by $\tilde{a}^{\alpha}(\omega)$:

$$\tilde{a}^{\alpha}(\omega) = [\tilde{a_i}^{\alpha}(\omega)] \qquad (2.34)$$

2.3 Results

2.3.1 Asynchronous states and balance equations of spike train cross-covariance functions

As we explained in the introduction of this chapter, we will use a definition of the asynchronous state that we will prove to be compatible with the one in Ginzburg and Sompolinsky, 1994. Assuming that the network is in such a state, we will derive some balance equations for the spike train cross-covariance functions that hold independently of the neuron model.

First, we calculate the population-averaged cross-covariance function of the total currents afferent to a pair of recurrent neurons. For simplicity, we will assume thereby that the synaptic filters for all kind of connections are identical, $j_{syn}^{\alpha\beta}(t) \equiv j_{syn}(t)$. A generalization for the case when they are different can be found in Appendix 2-C at the end of this chapter. From the definition of the total afferent current and after averaging over neurons and Fourier transforming them, one can easily arrive to the following expression (see details in Appendix 2-B):

$$\begin{aligned}\tilde{c}^{\alpha\alpha'}(\omega) &= p^2 \sum_{\beta} \gamma_{\beta}^{-1} j^{\alpha\beta} j^{\alpha'\beta} \tilde{\phi}_{syn}(\omega) \tilde{a}^{\beta}(\omega) + p^2 \sum_{\beta\beta'} N \bar{\jmath}^{\alpha\beta} \bar{\jmath}^{\alpha'\beta'} \tilde{\phi}_{syn}(\omega) \tilde{r}^{\beta\beta'}(\omega) \; = \\ &= p^2 \sum_{\beta} \gamma_{\beta}^{-1} j^{\alpha\beta} j^{\alpha'\beta} |\tilde{\jmath}_{syn}(\omega)|^2 \tilde{a}^{\beta}(\omega) + p^2 \sum_{\beta\beta'} N \bar{\jmath}^{\alpha\beta} \bar{\jmath}^{\alpha'\beta'} |\tilde{\jmath}_{syn}(\omega)|^2 \tilde{r}^{\beta\beta'}(\omega) \quad (2.35)\end{aligned}$$

where $\alpha, \alpha' = E, I$. In the last expression we have used the definition of $\gamma_{\beta} \equiv \frac{N}{N_{\beta}}$ and:

$$\tilde{\phi}(\omega) \equiv \mathcal{F}[\phi(\tau)] = \tilde{\jmath}_{syn}^{*}(\omega) \tilde{\jmath}_{syn}(\omega) = |\tilde{\jmath}_{syn}(\omega)|^2. \quad (2.36)$$

For a fixed value of $\omega = \omega_0$ we assume that a Taylor series in the parameter $\epsilon \equiv 1/\sqrt{N}$ exists for $\tilde{c}^{\alpha\alpha'}(\omega_0)$, i.e., $\tilde{c}^{\alpha\alpha'}(\omega_0) = \sum_n \tilde{c}^{\alpha\alpha'\,(n)}(\omega_0)\epsilon^n$. A reasonable assumption is that, in the asynchronous state, this magnitude is small. Thus, we impose, by definition, that in the asynchronous state $\tilde{c}^{\alpha\alpha'}(\omega)$ cancels to leading order for all the values of ω:

$$\tilde{c}^{\alpha\alpha'\,(0)}(\omega) = 0. \quad (2.37)$$

This assumption is reasonable, because it assumes that, if the inputs to a pair of neurons (afferent currents) are decorrelated, their outputs (spike trains) also are. Notice that

the condition in eq. 2.37 is only a constraint about the cross-covariance functions of the currents afferent to pairs of neurons in the recurrent populations ($\alpha, \alpha' = E, I$). To complete our definition of asynchronous state, we need another constraint that includes the external neurons. However, external neurons do not receive any current, but their activity is determined by a random process. We still can calculate the population-averaged cross-covariance function of an external spike train and the total current afferent to a neuron in a recurrent population, $\mathcal{A}^{X\alpha}(\tau) \equiv [< \delta y_i^X(t)\delta I_j^\alpha(t+\tau) >]$, $(\alpha = E, I)$. In the frequency space, it reads as:

$$\tilde{\mathcal{A}}^{X\alpha}(\omega) = p\tilde{j}_{syn}(\omega)(\frac{j^{\alpha X}}{\sqrt{N}}\tilde{a}^X(\omega) + \sqrt{N}\sum_{\beta=E,I} j^{\beta X} r^{X\beta}(\omega)) \tag{2.38}$$

One would also expect that, in the asynchronous state, the cross-correlations between the activities of external and recurrent neurons are small. Because the activity of a recurrent neuron is determined by its input, one can expect that in the asynchronous state $\tilde{\mathcal{A}}^{X\alpha}(\omega)$ is small. As before, we impose by definition, that in the asynchronous state this magnitude cancels to leading order in the parameter ϵ for all the values of ω:

$$\tilde{\mathcal{A}}^{X\alpha\,(0)}(\omega) = 0. \tag{2.39}$$

Assuming these cancellations, one can solve the system of equations, by noticing that, by definition $r^{\alpha\alpha'}(\tau) = r^{\alpha'\alpha}(-\tau)$ so $\tilde{r}^{\alpha\alpha'}(\omega) = \tilde{r}^{\alpha'\alpha *}(\omega)$. In the time space, the balance equations for the spike train cross-covariance functions read as:

$$r^{XE}(\tau) = r^{EX}(\tau) = \epsilon^2 A_E a^X(\tau) \tag{2.40}$$
$$r^{XI}(\tau) = r^{IX}(\tau) = \epsilon^2 A_I a^X(\tau) \tag{2.41}$$
$$r^{EE}(\tau) = \epsilon^2(A_E^2 a^X(\tau) - \gamma_E a^{E\,(0)}(\tau)) \tag{2.42}$$
$$r^{II}(\tau) = \epsilon^2(A_I^2 a^X(\tau) - \gamma_I a^{I\,(0)}(\tau)) \tag{2.43}$$
$$r^{EI}(\tau) = r^{IE}(\tau) = \epsilon^2 A_E A_I a^X(\tau). \tag{2.44}$$

where A_α are the constants that relate population-averaged mean firing rates of the recurrent population α with the external one in balanced networks (see Appendix 2-A).

Notice that although we have imposed that the population-averaged current cross-covariance functions of the total afferent currents cancel to leading order, the population-averaged cross-covariance functions of the current components, $c^{\alpha\alpha'}_{\mathcal{I};\beta\beta'}(\tau)$, are $O(1)$. To see this, we write them in terms of $a^\beta(\tau)$ and $r^{\beta\beta'}(\tau)$:

$$c^{\alpha\alpha'}_{\mathcal{I};\beta\beta'}(\tau) = p^2\gamma_\beta^{-1}j^{\alpha\beta}j^{\alpha'\beta}\phi_{syn}(\tau)a^\beta(\tau)\delta_{\beta\beta'} + p^2N\bar{\jmath}^{\alpha\beta}\bar{\jmath}^{\alpha'\beta'}\phi_{syn}(\tau)r^{\beta\beta'}(\tau) \tag{2.45}$$

Substituting the expressions of $r^{\beta\beta'}(\tau)$ given by eqs. 2.40-2.44 one can see that $c^{\alpha\alpha'}_{\mathcal{I};\beta\beta'}(\tau)$ are $O(1)$.

If one considers recurrent networks composed only of inhibitory neurons and assumes the same definition of the asynchronous state given by eqs. 2.37 and 2.39, the spike train cross-covariance function balance equations are:

$$r^{XI}(\tau) = r^{IX}(\tau) = \epsilon^2 A a^X(\tau) \tag{2.46}$$
$$r^{II}(\tau) = \epsilon^2(A^2 a^X(\tau) - \gamma_I a^{I\,(0)}(\tau)) \tag{2.47}$$

where $A = \frac{j^{IX}}{|j^{II}|}$ is again the same constant that relates the population-averaged mean firing rates in balanced networks of only inhibitory neurons (see Appendix 2-A).

To finish, one can assume that the external spike trains are not completely decorrelated. However, in order for the variance of the incoming input not to be arbitrarily large, $r^{XX}(\tau)$ must be small. In fact, it has to be $O(1/N)$. Thus, we can write:

$$r^{XX}(\tau) = \epsilon^2 r^{XX\,(2)}(\tau) \tag{2.48}$$

In this case, it is easy to show that eqs. 2.37 and 2.39 imply:

$$r^{XE}(\tau) = r^{EX}(\tau) = \epsilon^2 A_E(a^X(\tau) + r^{XX\,(2)}(\tau)) \tag{2.49}$$
$$r^{XI}(\tau) = r^{IX}(\tau) = \epsilon^2 A_I(a^X(\tau) + r^{XX\,(2)}(\tau)) \tag{2.50}$$
$$r^{EE}(\tau) = \epsilon^2(A_E^2(a^X(\tau) + r^{XX\,(2)}(\tau)) - \gamma_E a^{E\,(0)}(\tau)) \tag{2.51}$$
$$r^{II}(\tau) = \epsilon^2(A_I^2(a^X(\tau) + r^{XX\,(2)}(\tau)) - \gamma_I a^{I\,(0)}(\tau)) \tag{2.52}$$
$$r^{EI}(\tau) = r^{IE}(\tau) = \epsilon^2 A_E A_I(a^X(\tau) + r^{XX\,(2)}(\tau)). \tag{2.53}$$

for a recurrent network of excitatory and inhibitory neurons, and:

$$r^{XI}(\tau) = r^{IX} = \epsilon^2 A(a^X(\tau) + r^{XX\,(2)}(\tau)) \tag{2.54}$$
$$r^{II}(\tau) = \epsilon^2(A^2(a^X(\tau) + r^{XX\,(2)}(\tau)) - \gamma_I a^{I\,(0)}(\tau)) \tag{2.55}$$

for a recurrent network of inhibitory neurons.

2.3.2 Balance equations for spike-count cross-correlations

A magnitude closely related to $r_{ij}^{\alpha\alpha'}(\tau)$ is the spike-count cross-covariance, $CC_{sc\,ij}^{\alpha\alpha'}(T)$ defined on a time window of size T:

$$CC_{sc\,ij}^{\alpha\alpha'}(T) \equiv < \delta n_{i;T}^{\alpha}(t)\delta n_{j;T}^{\alpha'}(t) > /T, \tag{2.56}$$

where $n_{i;T}^{\alpha}(t)$ denotes the spike-count of neuron (i,α) in a time window of duration T around the time t. $CC_{sc\,ij}^{\alpha\alpha'}(T)$ can be computed as [Tetzlaff et al., 2008]:

$$CC_{sc\,ij}^{\alpha\alpha'}(T) = \int_{-T}^{T} r_{ij}^{\alpha\alpha'}(\tau)\frac{T-|\tau|}{T}d\tau. \tag{2.57}$$

It is easy to show that $CC_{sc}^{\alpha\alpha'}(T) \equiv [CC_{sc\,ij}^{\alpha\alpha'}(T)]$ follows similar expressions as eqs. 2.49-2.53. For the case in which all the synaptic filters are identical we have:

$$CC_{sc}^{XE}(T) = \epsilon^2 A_E\, AC_{sc}^{X}(T) \tag{2.58}$$
$$CC_{sc}^{XI}(T) = \epsilon^2 A_I\, AC_{sc}^{X}(T) \tag{2.59}$$
$$CC_{sc}^{EE}(T) = \epsilon^2(A_E^2\, AC_{sc}^{X}(T) - \gamma_E AC_{sc}^{E\,(0)}(T)) \tag{2.60}$$
$$CC_{sc}^{II}(T) = \epsilon^2(A_I^2\, AC_{sc}^{X}(T) - \gamma_I AC_{sc}^{I\,(0)}(T)) \tag{2.61}$$
$$CC_{sc}^{EI}(T) = CC_{sc}^{IE}(T) = \epsilon^2 A_E A_I\, AC_{sc}^{X}(T). \tag{2.62}$$

where $AC_{sc}^{\alpha}(T) \equiv \int_{-T}^{T} a^{\alpha}(\tau)\frac{T-|\tau|}{T}\mathrm{d}\tau$ (α = E,I,X).

Spike-count cross-correlation coefficients, $\overline{CC}_{sc}(T)$, are related to the spike-count cross-covariances in the following way:

$$\overline{CC}_{sc\,ij}^{\alpha\alpha'}(T) = \frac{CC_{sc\,ij}^{\alpha\alpha'}(T)}{\sqrt{\int_{-T}^{T} a_i^{\alpha}(\tau)\,\frac{T-|\tau|}{T}\,\mathrm{d}\tau \int_{-T}^{T} a_j^{\beta}(\tau)\,\frac{T-|\tau|}{T}\,\mathrm{d}\tau}} \tag{2.63}$$

Assuming that the numerator and the denominator are independent magnitudes [Renart et al., 2010] we can estimate the population-averaged value of $\overline{CC}_{sc\,ij}^{\alpha\alpha'}(T)$ as:

$$\overline{CC}_{sc}^{\alpha\alpha'}(T) \equiv [\overline{CC}_{sc\,ij}^{\alpha\alpha'}(T)] = \frac{CC_{sc}^{\alpha\alpha'}(T)}{\sqrt{\int_{-T}^{T}[a^{\alpha}(\tau)\,\frac{T-|\tau|}{T}\,\mathrm{d}\tau \int_{-T}^{T} a^{\alpha'}(\tau)\,\frac{T-|\tau|}{T}\,\mathrm{d}\tau}}. \tag{2.64}$$

We have also assumed that in an asynchronous state the average of the terms in the denominator factorizes. $a^{\alpha}(\tau)$ being $O(1)$, it is straightforward to see from eq. 2.113 that the scaling of $\overline{CC}_{sc}$ and CC_{sc} is the same.

Notice that our definition of asynchronous states has turned out to be fully compatible to the one used previously for binary neurons [Ginzburg and Sompolinsky, 1994], i.e., where asynchronous states were characterized by activity cross-covariances scaling as $O(1/N)$.

2.3.3 Asynchrony and tracking of excitatory fluctuations

In this section we show that asynchronous states are equivalent to a dynamical phenomenon by which inhibitory activity precisely tracks the fluctuations of the excitatory one. Following Renart et al., 2010, we define the magnitude $\Delta_{\alpha X}(t)$:

$$\Delta_{\alpha X}(t) \equiv \frac{1}{\nu^{\alpha}} \sum_{(i,\alpha)}^{N_{\alpha}} y_i^{\alpha}(t)/N_{\alpha} - \frac{1}{\nu^{X}} \sum_{(j,X)}^{N} y_j^{X}(t)/N \tag{2.65}$$

The variance of $\Delta_{\alpha X}(t)$ measures the degree to which the average activity of neurons in population α tracks the external average fluctuations. It can be calculated as :

$$\begin{aligned} < (\Delta_{\alpha X}(t) &- < \Delta_{\alpha X}(t) >)^2 > = \\ &= \frac{1}{N_{\alpha}(\nu^{X})^2} \Big(\frac{a^{\alpha}(0) + (N_{\alpha}-1) r^{\alpha\alpha}(0)}{A_{\alpha}^2} + \gamma_{\alpha}^{-1} a^{X}(0) - 2N_{\alpha} \frac{r^{\alpha X}(0)}{A_{\alpha}} \Big) \end{aligned} \tag{2.66}$$

Replacing the value of $\tilde{r}^{\alpha X}(0)$ and $\tilde{r}^{\alpha\alpha}(0)$ previously found (eqs. 2.49-2.53) into this last expression one observes that the terms within the parentheses cancel each other at $O(1)$, thus $< (\Delta_{\alpha X}(t) - < \Delta_{\alpha X}(t) >)^2 >$ is at most $O(\epsilon^3)$, i.e, the standard deviation of the temporal fluctuations of the instantaneous difference in firing rates is at most $O(\epsilon^{3/2})$. On the other hand, it is easy to show that the standard deviation of the fluctuations of the population rates are $O(\epsilon)$. Thus, in the large N limit, the instantaneous activity of each recurrent population ($\alpha = E, I$) tracks the activity of the external one. Consequently, in the limit $N \to \infty$, one can write:

$$\nu^E(t) = \frac{\nu^E}{\nu^X}\nu^X(t) = A_E\nu^X(t) \quad (2.67)$$

$$\nu^I(t) = \frac{\nu^I}{\nu^X}\nu^X(t) = A_I\nu^X(t) \quad (2.68)$$

We have just shown that the balance of spike train cross-covariance functions allows tracking of external fluctuations. The reciprocal is also true. To show this, we write [2]:

$$\begin{aligned} < \delta\nu^E(t)\delta\nu^E(t+\tau) > &= \sum_{(i,E)}^{N_E} \delta y_i^E(t)/N_E \sum_{(j,E)}^{N_E} \delta y_j^E(t)/N_E = \\ &\simeq \frac{1}{N}(\gamma_E a^E(\tau) + (N-1)r^{EE}(\tau)). \end{aligned} \quad (2.69)$$

Assuming that the excitatory population tracks the external activity, eq. 2.68 allows us to write:

$$\begin{aligned} < \delta\nu^E(t)\delta\nu^E(t+\tau) > &= < A_E\delta\nu^X(t)A_E\delta\nu^X(t+\tau) >= \\ &= A_E^2 \sum_{i,X} y_i^X(t)/N \sum_{j,X} y_j^X(t)/N = \\ &= \frac{A_E^2}{N} a^X(\tau). \end{aligned} \quad (2.70)$$

Thus, comparing 2.69 and 2.70:

$$A_E^2 a^X(\tau) = \gamma_E a^E(\tau) + (N-1)r^{EE}(\tau) \quad (2.71)$$

Solving the last equation for $r^{EE}(\tau)$ to leading order one arrives to the balance expression for $r^{EE}(\tau)$, eq. 2.51. Thus, we have just shown that for heterogeneous networks tracking is a necessary and sufficient condition for decorrelation.

2.3.4 Distribution of spike-count cross-covariances and cross-correlation coefficients

Even if spike-count cross-correlation coefficients have been found to be small on average, experimental studies have reported wide distributions for them both dur-

[2] We restrict the demonstration to the magnitude $r^{EE}(\tau)$, although the proof for other cross-covariance functions, $r^{\alpha\alpha'}(\tau)$, is straightforward.

ing spontaneous activity states [Renart et al., 2010] and in animals receiving stimulus[Miura et al., 2012].

The theoretical frameworks we will develop in the next two chapters allow us to write the spike-count cross-covariance function $\tilde{r}_{ij}^{\alpha\alpha'}(\omega)$ as:

$$\begin{aligned}\tilde{r}_{ij}^{X\alpha}(\omega) &= \delta\tilde{y}_i^X(t)m_{ji}^{\alpha X}J_{ji}^{\alpha X}\tilde{K}_j^{\alpha}(\omega_0)\delta\tilde{y}_i^X(\omega) \\ &+ \delta\tilde{y}_i^X(\omega)\sum_{\substack{(k,\alpha')\\k\neq i}} m_{jk}^{\alpha\alpha'}J_{jk}^{\alpha\alpha'}K_j^{\alpha}(\omega)\delta\tilde{y}_k^{\alpha'}(\omega) \qquad (\alpha = E, I) \qquad (2.72)\end{aligned}$$

$$\begin{aligned}\tilde{r}_{+,\,ij}^{\alpha\beta}(\omega) &= \tilde{K}_j^{\beta}(\omega)\Big\{m_{ji}^{\beta\alpha}J_{ji}^{\beta\alpha}\tilde{a}_i^{\alpha}(\omega) + \sum_{\substack{(k,\alpha')\\\alpha'=E,I\\k\neq i}} m_{jk}^{\beta\alpha'}J_{jk}^{\beta\alpha'}r_{+\,ik}^{\alpha\alpha'}(\omega) \\ &+ \sum_{(k,X)} m_{jk}^{\beta X}J_{jk}^{\beta X}r_{+\,ik}^{\alpha X}(\omega)\Big\} \qquad (\alpha,\beta = E, I). \qquad (2.73)\end{aligned}$$

where $\tilde{K}_j^{\beta}(\omega)$ depends on the characteristic response of the neuron in the network and the synaptic filters (we have assumed that they are identical for all kinds of synapses). As we will see, eqs. 2.72, 2.73 are consequence of the fact that one can approximate the effect of an afferent current on the response of a neuron in a *linear* way. In fact, although we will focus on two specific cases, this is a rather general approximation and we consider it worth explaining how those equations determine the width of the distribution of spike-count cross-covariances and cross-correlation coefficients. In Appendix 2-D, we show that they predict wide distributions of spike-count cross-covariances and cross-correlation coefficients. Specifically, the widths of these distributions are $O(1/\sqrt{N})$. This fact, together with the much smaller value of their average ($O(1/N)$) predicts that individual pairs spike-count cross-covariances can take positive or negative values with more or less the same probability, as has been found to be the case [Renart et al., 2010]. Notice that previous studies that assume *weak* coupling [Ginzburg and Sompolinsky, 1994] cannot predict such a feature.

2.4 Discussion

Assuming a definition of asynchronous states compatible with the generally accepted one [Ginzburg and Sompolinsky, 1994] we have found expressions that relate spike train cross- and auto-covariance functions in heterogeneous networks of neurons *densely* connected and *strongly* interacting. The overall magnitude of these functions

is $O(1/N)$. We found that similar scaling and balance equations hold for magnitudes such as spike-count cross-covariances, and cross-correlation coefficients. The definition of asynchronous states imposes the cancellation to leading order of the population-averaged cross-covariance functions of total currents although it allows for finite values of current components' ones.

We also found that for heterogeneous networks, tracking of the excitatory activity by the inhibitory one is a *necessary* and *sufficient* condition for asynchrony to exist.

To finish, we showed that under quite general assumptions, in *densely* connected networks with *strong* interactions, the distribution of spike-count cross-covariances is wide.

The conclusions we derived from this study are independent of the neuron model. However, we did not show any proof that guarantees that an asynchronous state exists in this kind of networks. To show this, one has to focus on a specific neuron model and explicitly show the existence of such a state, either numerically or analytically. In the next two chapters we show that asynchronous states exist in networks of leaky-integrate-and-fire neurons in two different regimes using two different analytical approximations and computer simulations.

Appendix 2-A. Mean rates balance

In this appendix we extend the ideas in van Vreeswijk and Sompolinsky, 1996 of balanced binary neurons to general neuron models. We show that in the limit of large networks, the average firing rate of recurrent neurons can be calculated by just imposing the incoming total current not to be arbitrarily large. We first assume the synaptic filter is identical for all the synapses $j_{syn}^{\alpha\beta}(t) \equiv j_{syn}(t)$. Later we generalize for different synaptical filters.

We first calculate the mean total current that reaches neuron (i,α) $(\alpha = E, I)$:

$$\begin{aligned}
\mu_i^\alpha &\equiv < I_i^\alpha(t) > = < \sum_{(k,\alpha')} m_{ik}^{\alpha\alpha'} J_{ik}^{\alpha\alpha'} s_k^{\alpha'}(t) > = \\
&= < \int_{-\infty}^{\infty} \mathrm{d}t \Big(\sum_{(j,X)} m_{ij}^{\alpha X} J_{ij}^{\alpha X} j_{syn}(t) y_j^X(\tau - t) \\
&+ \sum_{(l,E)} m_{il}^{\alpha E} J_{il}^{\alpha E} j_{syn}(t) y_l^E(\tau - t) \Big) + \sum_{(k,I)} m_{ik}^{\alpha I} J_{ik}^{\alpha I} j_{syn}(t) y_k^I(\tau - t) \Big) > . \quad (2.74)
\end{aligned}$$

We now average over the population of neurons. From now on, we will assume that the dynamical properties of a neuron and the synaptic weights with which it connects to the others are independent magnitudes [Renart et al., 2010], i.e., for example: $[J_{ij}^{\alpha\beta} \delta y_j^\beta(t)] = [J_{ij}^{\alpha\beta}][\delta y_j^\beta(t)]$. Proceeding in this way, averaging over the population of neurons, yields:

$$\begin{aligned}
\mu^\alpha &\equiv [\mu_i^\alpha] = pN_X J^{\alpha X} [\int_{-\infty}^{\infty} \mathrm{d}t j_{syn}(t) y_j^X(\tau - t) >] \\
&+ pN_E J^{\alpha E} [< \int_{-\infty}^{\infty} \mathrm{d}t j_{syn}(t) y_l^E(\tau - t) >] + pN_I J^{\alpha I} [< \int_{-\infty}^{\infty} \mathrm{d}t j_{syn}(t) y_k^I(\tau - t) >] = \\
&= p\sqrt{N} \Big\{ \bar{\jmath}^{\alpha X} [< \int_{-\infty}^{\infty} \mathrm{d}t j_{syn}(t) y_j^X(\tau - t) >] + \bar{\jmath}^{\alpha E} [< \int_{-\infty}^{\infty} \mathrm{d}t j_{syn}(t) y_l^E(\tau - t) >] \\
&+ \bar{\jmath}^{\alpha I} [< \int_{-\infty}^{\infty} \mathrm{d}t j_{syn}(t) y_k^I(\tau - t) >] \Big\} = \\
&= p\sqrt{N} \int_{-\infty}^{\infty} \mathrm{d}t j_{syn}(t) \Big\{ \bar{\jmath}^{\alpha X} \nu^X + \bar{\jmath}^{\alpha E} \nu^E + \bar{\jmath}^{\alpha I} \nu^I \Big\} \quad (2.75)
\end{aligned}$$

where $\bar{\jmath}^{\alpha\beta} \equiv N_\beta / N j^{\alpha\beta}$. The terms on the right hand side represent the population-averaged mean afferent current components. Notice that they are $O(\sqrt{N})$. In order for μ^α not to be arbitrarily large the following system of equations must be satisfied:

$$\bar{j}^{IX}\nu^X + \bar{j}^{IE}\nu^E + \bar{j}^{II}\nu^I = O(\epsilon) \quad (2.76)$$

$$\bar{j}^{EX}\nu^X + \bar{j}^{EE}\nu^E + \bar{j}^{EI}\nu^I = O(\epsilon), \quad (2.77)$$

where we have defined $\epsilon \equiv \frac{1}{\sqrt{N}}$. We assume as in van Vreeswijk and Sompolinsky, 1996 that the network is heterogeneous, i.e., if $\alpha \neq \alpha'$, then $j^{\alpha\beta} \neq j^{\alpha'\beta}$ for, at least, one value of β. This system can easily be solved to leading order in ϵ:

$$\nu^I = \frac{\bar{j}^{IE}\bar{j}^{EX} - \bar{j}^{EE}\bar{j}^{IX}}{\bar{j}^{II}\bar{j}^{EE} - \bar{j}^{EI}\bar{j}^{IE}}\nu^X \equiv A_I\nu^X \quad (2.78)$$

$$\nu^E = \frac{\bar{j}^{IX}\bar{j}^{EI} - \bar{j}^{II}\bar{j}^{EX}}{\bar{j}^{II}\bar{j}^{EE} - \bar{j}^{EI}\bar{j}^{IE}}\nu^X \equiv A_E\nu^X. \quad (2.79)$$

In order for this solution to have a physical meaning some constraints should be taken into account. First, the fact that the rates are positive magnitudes imposes either of the conditions:

$$\frac{j^{EX}}{j^{IX}} > \frac{j^{EI}}{j^{II}} > \frac{j^{EE}}{j^{IE}} \quad (2.80)$$

or:

$$\frac{j^{EX}}{j^{IX}} < \frac{j^{EI}}{j^{II}} < \frac{j^{EE}}{j^{IE}}. \quad (2.81)$$

Besides, we want to avoid states in which either $\nu^\alpha = 0$ and μ^α is $O(\epsilon^{-1})$ and negative or the firing rate saturates, $\nu^\alpha = (\tau^\alpha_{ref})^{-1}$. Eq. 2.81 admits an unbalanced solution with $\nu^E = 0$. The population and temporal-averaged total current reaching a neuron of the excitatory population is, in this situation:

$$\mu^E = p\sqrt{N}\Big(j^{EX} + j^{EI}j^{IX}/j^{II}\Big)\nu^X. \quad (2.82)$$

Another undesirable solution can occur when $|\bar{j}^{EI}| < \bar{j}^{EE}$ and $|\bar{j}^{II}| < \bar{j}^{IE}$. In that case a state in which both populations reach their respective saturation firing rates exists even for $\nu^X = 0$. In this solution μ^α satisfies to leading order:

$$\mu^\alpha = p\sqrt{N}\Big(\bar{j}^{\alpha E}/\tau^E_{ref} + \bar{j}^{\alpha I}/\tau^I_{ref}\Big)\nu^X. \quad (2.83)$$

μ^α is $O(\epsilon^{-1})$ and positive. Thus, if we require solutions with no saturation values of firing rates the following relationships must be satisfied:

$$\frac{j^{EX}}{j^{IX}} > \frac{j^{EI}}{j^{II}} > \frac{j^{EE}}{j^{IE}} \tag{2.84}$$

$$|j^{EI}| > \frac{\tau^I_{ref} N_E}{\tau^E_{ref} N_I} j^{EE} \tag{2.85}$$

Notice that recurrent neurons composed only of inhibitory neurons present also a balanced state similar to the one we have described. To show this, we write an expression equivalent to eq. 2.77 for this case. The population-averaged mean current reaching an inhibitory neuron is:

$$\mu^I = p\sqrt{N}(\bar{j}^{IX}\nu^X + \bar{j}^{II}\nu^I) \tag{2.86}$$

Taking into consideration the same ideas as before, we arrive to the conclusion that the following equation must be satisfied:

$$\bar{j}^{IX}\nu^X + \bar{j}^{II}\nu^I = 0 \tag{2.87}$$

There is always a physical solution to this equation, provided j^{II} is negative:

$$\nu_I = \frac{\bar{j}^{IX}}{|\bar{j}^{II}|}\nu_X \tag{2.88}$$

To finish, we extend our result to the case in which synaptic filters are not identical. Denoting the synaptic filter as $j^{\alpha\beta}_{syn}$, one can easily prove that eqs. 2.78, 2.79, 2.88 and the relation are still valid just by redefining the synaptic couplings:

$$j'^{\alpha\beta} \to j^{\alpha\beta} \int_{-\infty}^{\infty} j^{\alpha\beta}_{syn}(t)\mathrm{d}t, \tag{2.89}$$

Appendix 2-B. Calculation of $\tilde{c}^{\alpha\alpha'}(\omega)$ and $\tilde{\mathcal{A}}^{X\alpha}(\omega)$

.

In this section we will derive the expressions for $\tilde{c}^{\alpha\alpha'}(\omega)$ and $\tilde{\mathcal{A}}^{X\alpha}(\omega)$ in eqs. 2.35 and 2.38.

We start by calculating $c_{ij}^{\alpha\alpha'}(\tau)$. From its definition (eq. 2.9) and using the expression of the total current in eq. 2.3 we find that:

$$\begin{aligned} c_{ij}^{\alpha\alpha'}(\tau) &= < \delta I_i^{\alpha}(t)\delta\tilde{I}_j^{\beta}(t+\tau) > = \\ &= < (j_{syn} * \sum_{(k,\beta)} m_{ik}^{\alpha\beta} J_{ik}^{\alpha\beta} \delta y_k^{\beta})(t)(j_{syn} * \sum_{(l,\beta')} m_{jl}^{\alpha'\beta'} J_{jl}^{\alpha'\beta'} \delta y_l^{\beta'})(t+\tau) > = \\ &= \Big(\phi_{syn} * (\sum_{(k,\beta)} m_{ik}^{\alpha\beta} m_{jk}^{\alpha'\beta} J_{ik}^{\alpha\beta} J_{jk}^{\alpha'\beta} a_k^{\beta} + \sum_{\substack{(k,\beta)\\(l,\beta')\\k\neq l}} m_{ik}^{\alpha\beta} m_{jl}^{\alpha'\beta'} J_{ik}^{\alpha\beta} J_{jl}^{\alpha'\beta'} r_{kl}^{\beta\beta'})\Big)(\tau) \end{aligned} \quad (2.90)$$

where:

$$\phi_{syn}(\tau) \equiv \int_{-\infty}^{+\infty} j_{syn}(t) j_{syn}(t+\tau) \mathrm{d}t \quad (2.91)$$

and * is the convolution operator. After Fourier transforming, we can write eq. 2.90 as:

$$\tilde{c}_{ij}^{\alpha\alpha'}(\omega) = \tilde{\phi}_{syn}(\omega)\Big(\sum_{(k,\beta)} m_{ik}^{\alpha\beta} m_{jk}^{\alpha'\beta} \tilde{J}_{ik}^{\alpha\beta} J_{jk}^{\alpha'\beta} a_k^{\beta}(\omega) + \sum_{\substack{(k,\beta)\\(l,\beta')\\k\neq l}} m_{ik}^{\alpha\beta} m_{jl}^{\alpha'\beta'} J_{ik}^{\alpha\beta} J_{jl}^{\alpha'\beta'} \tilde{r}_{kl}^{\beta\beta'}(\omega)\Big) \quad (2.92)$$

Averaging over the populations of neurons and using the $O(1)$ synaptic couplings, $j^{\alpha\beta}$, we have:

$$\begin{aligned} \tilde{c}^{\alpha\alpha'}(\omega) &= p^2 \sum_{\beta} \gamma_{\beta}^{-1} j^{\alpha\beta} j^{\alpha'\beta} \tilde{\phi}_{syn}(\omega) \tilde{a}^{\beta}(\omega) + p^2 \sum_{\beta\beta'} N \bar{\jmath}^{\alpha\beta} \bar{\jmath}^{\alpha'\beta'} \tilde{\phi}_{syn}(\omega) \tilde{r}^{\beta\beta'}(\omega) = \\ &= p^2 \sum_{\beta} \gamma_{\beta}^{-1} j^{\alpha\beta} j^{\alpha'\beta} |\tilde{\jmath}_{syn}(\omega)|^2 \tilde{a}^{\beta}(\omega) + p^2 \sum_{\beta\beta'} N \bar{\jmath}^{\alpha\beta} \bar{\jmath}^{\alpha'\beta'} |\tilde{\jmath}_{syn}(\omega)|^2 \tilde{r}^{\beta\beta'}(\omega) \end{aligned} \quad (2.93)$$

which is eq. 2.35 in *Results*, section 2.3.1.

We will now deduce eq. 2.38. We start by calculating:

$$\mathcal{A}_{ij}^{X\alpha}(\tau) = < \delta y_i^X(t) \delta I_j^{\alpha}(t+\tau) > = (j_{syn} * (j^{\alpha X} m_{ji}^{\alpha X} J_{ji}^{\alpha X} a_i^X + \sum_{(k,\beta)} m_{ik}^{\beta X} J_{ik}^{\beta X} r_{ik}^{X\beta})(\tau)) \quad (2.94)$$

After Fourier transforming, averaging over neurons and using the $j^{\alpha\beta}$ synaptic couplings, we have:

$$\tilde{\mathcal{A}}^{X\alpha}(\omega) = p\tilde{j}_{syn}(\omega)(\frac{j^{\alpha X}}{\sqrt{N}}\tilde{a}^{X}(\omega) + \sqrt{N}\sum_{\beta=E,I} j^{\beta X} r^{X\beta}(\omega)) \tag{2.95}$$

which is eq. 2.38 in *Results*, section 2.3.1.

Appendix 2-C. Asynchrony in networks with different synaptic filters

In this appendix we generalize the previous calculations to the case in which synaptic filters depend on the type of neuron (E, I). In this case, eqs. 2.35 and 2.38 become:

$$\tilde{c}^{\alpha\alpha'}(\omega) = p^2 \sum_{\beta} \gamma_{\beta}^{-1} j^{\alpha\beta} j^{\alpha'\beta} \tilde{\jmath}_{syn}^{\alpha\beta}(\omega) \tilde{\jmath}_{syn}^{\alpha'\beta\,*}(\omega) \tilde{a}^{\beta}(\omega) + p^2 \sum_{\beta\beta'} N \bar{\jmath}^{\alpha\beta} \bar{\jmath}^{\alpha'\beta'} \tilde{\jmath}_{syn}^{\alpha\beta}(\omega) \tilde{\jmath}_{syn}^{\alpha'\beta\,*}(\omega) \tilde{r}^{\beta\beta'}(\omega) \quad (2.96)$$

$$\tilde{\mathcal{A}}^{X\alpha}(\omega) = p(\frac{j^{\alpha X}}{\sqrt{N}} \tilde{\jmath}_{syn}^{\alpha X}(\omega) \tilde{a}^{X}(\omega) + \sqrt{N} \sum_{\beta=E,I} j^{\beta X} \tilde{\jmath}_{syn}^{\beta X}(\omega) r^{X\beta}(\omega)) \quad (2.97)$$

We make the following definition:

$$\tilde{j}^{'\,\alpha\beta}(\omega) \to \tilde{\jmath}_{syn}^{\alpha\beta}(\omega) j^{\alpha\beta}, \quad (2.98)$$

For a fixed value of $\omega = \omega_0$ expressions formally identical to eqs. 3.61-3.65 hold true.

$$\tilde{r}^{XE}(\omega_0) = \tilde{r}^{EX\,(2)*}(\omega_0) = \epsilon^2 \tilde{A}'_E(\omega_0) \tilde{a}^X(\omega_0) \quad (2.99)$$

$$\tilde{r}^{XI}(\omega_0) = \tilde{r}^{IX\,(2)*}(\omega_0) = \epsilon^2 \tilde{A}'_I(\omega_0) \tilde{a}^X(\omega_0) \quad (2.100)$$

$$\tilde{r}^{EE}(\omega_0) = \epsilon^2 (|\tilde{A}'_E(\omega_0)|^2 \tilde{a}^X(\omega_0) - \tilde{a}^{E\,(0)}(\omega_0)) \quad (2.101)$$

$$\tilde{r}^{II}(\omega_0) = \epsilon^2 (|\tilde{A}'_I(\omega_0)|^2 \tilde{a}^X(\omega_0) - \gamma_I \tilde{a}^{I\,(0)}(\omega_0)) \quad (2.102)$$

$$\tilde{r}^{EI}(\omega_0) = \tilde{r}^{EI\,(2)*}(\omega_0) = \epsilon^2 \tilde{A}'^{*}_E(\omega_0) \tilde{A}'_I(\omega_0) \tilde{a}^X(\omega_0). \quad (2.103)$$

where $\tilde{A}'_E(\omega_0)$ and $\tilde{A}'_I(\omega_0)$ are defined analogously to A_E and A_I but using the values $\tilde{j}^{'\,\alpha\beta}(\omega_0)$ given by eq. 2.98.($\tilde{A}'^{*}_{\alpha}(\omega_0)$ denotes the complex conjugate of $\tilde{A}'_{\alpha}(\omega_0)$)

It is easy to calculate $CC_{sc}(T)$. To do this, one calculates the inverse Fourier transform of eqs. 2.99-2.103 and use the definition of $CC_{sc}(T)$. Because of the linearity of all the calculations the scaling of $CC_{sc}(T)$ is $O(1/N)$.

We finish by showing, the equivalence of asynchrony and tracking of external (excitatory) fluctuations in heterogeneous networks with different synaptic filters. We find it useful to define a magnitude similar to the one in eq. 2.65:

$$\Delta'_{\alpha X}(\tau) \equiv \sum_{(i,\alpha)}^{N_\alpha} y_i^{\alpha}(t)/N_\alpha - \sum_{(j,X)}^{N} (A'_\alpha * y_j^X)(t)/N \quad (2.104)$$

where A'_α is the Fourier inverse of $\tilde{A}'_\alpha(\omega)$. We calculate the variance of $\Delta'_{\alpha X}(t)$:

$$\begin{aligned} < (\Delta'_{\alpha X}(t) \quad - \quad & < \Delta'_{\alpha X}(t) >)^2 >= \\ = \quad & \frac{1}{N_\alpha}\Big(a^\alpha(0) + (N_\alpha - 1)(A'_\alpha * A'_\alpha * r^{\alpha\alpha})(0) + \gamma_\alpha^{-1} a^X(0) - 2N_\alpha (A'_\alpha * r^{\alpha X})(0)\Big) = \\ = \quad & \frac{1}{2\pi}\int_{-\infty}^{\infty} \Big(\tilde{a}^\alpha(0) + (N_\alpha - 1)|\tilde{A}'_\alpha(\omega)|^2 \tilde{r}^{\alpha\alpha}(\omega) + \gamma_\alpha^{-1}\tilde{a}^X(\omega) - 2N_\alpha(\tilde{A}'_\alpha(\omega)\tilde{r}^{\alpha X})(\omega)\Big)\mathrm{d}\omega \end{aligned} \quad (2.105)$$

Substituting the value of the cross-covariances given by eq. 2.99-2.103 in the frequency space one can see that the integrand cancels to leading order. Thus $< (\Delta'_{\alpha X}(t) - < \Delta'_{\alpha X}(t) >)^2 >$ is at most $O(\epsilon^3)$, i.e, the standard deviation of $\tilde{\Delta}'_{\alpha X}(\omega)$ is at most $O(\epsilon^{3/2})$. As before, one can see that the standard deviation of $\sum_i^{N_\alpha} \tilde{y}_i^\alpha(\omega)/N_\alpha$ and that of $\frac{1}{\nu^X}\sum_j^N \tilde{y}_j^X(\omega)/N$ are $O(\epsilon)$. Thus, in the large N limit, we have:

$$\nu^\alpha(\tau) \quad = \quad \int_{-\infty}^{\infty} A'_\alpha(t - t')\nu^X(t')\mathrm{d}t' \quad (2.106)$$

Thus, when the synaptic filters are different, the recurrent population activity tracks the external one once it is filtered by $A'_\alpha(t)$. It is straightforward to show that this tracking also implies decorrelation in this case. To do this, one uses the definition of $\tilde{\Delta}'_{\alpha X}(\omega)$ and follows the demonstration for the case with identical synaptic filters.

Appendix 2-D. Spike-count cross-covariances distributions

In this appendix we show how eq. 2.72 predicts a spike-count cross-covariance distribution whose width is $O(1/\sqrt{N})$. The demonstration for eq. 2.73 is formally identical.

From eq. 2.72, keeping $\omega = \omega_0$ and using the notation $\Delta\tilde{r}_{ij}^{X\alpha}(\omega_0) \equiv \tilde{r}_{ij}^{X\alpha}(\omega_0) - [\tilde{r}_{ij}^{X\alpha}(\omega_0)]$ one can write:

$$\begin{aligned}
[(\Delta\tilde{r}_{ij}^{X\alpha}(\omega_0))^2] &= [(\tilde{K}_j^{\alpha}(\omega_0))^2]\Big\{p^2\frac{j^{(2)\,\alpha X}}{N}[(\Delta\tilde{a}_i^X(\omega_0))^2] \\
&+ p\sum_{(k,\alpha')}(\bar{\jmath}^{\alpha\alpha'})^2[(\Delta\tilde{r}_{ik}^{X\alpha'}(\omega_0))^2] \\
&+ p(Np-1)\sum_{\substack{(k,\alpha')\\(l,\alpha'')}}\bar{\jmath}^{\alpha\alpha'}\bar{\jmath}^{\alpha\alpha''}[\Delta\tilde{r}_{ik}^{X\alpha'}(\omega_0)\Delta\tilde{r}_{il}^{X\alpha''}(\omega_0)]_{k\neq l} \\
&+ \frac{2}{N}j^{\alpha X}p\sum_{(k,\alpha')}\bar{\jmath}^{\alpha\alpha'}[\Delta\tilde{r}_{ik}^{X\alpha'}(\omega_0)\Delta\tilde{a}_i^X(\omega_0)]\Big\} \qquad (2.107)
\end{aligned}$$

Last expression represents a matrix equation for $[(\Delta\tilde{r}_{ij}^{X\alpha}(\omega_0))^2]$. Notice that some unknown terms also appear: $[\Delta\tilde{r}_{ik}^{X\alpha'}(\omega_0)\Delta\tilde{r}_{il}^{X\alpha''}(\omega_0)]_{k\neq l}$ and $[\Delta\tilde{r}_{ik}^{X\alpha'}(\omega_0)\Delta\tilde{a}_i^X(\omega_0)]$. We can write equations for them also from eq. 2.72:

$$\begin{aligned}
[\Delta\tilde{r}_{ij}^{X\alpha}(\omega_0)\Delta\tilde{r}_{im}^{X\alpha'}(\omega_0)]_{j\neq m} &= [(K_j^{\alpha}(\omega_0))^2]\Big\{p^2\frac{j^{\alpha X}j^{\alpha' X}}{N}[(\Delta\tilde{a}_i^X(\omega_0))^2] \\
&+ p^2\sum_{(k,\alpha'')}\bar{\jmath}^{\alpha\alpha''}\bar{\jmath}^{\alpha\alpha''}[(\Delta\tilde{r}_{ik}^{X\alpha''}(\omega_0))^2] \\
&+ p^2(N-1)\sum_{\substack{(k,\alpha'')\\(l,\alpha''')}}\bar{\jmath}^{\alpha\alpha''}\bar{\jmath}^{\alpha'\alpha'''}[\Delta\tilde{r}_{ik}^{X\alpha''}(\omega_0)\Delta\tilde{r}_{il}^{X\alpha'''}(\omega_0)]_{k\neq l} \\
&+ (j^{\alpha' X})p\sum_{(k,\alpha'')}\bar{\jmath}^{\alpha\alpha''}[\Delta\tilde{r}_{ik}^{X\alpha''}(\omega_0)\Delta\tilde{a}_i^X(\omega_0)] \\
&+ (j^{\alpha X})p\sum_{(k,\alpha'')}\bar{\jmath}^{\alpha'\alpha''}[\Delta\tilde{r}_{ik}^{X\alpha''}(\omega_0)\Delta\tilde{a}_i^X(\omega_0)] \qquad (2.108)
\end{aligned}$$

$$\begin{aligned}
[\Delta\tilde{r}_{ij}^{X\alpha}(\omega_0)\Delta\tilde{a}_i^X(\omega_0)] &= \tilde{K}_j^{\alpha}(\omega_0)p\Big\{\frac{j^{\alpha X}}{\sqrt{N}}[(\Delta\tilde{a}_i^X(\omega_0))^2] \\
&+ \sqrt{N}\sum_{(k,\alpha')}\bar{\jmath}^{\alpha\alpha'}[\Delta\tilde{r}_{ik}^{X\alpha'}(\omega_0)\Delta\tilde{a}_i^X(\omega_0)]\Big\} \qquad (2.109)
\end{aligned}$$

Taking into account that $[(\Delta\tilde{a}_i^X(\omega_0))^2]$ and $\tilde{a}^X(\omega_0)$ are $O(1)$, and assuming that $[\tilde{K}_j^\alpha(\omega_0)]$ and $[(\tilde{K}_j^\alpha(\omega_0))^2]$ are $\sim O(1)$[3] one can easily show that:

$$[\Delta\tilde{r}_{ij}^{X\alpha}(\omega_0)\Delta\tilde{a}_i^X(\omega_0)] \sim O(1/N) \quad (2.110)$$

$$[\Delta\tilde{r}_{ij}^{X\alpha}(\omega_0)\Delta\tilde{r}_{im}^{X\alpha}(\omega_0)]_{j\neq m} \sim O(1/N^2) \quad (2.111)$$

$$[(\Delta\tilde{r}_{ij}^{X\alpha}(\omega_0))^2] \sim O(1/N) \quad (2.112)$$

Thus, the standard deviation of the distribution of $\tilde{r}_{ij}^{X\alpha}(\omega_0)$ is $O(\epsilon)$. It is trivial to show that the distribution of spike-count cross-covariances $CC_{sc\,ij}^{X\alpha}(T)$ presents a standard deviation with the same scaling. To prove this, one computes $CC_{sc\,ij}^{X\alpha}(T)$ from $r_{ij}^{X\alpha}(\tau)$ (eq. 2.23) and calculate its standard deviation in terms of $[(\Delta r_{ij}^{X\alpha}(\tau))^2]$. Because of the linearity of the integral, $CC_{sc\,ij}^{X\alpha}(T)$ and $r_{ij}^{X\alpha}(\tau)$ scale in the same way. One can also show that the distributions of the spike count cross-correlation coefficients are also wide. To see this, we write:

$$[(\Delta\overline{CC}_{sc\,ij}^{X\alpha'}(T))^2] = \frac{[(\Delta CC_{sc\,ij}^{X\alpha'}(T)])^2}{\sqrt{\int_{-T}^{T}\Delta[(a_i^X(\tau))^2]\,\frac{T-|\tau|}{T}\,\mathrm{d}\tau\int_{-S}^{S}\Delta[(a_j^{\alpha'}(\tau))^2]\,\frac{T-|\tau|}{T}\,\mathrm{d}\tau}}. \quad (2.113)$$

where we have assumed the same factorization as in section, 2.3.2. $[(\Delta a_i^X(\tau))^2]$ is $O(1)$ by construction, and if one assumes that $[(\Delta a_j^\alpha(\tau))^2]$ is also $O(1)$ one can conclude that $[(\Delta\overline{CC}_{sc\,ij}^{X\alpha'}(T))^2]$ and $[(\Delta CC_{sc\,ij}^{X\alpha'}(T))^2]$ scale in the same way. We, thus, need to show that $a_j^\alpha(\tau)$ effectively is $O(1)$. Notice that $a_j^\alpha(\tau)$ is *univocally* determined by the incoming current auto-covariance function, $< I_j^\alpha(t)I_j^\alpha(t+\tau) >$. Thus, the spatial variance of $a_j^\alpha(\tau)$ and the spatial variance of $< \delta I_j^\alpha(t)\delta I_j^\alpha(t+\tau) >$ scale with N in the same way. One can express the spatial variance of $< \delta I_j^\alpha(t)\delta I_j^\alpha(t+\tau) >$ in terms of the spatial variance of the spike trains auto- and cross-covariance functions in a similar way as we did for $[(\Delta\tilde{r}_{ij}^{X\alpha}(\omega_0))^2]$. By doing so, one can convince oneself that the spatial variances of both $< \delta I_j^\alpha(t)\delta I_j^\alpha(t+\tau) >$ and $a_j^\alpha(\tau)$ *necessarily* have to be $O(1)$.

As we have mentioned, the demonstration for the spike-count cross-covariances of recurrent-recurrent pairs is very similar and the conclusion is the same.

[3] In the next chapters, we will see that the function $\tilde{K}_j^\alpha(\omega)$ represents the joint effect of a synaptic filter and the response of the neuron to an input. This response depends on the state of the network, typically it depends on the current statistics. In the limit of large networks currents are Gaussian variables, and thus, $\tilde{K}_j^\alpha(\omega)$ depends only on the mean and the variance of the current which are $\sim O(1)$.

In the general case of networks in which synaptic filters depend on the type of neurons, eqs. 2.72 and 2.73 become:

$$\begin{aligned}
\tilde{r}_{ij}^{X\alpha}(\omega) &= m_{ji}^{\alpha X} J_{ji}^{\alpha X} \tilde{K}_j^{\alpha}(\omega_0) \tilde{a}_i^X(\omega) \\
&+ \sum_{\substack{(k,\alpha') \\ k\neq i}} m_{jk}^{\alpha\alpha'} J_{jk}^{\alpha\alpha'} K_j^{\alpha}(\omega) \tilde{r}_{ik}^{X\alpha'}(\omega) \qquad \alpha = E, I \qquad (2.114) \\
\tilde{r}_{+,\,ij}^{\alpha\beta}(\omega) &= K_j^{\beta}(\omega) \Big\{ m_{ji}^{\beta\alpha} J_{ji}^{\beta\alpha} \tilde{a}_i^{\alpha}(\omega) \\
&+ \sum_{\substack{(k,\alpha') \\ \alpha'=E,I \\ k\neq i}} m_{jk}^{\beta\alpha'} J_{jk}^{\beta\alpha'} r_{+\,ik}^{\alpha\alpha'}(\omega) \\
&+ \sum_{(k,X)} m_{jk}^{\beta X} J_{jk}^{\beta X} r_{+\,ik}^{\alpha X}(\omega) \Big\} \qquad \alpha, \beta = E, I. \qquad (2.115)
\end{aligned}$$

where $\tilde{K}_{ji}^{\alpha\alpha'}(\omega)$ depends now on the pre- and postsynaptic neurons. Using the same techniques as in Appendix 2-C it is straightforward to show that the same scaling of the distributions' width is predicted.

Chapter 3

Decorrelation in LIF networks with fast synaptic kinetics

3.1 Introduction

Here we present a study on balanced heterogeneous networks of leaky-integrate-and-fire (LIF) neurons which are *densely* connected and interact *strongly*. This is the simplest spiking model that presents the most relevant biological features, such as synaptic and membrane potential time constants. Besides, the model is simple enough to understand some of the very basic phenomena that take place. We use the linear response approximation [Brunel and Hakim, 1999, Lindner and Schimansky-Geier, 2001, Lindner et al., 2005] to find self-consistent equations for the spike train cross-covariance functions. Such approximation has been proved to be valid in the case when neurons receive white noise input or background activity filtered through fast synapses [Fourcaud and Brunel, 2002].

The aim of this study is to show that decorrelated activity is possible in networks of LIF neurons and to understand the mechanisms that make this decorrelation possible.

3.2 Methods

3.2.1 Model

3.2.1.1 Network model

We consider a recurrent network with N_E excitatory (E) and N_I inhibitory (I) leaky integrate-and-fire neurons (LIF), in a 4:1 ratio. These two neural populations receive an input current from a population of external neurons (X), of the same size as the

excitatory population, $N_E = N_X \equiv N$.

Neurons in the recurrent network are randomly connected with connection probability $p = 0.2$, unless otherwise mentioned. External afferents are connected to cells in the network with the same probability p.

3.2.1.2 External neuron model

External neurons fire independently, with Poisson statistics and with a mean firing rate of 2.5 Hz.

3.2.1.3 Recurrent neuron model

Neurons in the recurrent network are modeled as LIF units, with current-based synaptic inputs. Neuron i in population α is indicated as neuron (i, α). Its state at time t is fully determined by its membrane potential, $V_i^\alpha(t)$, that, below a threshold value V_{Th}, evolves according to:

$$\tau_m \frac{dV_i^\alpha(t)}{dt} = -V_i^\alpha(t) + V_L^\alpha - I_i^\alpha(t), \tag{3.1}$$

where τ_m= 15 ms is the membrane characteristic time and $V_L^{E(I)}$= -60 (-59.5) mV is the leak potential. $I_i^\alpha(t)$ is the total pre-synaptic current to neuron (i, α). When the membrane potential reaches the value V_{Th}= -50 mV, an action potential is emitted and the voltage is reset to V_{Reset}= -59 mV, in which it remains during a refractory time (τ_{ref}^E= 2 ms for excitatory neurons and τ_{ref}^I= 1 ms for inhibitory neurons).

3.2.1.4 Synaptic currents

The spike train produced by neuron (j, β), denoted as $y_j^\beta(t)$, is:

$$y_j^\beta(t) \;=\; \sum_k \delta(t - t_j^{\beta,k}) \tag{3.2}$$

where $t_j^{\beta,k}$ is the spike time of the k-th action potential fired by the neuron. Spike trains are filtered through synapses as:

$$\tau_d \frac{ds_j^\beta(t)}{dt} = x_j^\beta(t) - s_j^\beta(t) \tag{3.3}$$

$$\tau_r \frac{dx_j^\beta(t)}{dt} = \tilde{\tau} y_j^\beta(t) - x_j^\beta(t), \tag{3.4}$$

where $s_j^\beta(t)$ is the filtered spike train, $x_j^\beta(t)$ is an auxiliary variable, τ_r= 0.5 ms and τ_d= 5 ms are the rise and decay synaptic time constants and the factor $\tilde{\tau}$= 1 ms ensures that the area under $s_j^\beta(t)$ is constant regardless of the rise and decay time constants.

The total input current afferent to neuron (i, α) is given by the sum of the filtered pre-synaptic spike trains, each weighted with the corresponding synaptic efficacy:

$$I_i^\alpha(t) = \sum_{(j,\beta)} m_{ij}^{\alpha\beta} J_{ij}^{\alpha\beta} s_j^\beta(t), \tag{3.5}$$

The sum runs over all neurons (j, β) in the network (including those in the external population, $\beta = X$); $J_{ij}^{\alpha\beta}$ is the synaptic efficacy from neuron (j, β) to neuron (j, α). The connectivity matrix, $m_{ij}^{\alpha\beta}$, is made of *one*s or *zero*s, according to whether neuron (i, α) is post-synaptic to neuron (j, β) or not. It can be easily proven that the filtering in eqs. 3.3 and 3.4 results in:

$$I_i^\alpha(t) = \sum_{(j,\beta)} m_{ij}^{\alpha\beta} J_{ij}^{\alpha\beta} (j_{syn} * y_j^\beta)(t), \tag{3.6}$$

where * is the convolution operator and $j_{syn}(t)$ is the synaptic filter:

$$j_{syn}(t) = \Theta(t) \frac{\tilde{\tau}}{\tau_d - \tau_r} (e^{-\frac{t}{\tau_d}} - e^{-\frac{t}{\tau_r}}) \tag{3.7}$$

where $\Theta(t)$ is the Heaviside step function. The total current consists of components $\mathcal{I}_i^{\alpha\beta}(t)$, defined as the sum of the pre-synaptic currents arriving to neuron (i, α) from neurons in the population $\beta = E, I, X$:

$$I_i^\alpha(t) = \sum_\beta \mathcal{I}_i^{\alpha\beta}(t) \quad ; \quad \mathcal{I}_i^{\alpha\beta}(t) = \sum_{j\in\beta} m_{ij}^{\alpha\beta} J_{ij}^{\alpha\beta} s_j^\beta(t). \tag{3.8}$$

Synaptic efficacies, $J_{ij}^{\alpha\beta}$, are sampled from Gaussian distributions with mean $J^{\alpha\beta}$ and standard deviation equal to 0.2 of the mean. Gaussian distributions were truncated at five standard deviations in order to prevent a change of sign for the synaptic couplings. We denote by $J^{(2)\,\alpha\alpha'}$ the second moment of the distribution of synaptic efficacies:

$$\begin{aligned} J^{(2)\,\alpha\alpha'} &\equiv [(J_{ij}^{\alpha\alpha'})^2] \\ &= \frac{1}{0.2J^{\alpha\alpha'}\sqrt{2\pi}} \int_{-J^{\alpha\alpha'}}^{J^{\alpha\alpha'}} x^2 e^{-\frac{(x-J^{\alpha\alpha'})^2}{2(0.2(J^{\alpha\alpha'})^2)}} \mathrm{d}x. \end{aligned} \tag{3.9}$$

It is easy to show that $J^{(2)\,\alpha\alpha'} \sim O(1/N)$.

3.2.1.5 Network scaling

The analysis of the network behavior is based on a scaling approach in which the network statistical properties are analyzed as a function of network size $N \equiv N_E$ (remember that $N_E = N_X = 4N_I$). Since we focus on the study of correlations in *densely* connected networks, the connection probability p between two cells does not depend on network size, i.e., the mean number of neurons connected to a given cell increases linearly with N. This guarantees that the mean fraction of common input does not vary with network size.

Synaptic efficacies are scaled as:

$$J^{\alpha\beta} = \frac{j^{\alpha\beta}}{\sqrt{N}} \tag{3.10}$$

with the following values of $j^{\alpha\beta}$: j^{EE} = 117.85 mV, j^{EI} = -445.8, j^{EX} = 481.8 mV, j^{IE} = 161.7 mV, j^{II} = -398.75 mV, j^{IX} = 410.2 mV.

For networks with N =32000, the IPSPs and EPSPs amplitudes are a few millivolts. Neurons connected with this kind of synapses ($J \sim 1/\sqrt{N}$) are said to interact *strongly*. With such a scaling the net input to a neuron coming from each population is $O(\sqrt{N})$. A balance in the average total afferent current is achieved because of a dynamical adjustment of the firing rates, as in van Vreeswijk and Sompolinsky, 1998, Renart et al., 2010, so that the total afferent current takes finite values. Besides, this scaling assures finite current fluctuations [Renart et al., 2007].

We find it useful to define the $O(1)$ magnitude $j^{(2)\,\alpha\alpha'}$:

$$J^{(2)\,\alpha\alpha'} \equiv \frac{j^{(2)\,\alpha\alpha'}}{N} \tag{3.11}$$

3.2.2 Parameter values

In table 3.1 we summarize the default value of all the parameters which describe the system.

	E	I
τ_m	15 ms	
τ^{α}_{ref}	2 ms	1 ms
τ_r	0.5 ms	
τ_d	5 ms	
V^{α}_{L}	-60 mV	-59.5 mV
V_{Th}	-50 mV	
V_{Reset}	-60 mV	
$j^{\alpha E}$	117.85 mV	161.7 mV
$j^{\alpha I}$	-445.8 mV	-398.75 mV
$j^{\alpha X}$	481.8 mV	410.2 mV
ν^X	2.5Hz	
p	0.2	

Table 3.1: Parameter's values

3.2.3 Current, membrane potential and spiking statistics

Statistical measures of the currents and spike trains were defined in chapter 2. We find it convenient to define here the statistical magnitudes related to the membrane potential employed in this chapter.

Temporal mean of the membrane potential of neuron (i, α), $< V^{\alpha}_{i}(t) >$, is calculated as:

$$< V^{\alpha}_{i}(t) >= \frac{1}{S}\int_{0}^{S} V^{\alpha}_{i}(t)\mathrm{d}t \tag{3.12}$$

where S is the simulation time. The cross-covariance function of membrane potentials of neurons (i,α) and (j,β), $c^{\alpha\beta}_{V,\,ij}(\tau)$, is calculated as:

$$\begin{aligned} c^{\alpha\beta}_{V,\,ij}(\tau) &\equiv < \delta V_i^{\alpha}(t)\delta V_j^{\beta}(t+\tau) > \\ &= \frac{1}{\Lambda(\tau)}\int_0^S \delta V_i^{\alpha}(t)\delta V_j^{\beta}(t+\tau)\mathrm{d}t. \end{aligned} \tag{3.13}$$

where $\Lambda(\tau) = S - |\tau|$. We find it useful to define the zero-lag cross-covariance and the cross-correlation coefficient:

$$CC^{\alpha\beta}_{V,\,ij} \equiv c^{\alpha\beta}_{V,\,ij}(0) \tag{3.14}$$

$$\overline{CC}^{\alpha\beta}_{V,\,ij} \equiv \frac{CC^{\alpha\beta}_{V,\,ij}}{\sigma_{V_i^{\alpha}}\sigma_{V_j^{\beta}}} \tag{3.15}$$

where $\sigma_{V_i^{\alpha}}$ is the standard deviation of V_i^{α}. The population-averaged values of these magnitudes are:

$$c^{\alpha\beta}_{V}(\tau) = [c^{\alpha\beta}_{V,\,ij}(\tau)] \tag{3.16}$$

$$CC^{\alpha\beta}_{V} = [c^{\alpha\beta}_{V,\,ij}(0)] \tag{3.17}$$

$$\overline{CC}^{\alpha\beta}_{V} = [\overline{CC}^{\alpha\beta}_{V,\,ij}] \tag{3.18}$$

3.2.4 Jittered spike trains

Jittered spike trains were constructed by adding to each spike time an independent random variable drawn from a uniform distribution in the interval [-0.5, 0.5] s . By doing this, one eliminates the cross-correlations between them in time-scales shorter than 0.5 s. As we will see, in the networks that we have simulated, cross-correlations are concentrated at time-scales of the order of some milliseconds, thus, jittered spike trains generated in this way are uncorrelated.

For each network simulation, we generated 100 surrogate data sets where spike trains were jittered in the described way. Histograms of spike-count cross-correlation coefficients and cross-covariances of jittered spike trains in fig. 3.6 (grey lines) were computed

by averaging the corresponding histograms obtained for each of the surrogate data sets of a given simulation.

3.2.5 Simulations

Equations for the evolution of the membrane potential (eq. 3.1) and pre-synaptic currents (eqs. 3.3-3.4) were integrated using Euler's method, with an integration step of $\mathrm{d}t = 0.05$ ms. Simulated network sizes were ($N \equiv N_X = N_E$): $N = 2000$, 4000, 8000, 16000, 32000).

For each run, simulation time was $S = 150$ s, except for fig. 3.6 where $S = 12000$ s. We recorded the membrane potential and the pre-synaptic current traces of 20 excitatory and 20 inhibitory neurons. We also recorded the spike times of 1000 neurons in each population. Population-averaged magnitudes were computed with these data. Figures showing the scaling of certain magnitudes with N were computed by averaging over 20 simulations with different realizations of the connectivity matrix. Error bars correspond to the standard errors. Although most of the figures report results for single excitatory cells or excitatory pairs, the results and conclusions hold true for single inhibitory neurons and inhibitory-inhibitory or excitatory-inhibitory pairs.

Simulations and data analysis were performed with custom codes written in C and Matlab. Spectral analysis was computed with Chronux toolbox.

3.3 Results

Fig. 3.1b shows the rastergram of inhibitory (red) and excitatory (green) neurons in a network with $N = 32000$ neurons. The firing pattern of each neuron looks independent of the others. This suggests that they fire in an asynchronous way. Neurons' firing patterns are also very irregular. Fig. 3.1c shows the incoming current to one randomly chosen excitatory cell in the network. Notice that the current components (part of the current that arrives from one specific population) are large but the total incoming current is small. This results in a firing state dominated by fluctuations characterized by a high value of the CV of the ISIs, fig. 3.1e. The distribution of firing rates has a long tail (fig. 3.1f), a typical feature of *balanced* networks [van Vreeswijk and Sompolinsky, 1998, Roxin et al., 2011]. Notice that the observed asynchrony is not a consequence of the small number of common inputs. In fig. 3.1d we show the

population-averaged cross- correlation coefficients of the current components and total currents reaching a pair of excitatory neurons as a function of the mean connectivity p for networks with $N = 32000$ neurons. The total current cross-correlation coefficients are small (one order of magnitude smaller than p), which explains the asynchrony of the system. However, notice that current components cross-correlation coefficients are very high.

In the following sections we will explain the mechanisms that lead to an asynchronous state as the one in fig. 3.1. To this end, we will employ both numerical and analytical methods. First, we present the general scheme of the theory that allows us to calculate cross-correlations in a self-consistent way. Then, we will show analytical and numerical results in *densely* connected networks of *strongly* interacting neurons, presenting qualitatively the results and conclusions that can be derived from the theory. We will finish by showing an analysis of the effect of the most relevant parameters on the asynchronous state. Theoretical results can be found in Appendices 3-A, 3-B and 3-C. Additional details and supplementary information are present in other appendices at the end of this chapter.

3.3.1 Self-consistent scheme

The theory is based on the linear response approximation [Brunel and Hakim, 1999, Lindner and Schimansky-Geier, 2001, Lindner et al., 2005] that relates small afferent currents with the spiking activity of the neuron. In this framework, the effect of a small incoming current on the spike train $y(t)$ of a neuron that receives background noise can be well approximated by [Lindner et al., 2005]:

$$y(t) \simeq y^{(0)}(t) + (R * I_s)(t) \tag{3.19}$$

where * denotes the convolution operator, $R(t)$ is the linear response kernel, $I_s(t)$ is a small current and $y^{(0)}(t)$ is the spike train generated only with the background noise. As explained in Brunel and Hakim, 1999, the liner response kernel depends on the characteristics of the neuron and on the statistics of the afferents it receives. In a recurrent network, the spike train emitted by a neuron acts as input to its post-synaptic cells, after being filtered by the synapses. This fact, together with the previous equation, are the ingredients necessary to develop self-consistent equations for the spike train cross-covariance functions. Notice that for the linear approximation to be valid,

$I_s(t)$ has to be small. For a given pair of cells, we find it convenient to split the total current arriving to a neuron into a current that is correlated with the firing of the other neuron and a current that is independent of it. The latter acts as the background noise that defines $y^{(0)}(t)$ while the former is assumed (and later proved) to be small. Proceeding like this, in Appendix 3-A2 we show that the population-averaged cross-covariance functions $r^{\alpha\beta}(\tau)$, $r^{X\alpha}(\tau)$ $(\alpha, \beta = E, I)$ can be expressed in a self-consistent way:

$$\begin{aligned} r_+^{\alpha\beta}(\tau) &= p\Big\{ \frac{j^{\beta\alpha}}{\sqrt{N}}(R^\beta * j_{syn} * a^\alpha)(\tau) + \sqrt{N}\Big(\bar{j}^{\beta X}(R^\beta * j_{syn} * r^{\alpha X})(\tau) \\ &+ \sum_{\alpha' \in E,I} \bar{j}^{\beta\alpha'}(R^\beta * j_{syn} * r_+^{\alpha\alpha'})(\tau)\Big)\Big\} \end{aligned} \tag{3.20}$$

$$r^{X\alpha}(\tau) = p\Big\{ \frac{\bar{j}^{\alpha X}}{\sqrt{N}}(R^\alpha * j_{syn} * a^X)(\tau) + \sum_{\alpha' \in E,I} \sqrt{N}\bar{j}^{\alpha\alpha'}(R^\alpha * j_{syn} * r^{X\alpha'})(\tau)\Big\}, \tag{3.21}$$

where p is the connection probability, $\bar{j}^{\alpha\beta} = N_\beta / N j^{\alpha\beta}$,* is the convolution operator and $a^\alpha(\tau)$ and $R^\alpha(\tau)$ are the population-averaged spike train auto-covariance function and linear response kernel of neurons in population α. The subscript + indicates that eq. 3.20 holds only for $\tau \geq 0$. For $\tau < 0$, we make use of the symmetry of the cross-covariance functions: $r^{\alpha\beta}(\tau) = r_+^{\alpha\beta}(-\tau)$ $(\tau < 0)$.

In Appendix 3-A, we solve eqs. 3.22 and 3.26 in the limit $N \to \infty$ (leading order). Population-averaged spike train cross-covariance functions are determined by a combination of spike train auto-covariance functions of external and recurrent neurons, which present a delta-shaped structure (fig. 3.4a):

$$r^{XE}(\tau) = \frac{1}{N} A_E a^X(\tau) \tag{3.22}$$

$$r^{XI}(\tau) = \frac{1}{N} A_I a^X(\tau) \tag{3.23}$$

$$r^{EE}(\tau) = \frac{1}{N}(A_E^2 a^X(\tau) - a^{E\,(0)}(\tau)) \tag{3.24}$$

$$r^{II}(\tau) = \frac{1}{N} A_I^2 a^X(\tau) - \gamma_I a^{I\,(0)}(\tau) \tag{3.25}$$

$$r^{EI}(\tau) = \frac{1}{N} A_E A_I a^X(\tau). \tag{3.26}$$

where $\gamma_I \equiv \frac{N}{N_I} \sim O(1)$ and A_α has been defined in eqs. 2.78 and 2.79 and can be

rewritten in matrix notation as:

$$A_\alpha = -\sum_\beta (\bar{J}^{\beta\alpha})^{-1} \bar{J}^{\alpha X} \tag{3.27}$$

Notice that these equations were derived in the previous chapter by assuming that the network is in an asynchronous state. In Appendix 3-A we arrive to eqs. 3.22-3.26 from 3.20-3.21 without making any assumption. Proceeding like this, we show that the cross-covariance functions are small, thus, the asynchronous state exists and all the results described in the previous chapter are valid. Eqs. 3.22-3.26 and their consequences are explained in detail in the next sections.

3.3.2 Scaling analysis of the network activity

In this section we present the results of the simulations and compare them with the predictions from the theory. We start by showing some of the features of *densely* and *strongly* connected networks in the limit $N \to \infty$. Population-averaged rates and mean currents behave asymptotically as predicted (figs. 3.2a,b). The current components increase as $\sqrt{N}$, due to the combined effect of the scaling of the synaptic efficacies (which are $O(1/\sqrt{N})$) and the increasing number of pre-synaptic connections, $O(N)$. The population and temporal average of the total current remains finite, a defining feature of balanced networks [van Vreeswijk and Sompolinsky, 1996, Renart et al., 2010]. The population-averaged standard deviation of the membrane potential of excitatory neurons (fig. 3.2c) reaches an asymptotic value in the biological range (fig. 3.2c) [Anderson et al., 2000a].

To analyze more quantitatively how the asynchronous regime develops, we evaluated cross-covariances in networks of several sizes. Figs. 3.2d-g show that population-averaged spike-count cross-covariances ($T = 80$ ms) decrease with N. In the asynchronous state the scaling of the population-averaged spike-count cross-covariances between a pair of neurons is $O(1/N)$ (see previous chapter):

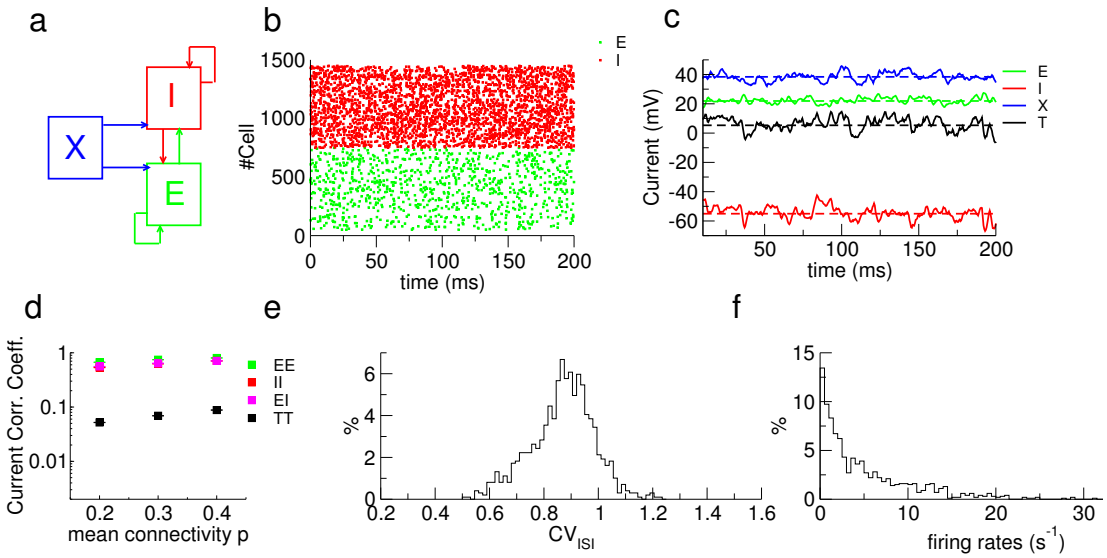

Figure 3.1: **Balanced and asynchronous network. a)** Network architecture. **b)** Rastergram of excitatory (green) and inhibitory (red) neurons for a network with N =32000. **c)** Temporal traces of currents afferent to a randomly chosen excitatory neuron : excitatory (E) current (green), inhibitory (I) current (red), external (X) current (blue) and total (T) current (black). Dashed lines correspond to the (temporal) mean value. **d)** Absolute value of the population-averaged cross-correlation coefficients between the current components and between the total currents afferent to a pair of excitatory neurons. Green: cross-correlation coefficients of the excitatory-excitatory current components; red: cross-correlation coefficients of the inhibitory-inhibitory current components; magenta: cross-correlation coefficients of the excitatory-inhibitory (their values without taking the absolute value are negative) current components; black: cross-correlation coefficients of the total currents. **e)** Distribution of the coefficient of variation (CV) of inter-spike-intervals of excitatory cells. **f)** Firing rate distribution of excitatory cells.

$$CC_{sc}^{XE}(T) = \frac{1}{N} A_E \; AC_{sc}^{X}(T) \tag{3.28}$$

$$CC_{sc}^{XI}(T) = \frac{1}{N} A_I \; AC_{sc}^{X}(T) \tag{3.29}$$

$$CC_{sc}^{EE}(T) = \frac{1}{N} (A_E^2 \; AC_{sc}^{X}(T) - AC_{sc}^{E\,(0)}(T)) \tag{3.30}$$

$$CC_{sc}^{II}(T) = \frac{1}{N} (A_I^2 \; AC_{sc}^{X}(T) - \gamma_I AC_{sc}^{I\,(0)}(T)) \tag{3.31}$$

$$CC_{sc}^{EI}(T) = \frac{1}{N} A_E A_I \; AC_{sc}^{X}(T). \tag{3.32}$$

where $\gamma_I \equiv \frac{N}{N_I}$ and the superscripts indicate the populations the neurons belong to (see *Methods* section for more details) and $AC_{sc}^{\alpha}(T) = \int_{-T}^{T} a^{\alpha\,(0)}(\tau) \frac{T-|\tau|}{T} \mathrm{d}\tau$ is the population-averaged auto-covariance of the spike-count in population α. The superscript (0) means that these magnitudes should be evaluated at order 0 in the perturbative parameter $1/\sqrt{N}$. Auto-covariance functions $a^{\alpha\,(0)}(\tau)$ are $O(1)$ magnitudes, i.e. at leading order they do not depend on N (fig. 3.4). The constants A_α depend on the synaptic couplings and coincide with the ones that relate recurrent mean firing rates with the rate of the external neurons (balance conditions similar to the ones in van Vreeswijk and Sompolinsky, 1996, see Appendix 2-A in the previous chapter). Figs. 3.2d-g show the theoretical prediction in eqs. 3.28-3.32 (dashed lines) and the computation directly from the rastergrams (squares). The agreement between theory and simulations is good for biologically relevant values of N ($N = 32000$). The dashed lines in figs. 3.2d-g were calculated with the value of $AC_{sc}^{\alpha\,(0)}(T)$ calculated from the simulation for $N = 32000$ (dark green and orange dashed lines) or assuming the firing statistics of recurrent neurons is Poisson-like, i.e, $AC_{sc}^{\alpha\,(0)}(T) = \nu^\alpha$ (light green and red dashed lines). This last approximation is justified because spike train auto-covariance function almost do not present any kind of structure apart from the peak at $\tau = 0$, which translates into flat auto-spectra (fig. 3.4a).

The population-averaged zero-lag cross-covariances of membrane potentials and their cross-correlation coefficients also decay as $\sim O(1/N)$ (figs. 3.2j,k). The membrane potential cross-correlation coefficients of cells whose spiking mechanism has been deactivated (fig. 3.2k, green symbols) scale in a similar way to those of neurons in which it was active (fig. 3.2k, black symbols). Fig. 3.2h shows the scaling of the population-averaged pre-synaptic current components and total current zero-lag cross-covariances. Theory predicts that the zero-lag cross-covariances of current components saturate to finite values for large N, while total current zero-lag cross-covariance should decrease as a negative power of $\sqrt{N}$. We see that the last one converges to a behavior compatible

with a $O(1/\sqrt{N})$ scaling, while the zero-lag cross-covariances of current components decay more slowly suggesting that the asymptotic limit is close to be reached. Cross-correlation coefficients of current components (fig. 3.2i) are already very close to their asymptotic values, while the total current cross-correlation coefficient decays also as $\sim O(1/\sqrt{N})$.

We additionally studied the population-averaged cross-covariance functions of spike trains, total currents and membrane potentials (figs. 3.3a-c). Qualitatively, one can see how these functions become flatter as the network gets larger. The temporal structure also changes as networks become larger and correlations become concentrated at shorter time-scales.

As we have previously mentioned the functions $a^{\alpha}(\tau)(\alpha = E, I)$ have almost no structure apart from the peak at $\tau = 0$. The progressive narrowing of the spike train cross-covariance functions (figs.3.3a-c) should be understood as part of the convergence to the asymptotic state defined by eqs. 3.22-3.26. In the frequency domain, one can see that for finite values of N the prediction is accurate for low frequencies, while a peak appears for higher values of ω (figs. 3.4b-d), reflecting the oscillatory character of the cross-covariance functions. This peak moves to higher frequencies as the network size increases in such a way that in the limit $N \to \infty$ the maximum discrepancy between theoretical and simulated values occurs for a frequency $\omega_c \to \infty$. At this point it should be reminded that eqs. 3.22-3.26 were derived in the case $N \to \infty$. In practice, one deals with networks of big but finite size. In section 3.4 we see how this narrowing is achieved and how the oscillatory character of the cross-covariance functions can be predicted assuming an approximation for the linear response kernel.

The fact that even for finite values of N low frequencies are well predicted has important consequences. It allows us to accurately predict magnitudes that require the computation of the integral of the cross-covariance functions $r^{\alpha\alpha'}(\tau)$ for all τ, such as, for example, the spike-count cross-covariance defined in large time windows.

For the total current and membrane potential cross-covariance functions, the value of the peak is the zero-lag cross-covariance and decreases in all the cases. In the next section we show that the fact that the characteristic time constant depends on N is important to understand the self-consistency of the decorrelation process.

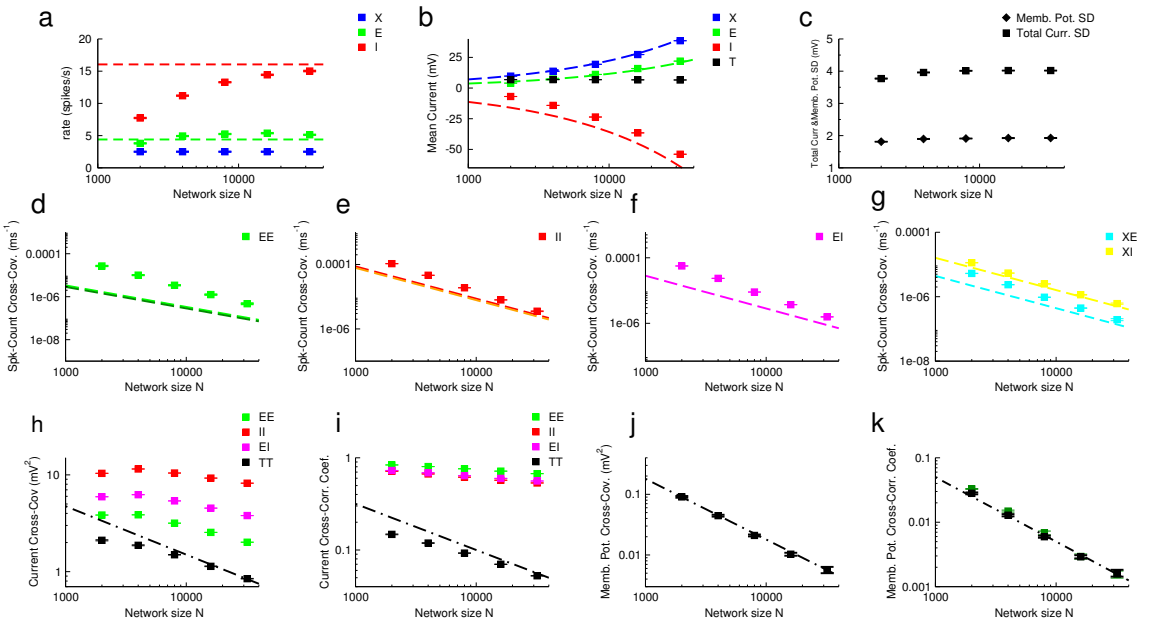

Figure 3.2: **Scaling of relevant magnitudes.** **a)** Population-averaged mean firing rates for different network sizes. Squares represent the values obtained in the simulation while dashed lines correspond to the asymptotic limits derived in Appendix 2-A. Color code: green, excitatory neurons; red, inhibitory neurons; blue, external neurons. **b)** Population-averaged mean currents afferent to excitatory neurons. The same code as before is used for identifying pre-synaptic current components with the addition of black referring to the total pre-synaptic currents. Dashed line corresponds to the theoretical values derived in Appendix 2-A. **c)** Population-averaged standard deviation of the membrane potential of excitatory neurons and of their total afferent current. **d)-g)** Population-averaged cross-covariances of the spike-count of pair of neurons ($T = 80$ ms) for different neuron pair types. Dashed lines correspond to the theoretical prediction in eqs. 3.28-3.32. In the case of figures **d)** and **g)** the value of $AC_{sc}^{\alpha\ (0)}(T)$ was numerically computed from the simulation of the largest network ($N = 32000$) (dark green and orange, respectively) or assuming that recurrent neurons are Poisson-like with a firing rate given by the theoretical values obtained in Appendix 2-A (light green and red). We show the results for $T = 80$ ms but a similar agreement between the prediction and the simulation can be found for all $T > 20$ ms (see Appendix 3-G). **d)** Excitatory-excitatory pairs (cyan) and external-inhibitory pairs (yellow). **e)** Inhibitory-inhibitory pairs. **f)** Excitatory-inhibitory pairs. **g)** External-excitatory pairs (cyan) and external-inhibitory pairs (yellow). **h)** Absolute value of the population-averaged zero-lag cross-covariances between the current components and between the total currents afferent to a pair of excitatory neurons. Dash-dotted black line corresponds to a $O(1/\sqrt{N})$ scaling. The same code as in panels d-g is used for identifying pre-synaptic current components with the addition of black to refer to the cross-correlation between total pre-synaptic currents. **i)** Absolute value of the population-averaged cross-correlation coefficients between the current components and between the total currents afferent to a pair of excitatory neurons. Same color convention as in panel h. **j)** Population-averaged zero-lag cross-covariances of the membrane potential of pairs of excitatory cells. Dash-dotted line corresponds to a $O(1/N)$ scaling. **k)** Population-averaged cross-correlation coefficients of the membrane potential of pairs of excitatory cells (black squares). Green squares correspond to neurons in which the membrane potential is never reset. Dash-dotted line corresponds to a $O(1/N)$ scaling.

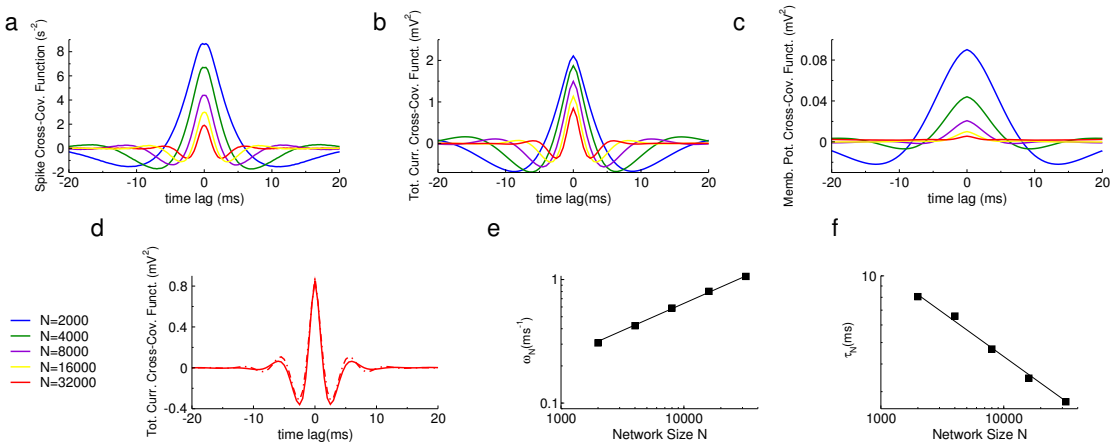

Figure 3.3: **Cross-covariance functions.** **a)** Population-averaged cross-covariance functions of spike trains. **b)** Population-averaged cross-covariance function of the total currents reaching excitatory neurons. **c)** Population-averaged cross-covariance functions of membrane potentials of excitatory cells. Colors represent different network sizes with the following convention, blue: $N = 2000$, green: $N = 4000$, violet: $N = 8000$, yellow: $N = 16000$, red: $N = 32000$. **d)** Population-averaged cross-covariance functions of the total currents reaching an excitatory neuron (solid line) and its fit to eq. 3.33 (dash-dotted line) ($N = 32000$). **e)** Scaling of the parameter ω_N in eq. 3.33 with N. Values of ω_N (black squares) were calculated by fitting the total current cross-covariance functions to eq. 3.33 with a least squares method. Solid line corresponds to a function $\sim N^{0.44}$ also obtained by a least squares adjustment of the previously calculated values of ω_N. **f)** Same as in **e)** but for the parameter τ_N in eq. 3.33. Solid line corresponds to a function $\sim N^{0.45}$

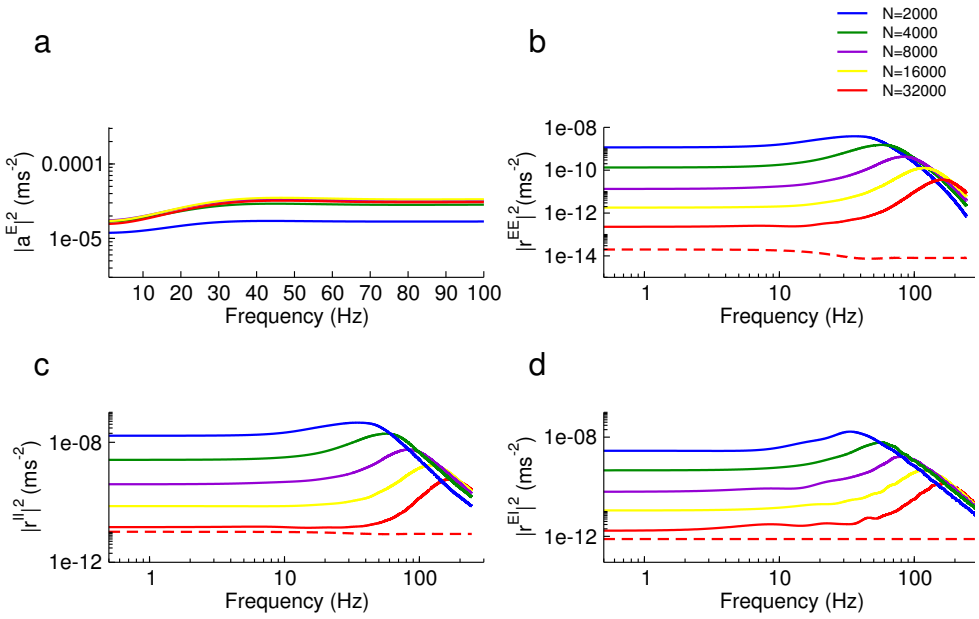

Figure 3.4: **Spectral analysis a)** $|\tilde{a}(\omega)^E|^2$. **b)** $|\tilde{r}^{EE}(\omega)|^2$. **c)** $|\tilde{r}^{II}(\omega)|^2$. **d)** $|\tilde{r}^{EI}(\omega)|^2$. Solid lines represent the results from the simulation. Color: blue: $N = 2000$, green: $N = 4000$, violet: $N = 8000$, yellow: $N = 16000$, red: $N = 32000$. Dashed lines correspond to the theoretical predictions for the largest value of N, calculated from eqs. 3.63-3.65 using a numerical evaluation of $a^\alpha(\omega)$.

3.3.3 Explaining the different steps of the decorrelation

To understand *qualitatively* how the different steps of the decorrelation process are related, we now look more carefully at the results in fig. 3.2. Starting from an asynchronous state characterized by spike-count cross-correlations behaving as $O(1/N)$ (eqs. 3.28-3.32), we will explain the scaling of total current and membrane potential zero-lag cross-covariances obtained with simulations and their consistency with the asynchronous state. More precisely, we first show how $O(1/N)$ decorrelated spike trains give rise to non-vanishing zero-lag cross-covariances for the various components of pre-synaptic currents. Secondly, we relate the predicted $O(1/\sqrt{N})$ decorrelated total currents to the $O(1/N)$ decorrelated membrane potentials. Finally, we close the loop by linking membrane potential and spike-count cross-correlation coefficients.

Let us start by relating the different scalings of spike-count and current zero-lag cross-covariances. In order to obtain the zero-lag cross-covariances of the total current one needs to calculate the product of filtered pre-synaptic spike trains. These are weighted by a $O(1/\sqrt{N})$ synaptic coupling. Besides, the computation also requires summing over all the pre-synaptic spike train pairs, $O(N^2)$. These facts, together with the scaling of spike-count cross-covariances ($O(1/N)$) could make us expect that current cross-covariances are $O(1)$. In Appendix 3-A4 we show that this is actually the case for the current components zero-lag cross-covariances. However, for the total current cross-covariance function a cancellation at $O(1)$ occurs, due to the different signs of the synaptic couplings in agreement with fig. 3.2h. Current cross-correlation coefficients are also predicted to scale in the same way (fig. 3.2i).

We study now the transmission of cross-correlations from input currents to membrane potentials. Population-averaged zero-lag cross-covariances of membrane potentials scale as $O(1/N)$ (fig. 3.2j). How can one understand that membrane potential and total current zero-lag cross-covariances scale differently? In Appendix 3-B we show that the membrane potential zero-lag cross-covariances can be evaluated as a convolution of the current cross-covariance functions with a kernel whose characteristic time is the membrane time constant. This indicates that the shape of the total current cross-covariance functions, and not just its peak value, determines the scaling behavior of voltage zero-lag cross-covariances. Fig. 3.3d shows the population-averaged total current cross-covariance function for pairs of excitatory neurons ($N = 32000$) and its fit to a damped oscillation. For different values of N, the population-averaged total current cross-covariance function can be well fitted by a damped oscillation:

$$c^{EE}(\tau) \;=\; A_N e^{-\frac{|\tau|}{\tau_N}} cos(\omega_N \tau). \tag{3.33}$$

Let us analyze in detail the behavior of the parameters A_N, ω_N and τ_N with network size. The amplitude, A_N, is the value at the peak of the cross-covariance functions at $\tau = 0$ ms. This is our definition of the zero-lag cross-covariance for continuous magnitudes, and is represented in fig. 3.2b (black symbols). The other two parameters can be evaluated by means of a least squares fit of the current cross-covariance functions, with the parameterization in eq. 3.33. The dependence with network size of ω_N and τ_N is shown in figs. 3.3e,f. Regression curves yield the behavior $\omega_N \sim N^{\gamma}$ and $\tau_N \sim N^{\zeta}$, with $\gamma = 0.45$ and $\zeta =$ -0.44.

The scaling with N of the three parameters, A_N, τ_N and ω_N, can be used to predict the scaling of the membrane potential zero-lag cross-covariances (see Appendix 3-B):

$$CC_V^{EE} \;=\; [c_{V,\,ij}^{EE}(0)] \propto A_N \frac{\tau_m + \tau_N}{\tau_m^2 \tau_N \omega_N^2} \left(1 + \left(\frac{\tau_m + \tau_N}{\omega_N \tau_N \tau_m}\right)^2\right)^{-1}. \tag{3.34}$$

Assuming $A_N \sim O(1/\sqrt{N})$ and using the previously found network size behavior of ω_N and τ_N, we obtain $CC_V \sim O(A_N \omega_N \tau_N^2) = O(N^{-(\frac{1}{2}+\zeta+2\gamma)})$ in good agreement with the $O(1/N)$ scaling of the population-averaged cross-covariances of membrane potentials obtained in the numerical simulation (fig. 3.2j). Notice that the product $\omega_N(\tau_N)^2$ has units of time. It determines a fast time-scale ($O(1/\sqrt{N})$). This parameterization sheds some light on the different scaling of current components and membrane potential zero-lag cross-covariances. It predicts that membrane potential zero-lag cross-covariances decay as $O(1/N)$ due the combined effect of the fast ($O(1/\sqrt{N})$ and small amplitude ($O(1/\sqrt{N})$) scaling of the total current cross-covariance function. The emergence of fast time-scales in *densely* connected networks of *strongly* coupled neurons has been pointed out previously in binary neurons [Renart et al., 2010] and in rate models [Bernacchia and Wang, 2013]. At this point of the discussion we have empirically observed the emergence of this fast time-scale. In section 3.4 we analytically study it. In Appendix 3-F we show that such a time-scale does not appear for different scaling of the parameters.

To close the loop we need to relate membrane potential and spike-count cross-correlations. It is worth pointing out that the theory explained in Appendix 3-A allows us to describe the neurons' activities in terms of their afferent currents, and write self-consistent

equations for spike train cross-covariance functions. Membrane potential, thus, is not a fundamental variable in the mathematical description presented in Appendix 3-A, but we consider that it is worth explaining qualitatively this issue. A simple analysis using a statistical model for the joint distribution of the voltages of pairs of neurons [Dorn and Ringach, 2003] (see Appendix 3-C) shows that the scaling of cross-correlation coefficients of the membrane potential is the same as the one of spike-count cross-correlation coefficients.

To summarize, we have qualitatively explained the decorrelation process in three different stages. First, we have seen that $O(1/N)$ correlated firing activity gives rise to highly correlated current components, due to the large amount of common input. Second, these correlations cancel each other in such a way that the total currents afferent to a pair of neurons are $O(1/\sqrt{N})$ correlated. Cell's membranes contribute to decorrelate these currents by means of the integration of the temporal structure of input correlations. Finally, a statistical model relates membrane potential and spike-count cross-correlations in a linear way.

3.3.4 Tracking of excitatory activity by inhibitory cells

In the last sections we have shown the scaling of the cross-correlations of different magnitudes and have explained qualitatively how they are related. Notice however that we did not answer to the question about which mechanism allows the neurons to fire in an asynchronous way. In simpler models with binary neurons, the absence of correlated activity is dynamically achieved by means of very fast tracking of excitatory activity by the inhibitory one [Renart et al., 2010]. As we have explicitly shown in the previous chapter, this is actually a general result that holds whatever the neuron model is. We have shown that in the limit $N \to \infty$ the instantaneous population rates of recurrent neurons in each population track each other and the external firing rate:

$$\nu^E(t) = A_E \nu^X(t) \tag{3.35}$$

$$\nu^I(t) = A_I \nu^X(t). \tag{3.36}$$

where the constants A_α depend on the synaptic couplings and are the same as the ones that relate mean firing rates in the balanced regime [van Vreeswijk and Sompolinsky, 1996].

A numerical and qualitative study of the tracking phenomenon is presented here. We have looked at the population-averaged cross-covariance function between the excitatory and inhibitory current components afferent to a given cell pair. Fig. 4.5a shows these functions for different network sizes. All of them exhibit a peak located at a positive time lag, indicating that inhibitory currents are delayed with respect to the excitatory component. This delay becomes shorter for larger networks. To quantify this phenomenon, we have fitted these functions close to their maximum (-3 ms$< \tau <$3 ms)to:

$$c^{EE}_{\mathcal{I};EI} = -A'_N(\tau - \tau^0_N)^2. \tag{3.37}$$

where τ^0_N represents the value at which the cross-covariance function of a network of size N reaches its peak. This parameter behaves as $\sim O(1/\sqrt{N})$ (a least squares fit for $c^{EE}_{\mathcal{I};EI}$ gives $\tau^0_N \sim O(N^{-0.45})$)(fig. 4.5b) confirming that tracking takes place in a similar time-scale as the one found before. Temporal traces of the current components show, in a more qualitative way, that tracking occurs, and that it improves as the number of neurons increases (fig. 4.5d,e).

Fig. 4.5c presents an indirect evidence of tracking of excitation by inhibitory activity being the mechanism responsible for decorrelation. Our hypothesis is that if this tracking decorrelates the network activity, the decorrelation process has to take time to occur, due to the fact that at finite value of N, the tracking is not instantaneous. To test this hypothesis, we have measured the spike-count cross-correlation coefficients in different time windows and for different values of the connection probability for a network of size $N = 8000$ neurons. As it is shown in fig. The spike-count cross-correlation coefficients measured in windows of $T = 0.25$ ms grow with p (fig. 4.5c, black squares), suggesting that the number of common inputs is relevant. For larger time windows, $T = 2$ ms (blue squares), the decorrelation mechanism has already taken place and the degree of correlation in the spike-count is not dependent on p, except for values very close to $p = 1.0$ (not shown).

3.3.5 Distribution of spike-count cross-covariances and cross-correlation coefficients

It has been experimentally reported that, although the spike-count cross-correlations can be small on average, their distribution is wide, both in spontaneous activity states

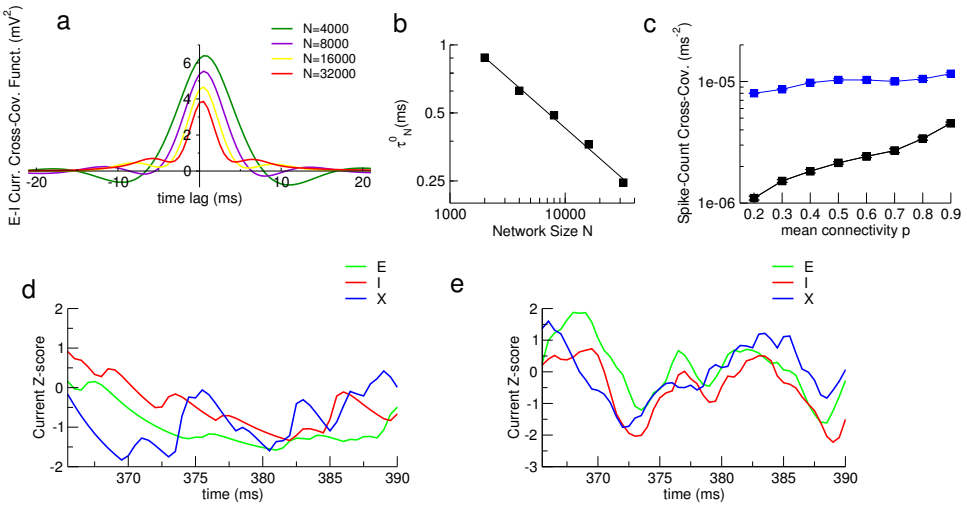

Figure 3.5: **Tracking of excitatory currents by inhibition.** **a)** Population-averaged cross-covariance functions of excitatory and inhibitory currents afferent to a pair of excitatory neurons. **b)**. τ_N^0 as a function of the number of neurons N. Values of τ_N^0 (black squares) were calculated by fitting the total current cross-covariance functions to eq. 3.37 with a least squares method. Solid line corresponds to a function $\sim N^{0.45}$ also obtained by a least squares adjustement of the previously calculated values of τ_N^0. **c)** Spike-count cross-correlation coefficients of excitatory-excitatory pairs. Black squares were calculated with $T = 2$ ms and blue squares with $T = 0.25$ ms. **d), e)** Temporal traces of external (blue), excitatory (green) and inhibitory (red) current components for a network with $N = 4000$ (**d**) and $N = 32000$ (**e**) neurons.

[Renart et al., 2010] and in animals receiving stimulus [Miura et al., 2012]. As we showed in Appendix 2-D, our theory predicts that the scaling of the standard deviations of the spike-count cross-covariances is larger than its average ($O(1/\sqrt{N})$ vs $O(1/N)$).

In fig. 3.6 we illustrate this fact by showing the distribution of pairwise spike-count cross-correlation coefficients for the largest simulated network $N = 32000$.

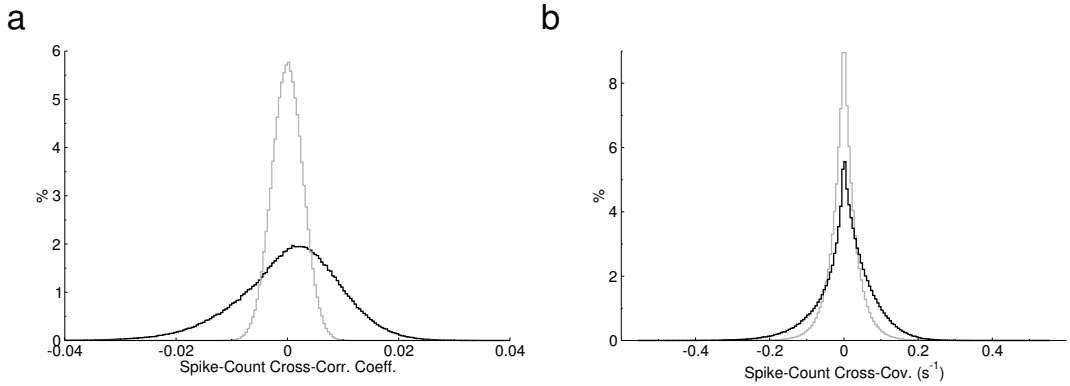

Figure 3.6: **Spike-count correlation coefficients and cross-covariances distributions. a)** Distribution of the spike-count correlation coefficients of EE pairs (black) and that of jittered spike trains (grey, jitter time is ±500 ms) ($T = 80$ ms, $N = 32000$). **b)** Distribution of the spike-count cross-covariances of EE pairs (black) and that of jittered spike trains (grey, jitter time is ±500 ms) ($T = 80$ ms, $N = 32000$)

3.4 Finite-size solution

In the previous sections we have described the asymptotic limit $N \to \infty$. As we pointed out, spike train cross-covariance functions tend to eqs. 3.22-3.26. However, it is obvious from fig. 3.4 that this solution was only accurate for low frequencies. As we have previously said, as N increases the range of frequencies for which the leading order solution is accurate also does. In this section we focus on how this asymptotic limit is achieved. In Appendix 3-A6 we derive the finite-size solution of eqs. 3.20-3.21. In order to calculate it analytically, an assumption about the shape of the linear response kernel must be made. We employ the approximation of the dominant time-scale. Basically, we approximate the product $\tilde{R}(\omega)\tilde{\jmath}_{syn}(\omega)$ by:

$$\tilde{R}^{\alpha}(\omega)\tilde{\jmath}_{syn}(\omega) \simeq \frac{k^{\alpha}}{\bar{\tau}_{\alpha}^{-1} + i\omega} \tag{3.38}$$

This approximation is similar to the one in Ostojic et al., 2009 [1]. We assume that we are in a parameter region in which no resonance for the function $\tilde{R}^{\alpha}(\omega)\tilde{j}_{syn}(\omega)$ appears, i.e., $\tau_{k,\alpha}$ is real. As explained, in Ostojic et al., 2009 this is the case provided that the synaptic noise is large enough. Notice that the approximation in eq. 3.38 reads as $(R^{\alpha} * j_{syn})(\tau) = \Theta(\tau)k^{\alpha}e^{-\frac{\tau}{\bar{\tau}_{\alpha}}}$ in the time domain. Besides, we assume that the auto-covariance functions of the recurrent neurons do not have any structure but the delta peak at $\tau = 0$. This is just an approximation, but as we have seen before, some results were well predicted only by assuming this (see, for example, fig. 3.2). One can then solve the systems of eqs. 3.20-3.21 (see details in Appendix 3-A6). Spike train cross-covariance functions are:

$$r^{XE}(\tau) = \Theta(\tau)\Gamma^{E}\nu^{X}k^{E}p\frac{j^{EX}}{\sqrt{N}}e^{-(v\sqrt{N})\tau}\cos(w\sqrt{N}\tau + \phi^{E}) \tag{3.39}$$

$$r^{XI}(\tau) = \Theta(\tau)\Gamma^{I}\nu^{X}k^{I}p\frac{j^{IX}}{\sqrt{N}}e^{-(v\sqrt{N})\tau}\cos(w\sqrt{N}\tau + \phi^{I}) \tag{3.40}$$

$$\begin{aligned} r^{EE}(\tau) = {} & k^{E}p\Gamma^{E}\Big(\nu^{E}\frac{j^{EE}}{\sqrt{N}}\cos(w\sqrt{N}|\tau| + \phi^{E}) + \frac{\Gamma^{E}}{\sqrt{N}}\nu^{X}j^{EX}\bar{j}^{EX}k^{E}p(\Upsilon\cos(w\sqrt{N}|\tau| + 2\phi^{E} + \Phi) + \frac{1}{4v}\cos(w\sqrt{N}|\tau|))\Big) \\ & \times \; e^{-v\sqrt{N}|\tau|} \end{aligned} \tag{3.41}$$

$$\begin{aligned} r^{II}(\tau) = {} & k^{I}p\Gamma^{I}\Big(\nu^{I}\frac{j^{II}}{\sqrt{N}}\cos(w\sqrt{N}|\tau| + \phi^{I}) + \frac{\Gamma^{I}}{\sqrt{N}}\nu^{X}j^{IX}\bar{j}^{IX}k^{I}p(\Upsilon\cos(w\sqrt{N}|\tau| + 2\phi^{I} + \Phi) + \frac{1}{4v}\cos(w\sqrt{N}|\tau|))\Big) \\ & \times \; e^{-v\sqrt{N}|\tau|} \end{aligned} \tag{3.42}$$

$$r^{IE}(\tau) = \begin{cases} k^{I}p\Gamma^{I}\Big(\nu^{E}\frac{j^{IE}}{\sqrt{N}}\cos(-w\sqrt{N}\tau + \phi^{I}) \\ \quad + \frac{\Gamma^{E}}{\sqrt{N}}\nu^{X}j^{EX}\bar{j}^{IX}k^{E}p(\Upsilon\cos(-w\sqrt{N}\tau + \phi^{I} + \phi^{E} + \Phi) + \frac{1}{4v}\cos(-w\sqrt{N}\tau + \phi^{I} - \phi^{E}))\Big) \times \quad e^{v\sqrt{N}\tau}, \quad \tau \leq 0 \\ k^{E}p\Gamma^{E}\Big(\nu^{I}\frac{j^{EI}}{\sqrt{N}}\cos(w\sqrt{N}\tau + \phi^{E}) \\ \quad + \frac{\Gamma^{I}}{\sqrt{N}}\nu^{X}j^{IX}\bar{j}^{EX}k^{I}p(\Upsilon\cos(w\sqrt{N}\tau + \phi^{I} + \phi^{E} + \Phi) + \frac{1}{4v}\cos(w\sqrt{N}\tau + \phi^{E} - \phi^{I}))\Big) \times \quad e^{-v\sqrt{N})\tau}, \quad \tau > 0 \end{cases} \tag{3.43}$$

where the constants $\Gamma^{\alpha}, \phi^{\alpha}, \Upsilon, \Phi, v$ and w depend on k_{α} and $\bar{\tau}_{\alpha}$ (see expressions in Appendix 3-A6). The damping characteristic time and the frequency of the oscillation are predicted to be $O(1/\sqrt{N})$ and $O(\sqrt{N})$ respectively.

Least squares fits of the spike train cross-covariance functions calculated from the rastergrams (fig.3.7, solid line, see details of the fit in the caption) to the shape given by the theoretical prediction (fig.3.7, black dot-dashed lines) show that the scaling of

[1] In Ostojic et al., 2009 the function $\tilde{R}^{\alpha}(\omega)$ (instead of $\tilde{R}^{\alpha}(\omega)\tilde{j}_{syn}(\omega)$) is approximated by a function of the form given by the right hand side of eq. 3.38. This approximation consists in keeping only the first term of the Laurent series of $\tilde{R}^{\alpha}(\omega)$. In our case, we keep the first term of the Laurent series of the function $\tilde{R}^{\alpha}(\omega)\tilde{j}_{syn}(\omega)$

frequency and damping characteristic time constant are well predicted (figs. 3.7f-g). Notice that the final result of all our calculations depend on the magnitudes k^α and $\bar{\tau}^\alpha$. In a network where the in-degree of all neurons is the same and the synaptic couplings do not depend on the particular neuron but are the same for all the neurons in a given population, these magnitudes can be computed from only one neuron in each population. To estimate $\tilde{R}^\alpha(\omega)\tilde{\jmath}_{syn}(\omega)$ numerically for a given value of ω one can apply a sinusoidal perturbation with the same frequency to one neuron, convolve it with $j_{syn}(t)$ and compute how this perturbation modifies its firing rate. One repeats this for different frequencies and gets an estimate of the function $\tilde{R}^\alpha(\omega)\tilde{\jmath}_{syn}(\omega)$. In our case, the in-degree of the neurons is not the same and the synaptic couplings follow a random distribution. This makes the computation technically more difficult. Besides, the amount of data required for a good estimate of $\tilde{R}^\alpha(\omega)\tilde{\jmath}_{syn}(\omega)$ requires long simulation times. In Appendix 3-D we estimate the function $\tilde{R}^\alpha(\omega)\tilde{\jmath}_{syn}(\omega)$ computing the response to a small perturbation of a set of neurons receiving Poisson inputs with firing rates corresponding to the ones in the network (fig. 3.2). We then approximate the function computed in this way to eq. 3.38 and obtained an estimate of k^α and $\bar{\tau}^\alpha$. Red dashed lines in fig. 3.7 correspond to the computation of the spike train cross-covariance functions using these values of k^α and $\bar{\tau}^\alpha$. The damping time constant and the frequency are well predicted in all the cases. The theoretical amplitudes are also similar to the expected ones, although in some cases they are overestimated (especially for $r^{II}(\tau)$ and, to a lesser extent, $r^{EI}(\tau)$).

3.5 Which are the most relevant parameters for decorrelation?

We now analyze how changes in parameter values affect the decorrelation observed in the network studied above. Our aim is twofold: on one hand, we intend to show that decorrelation occurs in a reasonably wide region of the parameter space. On the other hand, by finding limits on the region in parameter space where the network stays in the asynchronous state, we expect to detect the determinant factors of the observed decorrelation. Although an exhaustive study of the parameter space is rather difficult and outside the scope of this work, we study those parameters that *a priori* seem to be more critical for the behavior of the model: connection probability, synaptic time constants and synaptic delay distributions. We proceed by varying their values and observing the effect on the network dynamics.

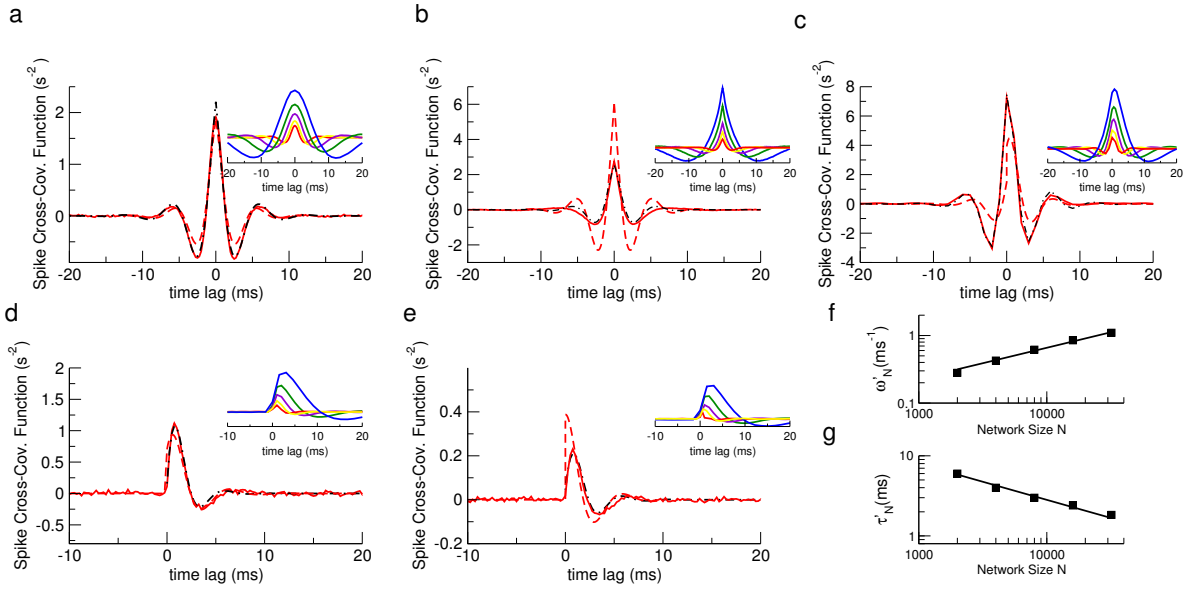

Figure 3.7: **Spike train cross-covariance functions** Population averaged cross-covariance functions of the spike train for different type of pairs of neurons ($N = 32000$). **a)** EE pairs. **b)** II pairs. **c)** EI pairs.**d)** XI pairs. **d)** XE pairs. Black dot-dashed lines correspond to least squares fit of the functions to eqs. 3.39-3.113. Red dashed lines are the cross-covariance functions computed using eqs. 3.39-3.113 with the parameters k^α and $\bar{\tau}^\alpha$ estimated in Appendix 3-D. Insets correspond to the cross-covariance functions for different network sizes. Same color code as in fig. 3.3a. **f)-g)** Scaling of the characteristic frequency (**f**) and damping time constant (**g**) of the function $r^{IX}(\tau)$. Squares correspond to the parameters ω'_N and τ'_N computed from a least square fit of $r^{XI}(\tau)$ to a function $r_N = \Theta(\tau)A'_N e^{-\frac{\tau}{\tau'_N}}\cos(\omega'_N\tau + \phi_N)$ for different values of N. Lines are the least squares fits of ω'_N (panel **f**) and τ'_N (panel **g**) to exponential functions ($\omega'_N \sim N^{0.46}$, $\tau'_N \sim N^{-0.45}$).

First, we have varied the connectivity parameter and repeated the analysis done above. The results for networks with $p = 0.3$ and $p = 0.4$ (fig. 3.8) are very similar to those obtained for $p = 0.2$ (fig. 3.2). We conclude that the decorrelation observed in the model is not a consequence of low connectivity.

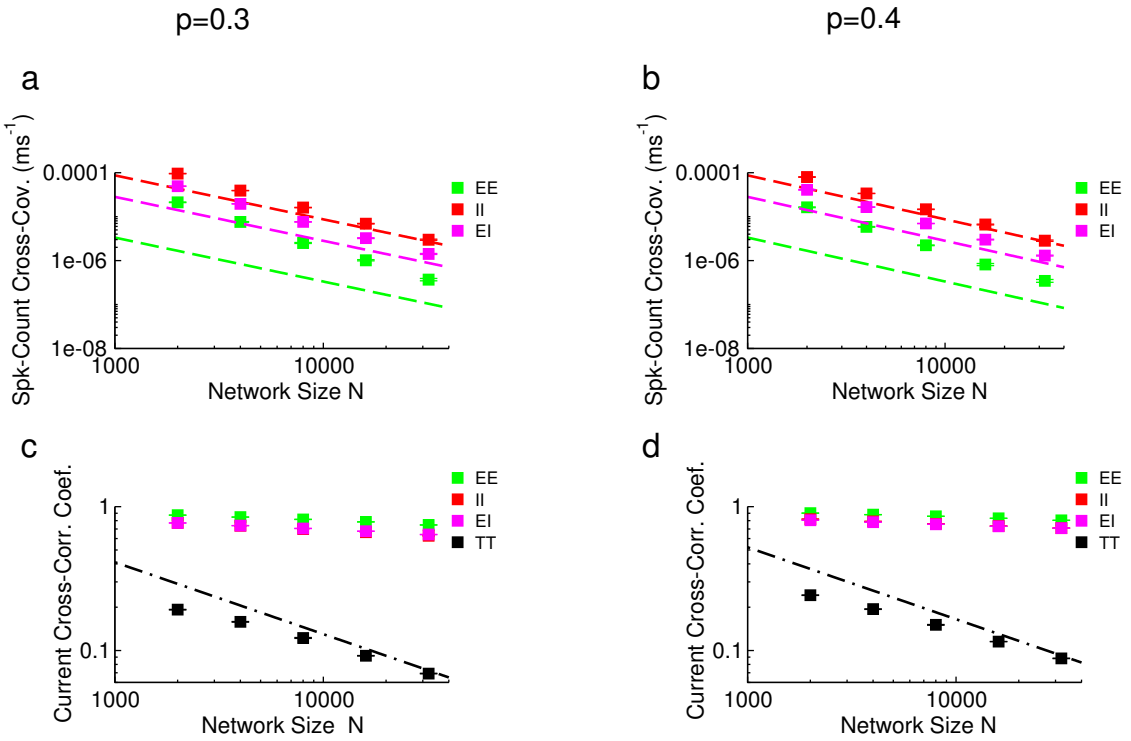

Figure 3.8: **Decorrelation for higher connection probability values. a), b)** Population-averaged cross-covariances of the spike-count of pair of neurons ($T = 80$ ms) for different neuron pair types for networks with $p = 0.3$ (**a**) and $p = 0.4$ (**b**). Dashed lines correspond to the theoretical limit in eqs. ($\sim O(1/N)$). **c), d)** Absolute value of the population-averaged cross-correlation coefficients between the current components and between the total currents afferent to a pair of excitatory neurons. Dashed black line corresponds to a $O(1/\sqrt{N})$ scaling. Same color conventions as in figure 3.2. Cross-correlation coefficients of excitatory-inhibitory current components (magenta squares) were originally negative.

Second, we studied the role of synaptic delays. As shown in section 3.3.4, the model has a fast tracking mechanism, which improves with network size. However, synaptic delays impose a limit in the way this tracking is achieved and, thus, could make the development of an asynchronous state difficult. To test this, we have simulated networks

with synaptic delays. We first study the case in which synaptic delays were taken from uniform distributions between 0.1 and 0.5 ms (figs. 3.9a,c). For the simulated values of N, spike-count cross-covariances show the expected scaling. The cancellation of the zero-lag current cross-covariances is not so pronounced as before, but the values remain smaller than the currents components cross-covariances. We have also studied the case in which the synaptic delays are higher and take the same value (0.8 ms) for all the synapses (figs. 3.9b,d). Although a certain degree of decorrelation is present for small values of N the high value of the synaptic delays do not allow the required precise tracking for large values of N and the network eventually reaches a highly correlated state that results in strong oscillations (fig. 3.9b, inset). The role of the delay in inhibition in generating network oscillations has been previously studied [Lindner et al., 2005].

These results reinforce the idea that tracking is a *necessary* condition for decorrelation to take place. In the previous chapter we have analytically shown that for *densely* connected networks of *strongly* coupled neurons, tracking is also a *sufficient* condition.

We finish this parameter study by introducing more realistic values of synaptic filters and membrane potential time constants. Inhibitory synaptic filters are slower than excitatory ones [Smith et al., 2000], something that is often used in modeling work [Brunel and Wang, 2003, Mazzoni et al., 2008]. The membrane time constant of excitatory neurons is longer than the membrane time constant of inhibitory cells [McCormick et al., 1985], a fact also used often in modeling studies [Brunel and Wang, 2003, Mazzoni et al., 2008]. In fig. 3.10 we show the results obtained for synaptic decay time constants $\tau_d^E = 3.5$ ms (70% of its original value), $\tau_d^I = 5$ ms and membrane time constants $\tau_m^E = 22$ ms and $\tau_m^I = 9$ ms. Rastergram in fig. 3.10a shows that neurons fire in an independent way. We quantify the cross-correlation by measuring spike-count cross-covariances. Up to the largest simulated networks, we observe that they tend to similar asymptotic limits[2], in a way similar to those obtained for the network discussed in fig. 3.2. Total current cross-correlation coefficients (fig. 3.10c) do not decay for the largest networks. It should be remembered that cross-correlation coefficients were computed from the zero-lag cross-covariance function and thus do not take into account the fast characteristic time-scale previously mentioned. When taken into account, one finds that membrane potential cross-correlations decay as $1/N$ (fig. 3.10d).

[2]Dashed lines in fig. 3.10 were calculated via eqs. 3.29-3.32 with the values of A_α computed when synaptic filters of excitation and inhibitions are different (see Appendix 3-A)

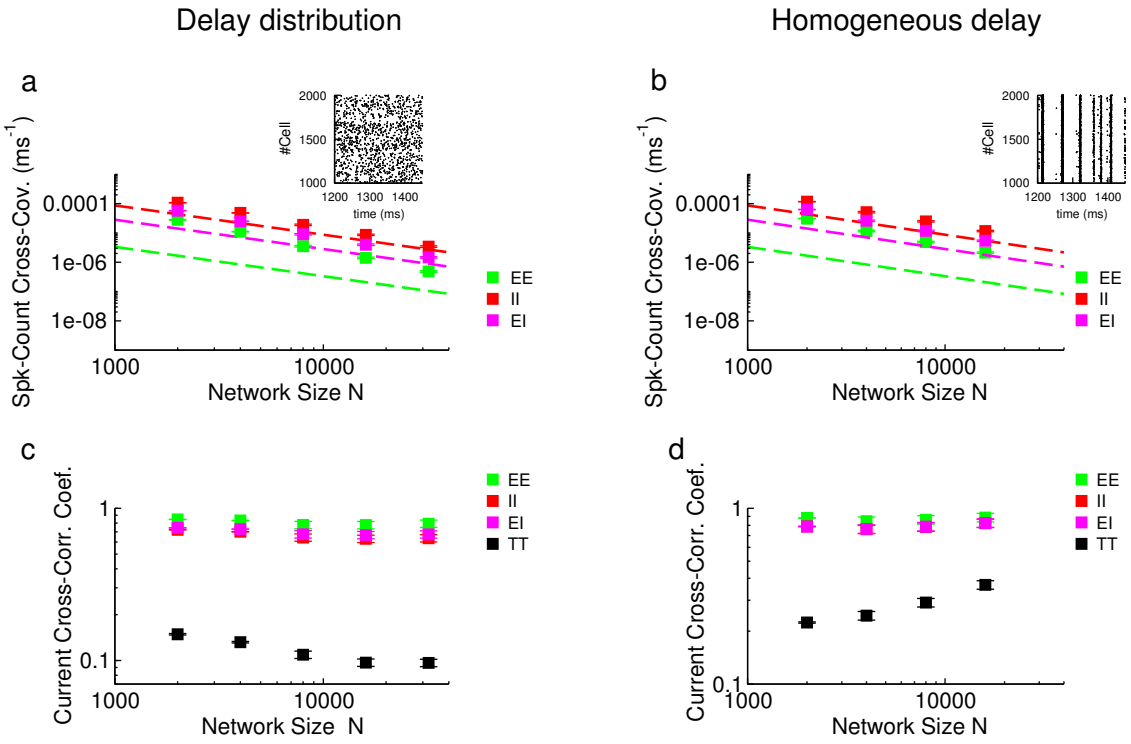

Figure 3.9: **Effect of synaptic delays**. **a)** Population-averaged cross-covariances of the spike-count of pair of neurons ($T = 80$ ms) for different neuron pair types for networks with a uniform distribution of synaptic delays (from 0.1 to 0.5 ms). Dashed lines correspond to the theoretical prediction in eqs. 3.28,3.29, 3.30 with the value of $AC^{\alpha\ (0)}(T)$ numerically computed from the simulation of the largest network ($N = 32000$) ($\sim O(1/N)$). Same color code as in 3.2. **b)** Same as in (a) but for a case where synaptic delays are the same for all the synapses (0.8 ms). Dashed lines were calculated from eqs. 3.28,3.29, 3.30 with the value of $AC^{\alpha\ (0)}(T)$ numerically computed from the simulation of $N = 16000$. Results for $N = 32000$ are not plotted. **b) Inset** Rastergram of 1000 excitatory cells ($N = 32000$). **c)** Absolute value of the population-averaged cross-correlation coefficients between the current components and between the total currents afferent to a pair of excitatory neurons in networks with uniform distribution of delays (from 0.1 to 0.5 ms). Same color conventions as in figure 3.2. Cross-correlation coefficients of excitatory-inhibitory current components (magenta squares) were originally negative. **d)** Same as before but for networks where synaptic delays are the same for all the synapses.

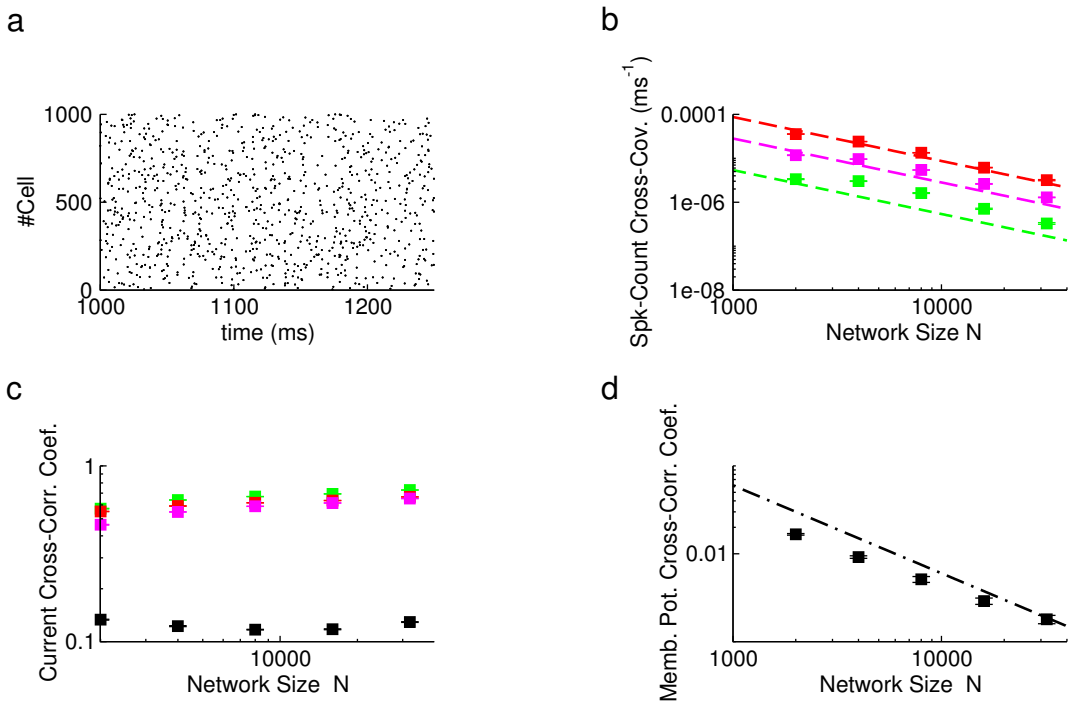

Figure 3.10: **Effect of different synaptic filters and membrane time constants**. Simulation of a network with synaptic delays, different synaptic time constants for excitatory and inhibitory synapses ($\tau_d^E = 3.5$ ms; $\tau_d^E = 5$ ms) and different membrane time constant for excitatory and inhibitory cells ($\tau_m^E = 22$ ms; $\tau_m^E = 9$ ms;). **a)** Rastergram of 1000 excitatory cells ($N = 32000$). **b)** Population-averaged cross-covariances of the spike-count of pair of neurons ($T = 80$ ms) . Dashed lines correspond to the theoretical prediction in eqs. 3.28-3.30 with the value of $AC^{\alpha\ (0)}(T)$ numerically computed from the simulation of the largest network ($N = 32000$) ($\sim O(1/N)$). Same color code as in 3.2. **c)** Absolute value of the population-averaged cross-correlation coefficients between the current components and between the total currents afferent to a pair of excitatory neurons. Same color conventions as in figure 3.2. Cross-correlation coefficients of excitatory-inhibitory current components (magenta squares) were originally negative. **d)** Population-averaged cross-correlation coefficients of membrane potentials of excitatory pairs of cells. Dashed line represents a $O(1/N)$ scaling.

In conclusion, the analysis of the effect of varying model parameters has revealed that time related parameters, such as synaptic delay distributions or synaptic time constants, have the largest impact on dynamic decorrelation and they impose limits to the region where the densely connected network stays in the asynchronous regime. We have shown that for realistic values of the parameters, the asynchronous state can be sustained. Interestingly, a larger connection probability does not disrupt the asynchronous regime, in spite of the larger interaction between neurons that it produces. Notice that biophysical models as the LIF are relevant for a study of time-related parameters, what is impossible to do in simpler models such as the one in Renart et al., 2010 with binary neurons, in which time-related parameters are defined in a rather artificial way.

3.6 Discussion

We have shown that asynchronous states are possible in balanced *densely* connected networks of *strongly* coupled LIF neurons. For the descriptional purpose, we separated the decorrelation process into three stages regarding the firing activity, synaptic currents and membrane potentials. By means of a self-consistent scheme we related these three different stages. We showed that the *components* of the synaptic currents (i.e. excitatory, inhibitory and external input) that arrive to a pair of neurons are highly correlated even if the firing activities of them are not. This is due to the large amount of inputs that neurons in the network share. Nevertheless, similarly to the case of binary neurons [Renart et al., 2010], *total* current cross-correlations are low. To see how these correlations are transmitted to the cell we have found that, not just the peak value of total current cross-correlations but the whole cross-covariance function determines the smaller cross-correlations of neuron's membrane potentials. Finally, a statistical model was proposed to explain the transfer of cross-correlation from membrane potentials to spike-counts.

The scaling defined in this work is the same as the one employed in Renart et al., 2010 for the study of binary networks and the results are compatible. In Ginzburg and Sompolinsky, 1994, *dense* networks ($p \sim O(1)$) of *weakly* connected ($J's \sim O(1/N)$) binary neurons were studied. In such case, the degree of correlation is small and depends exclusively on the values of the couplings: the stronger the couplings the stronger the correlations. Similar scaling can be found in Toyoizumi et al., 2008 for spiking neurons. However, it is easy to show that this scaling implies a vanishing recurrent input noise

in the limit $N \to \infty$. Besides, it cannot account for the experimentally found high values of current components cross-correlations [Renart et al., 2010, Graupner and Reyes, 2013].

One important conclusion of our work is that the activity of the excitatory neurons is tracked by the inhibitory ones. This *recurrent* mechanism was found to be the final cause of decorrelation in binary networks [Renart et al., 2010]. We reported that it is also the responsible for decorrelation in LIF networks. Our study suggests that if synapses have a short but finite delay in the transmission of spikes to inhibitory cells then there might exist a network size from which the decorrelation mechanism no longer works correctly. However, we have shown that for realistic network sizes and synaptic delay distributions our results are still valid. We have also shown that for typical values of synaptic and membrane potential time constants, decorrelated states are possible. This type of parameter study cannot be performed with binary neurons [Renart et al., 2010], where characteristic time constants are defined in a rather artificial way with no clear biophysical meaning.

Recent works have pointed out the role of inhibition in decorrelation. In Tetzlaff et al., 2012, inhibition was found to diminish the value of spike-count cross-covariances in finite size homogeneous networks of LIF neurons. As mentioned in previous chapters, the results for this kind of networks are qualitatively different (see Appendix 3-A5). We find that in *strongly* and *densely* connected heterogeneous networks tracking of excitatory fluctuations by the inhibition is a *necessary* and *sufficient* condition for decorrelation to take place (see previous chapter for more details).

In Bernacchia and Wang, 2013 the suppression of cross-correlations by recurrent inhibition was studied with a rate model. The scaling of parameters is the same as the one described here. They found that the peak of the rate cross-covariance function and its characteristic time constant behave as $O(1/\sqrt{N})$. Although rate models have proved to be useful, equations in those models are intrinsically phenomenological. Here, we have found similar results in more realistic and biophysically supported spiking networks. The fast time-scale appears as a consequence of the convergence to an asymptotic state in which spike-train cross-covariance functions are determined by the delta-shaped auto-covariance functions.

Apart from the already mentioned works, some efforts have been put recently on the study of cross-correlations in the LIF networks using the linear response approximation.

In Pernice et al., 2011, Trousdale et al., 2012 a method to compute cross-correlations is described. Such method is based on decomposing the networks into *motifs* and adding their contribution to the total cross-correlation. *Motifs* are described as subnetworks connecting two neurons through a number of intermediate neurons, that determine the order of the motif. This theory can be useful to compute cross-correlations for more complex architectures. Computations in these works were done assuming the synaptic coupling are $O(1/N)$, i.e, $J = \frac{j}{N}$, with $j \sim O(1)$. The theory works very well for small values of the j's although the accuracy is small for high values of the j's [Trousdale et al., 2012]. The contribution of inhibition to decorrelate the network is also pointed out. Notice that, as we mentioned above, the scaling of the synaptic couplings employed cannot explain the high values of cross-correlation between current components if one assumes *dense* connectivity.

Experimental studies have pointed out that inhibitory currents follow excitatory ones with delays in the order of some milliseconds [Pouille and Scanziani, 2001, Wehr and Zador, 2003, Gabernet et al., 2005]. This tracking has been revealed to be a good mechanism for the neurons to operate as coincidence detectors [Pouille and Scanziani, 2001, Wehr and Zador, 2003] and to sharpen tuning to specific stimuli [Cafaro and Rieke, 2010]. Here we suggest that the observed tracking is a fundamental part of the decorrelation process in natural neural networks.

Appendix 3-A. Cross-correlations self-consistent theory

In this appendix we show analytically the cancellation of cross-correlations of neurons' activities in networks of LIF neurons with fast synaptic filters. The scheme of the demonstration is based on the one presented in Renart et al., 2010. We first assume that the network is asynchronous in the steady states. With this assumption, we will develop equations to obtain self-consistent expressions for the population-averaged spike train cross-covariance functions. After this, we will show that there are solutions to these equations in which the network is indeed asynchronous.

As an approximation to the response of one neuron to a synaptic current we will adopt the linear response approach [Brunel and Hakim, 1999, Lindner and Schimansky-Geier, 2001, Lindner et al., 2005]. Such a framework describes the response of a neuron to a small current when the neuron is receiving noise[3]. The state of the neuron when receiving only noise can be considered the non-perturbed state and the response to the small current a perturbation. In the next section we will characterize both the non-perturbed state and the perturbation in a recurrent network by means of a study of the synaptic currents. Later we will derive self-consistent equations for the cross-covariance functions and solve them using a perturbative technique.

3-A1. Characterizing input currents in terms of neuronal activity

We first study the statistics of the synaptic currents in the network. Let $I_i^\alpha(t)$ be the total current that reaches neuron (i,α):

$$\begin{aligned} I_i^\alpha(t) &= \sum_{(j,\beta)} m_{ij}^{\alpha\beta} J_{ij}^{\alpha\beta} s_j^\beta(t) = \\ &= \sum_{(j,\beta)} m_{ij}^{\alpha\beta} J_{ij}^{\alpha\beta} (j_{syn} * y_j^\beta)(t) \end{aligned} \tag{3.44}$$

where $m_{ij}^{\alpha\beta}$ is the connectivity matrix and we have assumed that the synaptic filter $j_{syn}(t)$ is identical for all the neurons. The current temporal average value is:

[3]Linear response kernel for white noise has been analytically calculated in Brunel and Hakim, 1999, Lindner and Schimansky-Geier, 2001 while white noise filtered by fast synapses was calculated in Fourcaud and Brunel, 2002

$$< I_i^\alpha(t) > \;=\; \sum_{(j,\beta)} m_{ij}^{\alpha\beta} J_{ij}^{\alpha\beta} G \nu_j^\beta, \tag{3.45}$$

where $G \equiv \int_{-\infty}^{\infty} j_{syn}(t)\mathrm{d}t$ and ν_j^β is the rate of neuron j in population β. Averaging over the neurons in a given population we have:

$$< I^\alpha(t) > \;\equiv\; \mu^\alpha \;=\; G \sum_\beta N_\beta p J^{\alpha\beta} \nu^\beta, \tag{3.46}$$

where p is the connection probability and N_β is the number of neurons in population β. The firing rate can be calculated by imposing that the population-averaged mean current is $O(1)$ (see Appendix 2-A). Using the notation $\delta x \equiv x - < x >$, we calculate the variance of the current as:

$$< (\delta I_i^\alpha(t))^2 > \;=\; < \sum_{(j,\beta)} m_{ij} J_{ij}^{\alpha\beta} (j_{syn} * \delta y_j^\beta)(t) \sum_{(k,\beta')} m_{ik} J_{ik}^{\alpha\beta'} (j_{syn} * \delta y_k^{\beta'})(t) > \tag{3.47}$$

Averaging over neurons, we can write:

$$[< (\delta I_i^\alpha(t))^2 >] \;=\; \sum_\beta N_\beta p(1-p) J^{(2)\ \alpha\beta} [< ((\phi_{syn} * \delta y_j^\beta)(0))^2 >] + c^{\alpha\alpha}(0) \tag{3.48}$$

where $c^{\alpha\alpha}(0)$ is the population-averaged zero-lag cross-covariance of the synaptic currents of neurons in population α and $\phi_{syn}(\tau)$ is:

$$\phi_{syn}(\tau) \;=\; \int_{-\infty}^{\infty} j_{syn}(\tau) j_{syn}(\tau + t)\mathrm{d}t. \tag{3.49}$$

3-A2. Self-consistent equations

Recurrent-recurrent pairs

In this section we will derive equations for the population-averaged cross-covariance functions of spike trains. We proceed as follows: we are interested in calculating the effect of the activity of neuron (i, α) on neuron (j, β). To do this, we assume that neuron (i, α) emits a spike train $y_i^\alpha(t)$, without caring about how the other neurons contribute to that spike train. We calculate the effect of the spike train $y_i^\alpha(t)$ on the activity of neuron (j, β). By proceeding like this we are artificially breaking the recurrency of the

network and transforming the problem into a feedforward one. Since the recurrency loop is not closed we expect our equations for $r_{ij}^{\alpha\beta}(\tau) \equiv < \delta y_i^\alpha(t)\delta y_j^\beta(t+\tau) >$ to be valid only for values of $\tau \geq 0$ and will denote this part of the solution as $r_{+,\,ij}^{\alpha\beta}(\tau)$. Notice that to calculate the cross-covariance function for $\tau < 0$ we can just interchange the roles of neuron (i,α) and (j,β), or take into account the symmetry relation: $r_{ij}^{\alpha\beta}(\tau) = r_{ji}^{\beta\alpha}(-\tau)$

To start with, we assume that the total current arriving to neuron (j,β), $I_j^\beta(t)$, is a Gaussian random variable. We can decompose this current into two uncorrelated contributions, $\bar{I}_c^{ji}(t)$ and $\bar{I}_j^{\beta;(0)}(t)$, where the current $\bar{I}_{ji}^{\beta;(0)}(t)$ is also uncorrelated to the spike train $y_i^\alpha(t)$[4]:

$$I_j^\beta(t) \;=\; \bar{I}_c^{ji}(t) + \bar{I}_{ji}^{\beta;(0)}(t) \tag{3.50}$$

Assuming that in the asynchronous state $\bar{I}_c^{ji}(t)$ is a small current, the spike train, $y_j^\beta(t)$ can be approximated using the linear response equation:

$$y_j^\beta(t) \;\simeq\; \bar{y}_j^{\beta;(0)}(t) + \int_0^\infty R_j^\beta(t')\delta\bar{I}_c^{ji}(t-t')\mathrm{d}t', \tag{3.51}$$

where $\bar{y}_j^{\beta;(0)}(t)$ is the spike train produced in the absence of $\delta\bar{I}_c^{ji}(t)$ and $R_j^\beta(t)$ is the linear response kernel, which should be computed with the value of the mean and variance of the current given by eqs. 3.46 and 3.47 [5]. We calculate the cross-covariance function as:

$$\begin{aligned} r_{+\,ij}^{\alpha\beta}(\tau) \;&=\; < \delta y_i^\alpha(t)\delta y_j^\beta(t+\tau) > \;\;=\; < \delta y_i^\alpha(t)\delta\bar{y}_j^{\beta;(0)}(t+\tau) > \\ &\qquad + < \delta y_i^\alpha(t)(R_j^\beta * \delta\bar{I}_c^{ji})(t+\tau) >, \end{aligned} \tag{3.52}$$

where * denotes the convolution operator. Notice that, by construction, the first term on the right hand side is zero, while the second one can be written as:

$$\begin{aligned} < \delta y_i^\alpha(t)(R_j^\beta * \delta\bar{I}_c^{ji})(t+\tau) > \;&=\; < \delta y_i^\alpha(t)\left((R_j^\beta * \delta I_j^\beta)(t+\tau) - (R_j^\beta * \delta\bar{I}_{ji}^{\beta;(0)})(t+\tau)\right) > = \\ &=\; < \delta y_i^\alpha(t)(R_j^\beta * \delta I_j^\beta)(t+\tau) >, \end{aligned} \tag{3.53}$$

[4]It can be shown that this decomposition is always possible if $I_j^\beta(t)$ and $y_i^\alpha(t)$ are not fully correlated, i.e., their correlation coefficient is <1. In our case, we assume (and later prove) that the correlation between the two magnitudes is small and so the approach is valid.

[5]More precisely, R_j^β should be evaluated with the values of the temporal mean current and variance in eq. 3.45 and 3.47 once we have subtracted the contribution of $\bar{I}_c^{ji}(t)$. $\bar{I}_c^{ji}(t)$ will be proved to be small and one can omit the previous subtraction in the computation of $R_j^\beta(t)$

because, by construction, $\delta\bar{I}_{ji}^{\beta;(0)}$ is uncorrelated to $y_i^\alpha(t)$. Expressing the current $I_j^\beta(t+\tau)$ as a sum of the filtered pre-synaptic spike trains, we have:

$$\begin{aligned} r_{+,\,ij}^{\alpha\beta}(\tau) &= <\delta y_i^\alpha(t)(m_{ji}^{\beta\alpha}J_{ji}^{\beta\alpha}R_j^\beta * j_{syn} * \delta y_i^\alpha)(t+\tau)> \\ &+ <\delta y_i^\alpha(t)\sum_{\substack{(k,\alpha')\\ k\neq i}}(m_{jk}^{\beta\alpha'}J_{jk}^{\beta\alpha'}R_j^\beta * j_{syn} * \delta y_k^{\alpha'})(t+\tau)> . \end{aligned} \tag{3.54}$$

An equation equivalent to eq. 3.54 can be found in Tetzlaff et al., 2012, Helias et al., 2013. In those works, the current generated by the spike pre-synaptic cell is considered to be small in order to apply the linear response approximation. In our case, the relevant small magnitude is the correlated part of the current $\bar{I}_c^{ji}(t)$. We will find that the network is in an asynchronous state and, thus, $\bar{I}_c^{ji}(t)$ is necessarily small.

After Fourier transforming eq. 3.54, we obtain:

$$\begin{aligned} \tilde{r}_{+,\,ij}^{\alpha\beta}(\omega) &= \delta\tilde{y}_i^\alpha(\omega)\tilde{R}_j^\beta(\omega)\delta\tilde{I}_j^\beta(\omega) = \\ &= \tilde{R}_j^\beta(\omega)\tilde{j}_{syn}(\omega)\Big\{m_{ji}^{\beta\alpha}J_{ji}^{\beta\alpha}\tilde{a}_i^\alpha(\omega) \\ &+ \sum_{\substack{(k,\alpha')\\ \alpha'\in E,I\\ k\neq i}} m_{jk}^{\beta\alpha'}J_{jk}^{\beta\alpha'}\tilde{r}_{+\,ik}^{\alpha\alpha'}(\omega) \\ &+ \sum_{(k,X)} m_{jk}^{\beta X}J_{jk}^{\beta X}\tilde{r}_{+\,ik}^{\alpha X}(\omega)\Big\}. \end{aligned} \tag{3.55}$$

We assume that, when averaging over pairs, the dynamical properties of the network and the synaptic couplings are independent magnitudes [Renart et al., 2010], i.e., for example: $[J_{ji}^{\beta\alpha}\delta\tilde{a}_i^\alpha(\omega)] = [J_{ji}^{\beta\alpha}][\delta\tilde{a}_i^\alpha(\omega)]$. Averaging eq. 3.55 over neurons in each population, we have:

$$\tilde{r}_+^{\alpha\beta}(\omega) = \tilde{R}^\beta(\omega)\tilde{j}_{syn}(\omega)p\Big\{J^{\beta\alpha}\tilde{a}^\alpha(\omega) + N_X J^{\beta X}\tilde{r}^{\alpha X}(\omega) + \sum_{\alpha'\in E,I} N_{\alpha'}J^{\beta\alpha'}\tilde{r}_+^{\alpha\alpha'}(\omega)\Big\} \tag{3.56}$$

where we have defined $\tilde{R}^\beta(\omega) \equiv [\tilde{R}_j^\beta(\omega)]$. Making the dependence of the synaptic couplings on N explicit:

$$\tilde{r}_+^{\alpha\beta}(\omega) = \tilde{R}^\beta(\omega)\tilde{j}_{syn}(\omega)p\Big\{\frac{j^{\beta\alpha}}{\sqrt{N}}\tilde{a}^\alpha(\omega) + \sqrt{N}\Big(\bar{j}^{\beta X}\tilde{r}^{\alpha X}(\omega) + \sum_{\alpha'\in E,I}\bar{j}^{\beta\alpha'}\tilde{r}_+^{\alpha\alpha'}(\omega)\Big)\Big\}, \tag{3.57}$$

where $j^{\beta\alpha}$ and $\bar{j}^{\beta\alpha} \equiv \frac{N_\alpha}{N}j^{\beta\alpha}$ are $O(1)$ (see *Methods*). Eq. 3.57 is the Fourier transform of eq. 3.20 in *Results* (section 2.3.1).

External-recurrent pairs

In the previous derivation, one can assume that neuron i belongs to the population X and proceed exactly in the same way as before to calculate $r^{X\alpha}(\tau)$. Notice that in this case the equations that we find are valid for all values of τ, because the causality conflict due to the recurrence in the network mentioned before is not present (the connection of external neurons to recurrent neurons is purely feedforward):

$$\begin{aligned} r_{ij}^{X\alpha}(\tau) &= < \delta y_i^X(t)(m_{ji}^{\alpha X} J_{ji}^{\alpha X} R_j^\alpha * j_{syn} * \delta y_i^X)(t+\tau) > \\ &+ < \delta y_i^X(t) \sum_{\substack{(k,\alpha') \\ (k\neq i)}} (m_{jk}^{\alpha\alpha'} J_{jk}^{\alpha\alpha'} R_j^\alpha * j_{syn} * \delta y_k^{\alpha'})(t+\tau) > . \end{aligned} \tag{3.58}$$

As mentioned, this last equation was derived for a feedforward connection and, thus, is valid for all values of τ. It is formally identical to the one in Ostojic et al., 2009 for this kind of architecture.

In frequency domain the equation for the average external-recurrent cross-covariance function reads as:

$$\tilde{r}^{X\alpha}(\omega) = \tilde{R}^\alpha(\omega)\tilde{j}_{syn}(\omega)p\Big\{ J^{\alpha X}\tilde{a}^X(\omega) + \sum_{\alpha'\in E,I} N^{\alpha'} J^{\alpha\alpha'}\tilde{r}^{X\alpha'}(\omega)\Big\}. \tag{3.59}$$

Making the dependence of $J^{\alpha X}$ on N explicit, we have:

$$\tilde{r}^{X\alpha}(\omega) = \tilde{R}^\alpha(\omega)\tilde{j}_{syn}(\omega)p\Big\{ \frac{j^{\alpha X}}{\sqrt{N}}\tilde{a}^X(\omega) + \sum_{\alpha'\in E,I} \sqrt{N}\bar{j}^{\alpha\alpha'}\tilde{r}^{X\alpha'}(\omega)\Big\}. \tag{3.60}$$

3-A3. Leading-order solution

Here we propose a perturbative approach to solve eqs. 3.57 and 3.60. We will use a regular perturbation technique, similar to the one employed in Renart et al., 2010.

For a fixed value of $\omega = \omega_0$, eqs. 3.57 and 3.60 can be solved by proposing a Taylor series expansion of the form $\tilde{r}^{\alpha\beta}(\omega_0) = \sum_n \tilde{r}^{\alpha\beta\,(n)}(\omega_0)\epsilon^n$, where $\epsilon \equiv 1/\sqrt{N}$. The solution to leading order is [6]:

[6] To arrive to this solution one has to take into account that $\tilde{R}^\alpha(\omega_0)$ is $O(1)$. The linear response kernel, depends on the statistics of the background noise. If a neuron receives a large number of inputs, the afferent current is Gaussian and, as we have already seen, the mean and variance of the current are $O(1)$ for the studied regime (see fig. 3.2)

$$\tilde{r}^{XE\,(2)}(\omega_0) = A_E\tilde{a}^X(\omega_0) \quad (3.61)$$
$$\tilde{r}^{XI\,(2)}(\omega_0) = A_I\tilde{a}^X(\omega_0) \quad (3.62)$$
$$\tilde{r}_+^{EE\,(2)}(\omega_0) = A_E^2\tilde{a}^X(\omega_0) - \tilde{a}^{E\,(0)}(\omega_0) \quad (3.63)$$
$$\tilde{r}_+^{II\,(2)}(\omega_0) = A_I^2\tilde{a}^X(\omega_0) - \gamma_I\tilde{a}^{I\,(0)}(\omega_0) \quad (3.64)$$
$$\tilde{r}_+^{EI\,(2)}(\omega_0) = \tilde{r_+}^{IE\,(2)}(\omega_0) = A_EA_I\tilde{a}^X(\omega_0). \quad (3.65)$$

where $\gamma_I \equiv \frac{N}{N_I} \sim O(1)$ and A_α has been defined in eqs. 2.78 and 2.79 and can be rewritten in matrix notation as:

$$A_\alpha = -\sum_\beta (\bar{J}^{\beta\alpha})^{-1}\bar{J}^{\alpha X} \quad (3.66)$$

We have assumed that $j^{\beta\alpha}$ is invertible. This is always the case if the networks are not homogeneous [7] and we are in the balanced regime described in Appendix 2-A. For homogeneous networks it is easy to show that the system is degenerate, thus other techniques must be used. The differences between homogeneous and heterogeneous networks are not trivial and conclusions derived in homogeneous networks do not extrapolate to heterogeneous ones. Here, we restrict our conclusions to the latter, which we consider is the physically meaningful one. We will discuss the case of homogeneous networks in section 3-A5.

Proceeding in this way for all values of ω, we can take the inverse Fourier transform of eqs. 3.61-3.65. Taking into account the symmetry $r^{\alpha\alpha'}(-\tau) = r^{\alpha'\alpha}(\tau)$ we arrive to:

$$r^{XE}(\tau) = \epsilon^2 A_E a^X(\tau) \quad (3.67)$$
$$r^{XI}(\tau) = \epsilon^2 A_I a^X(\tau) \quad (3.68)$$
$$r^{EE}(\tau) = \epsilon^2(A_E^2 a^X(\tau) - a^{E\,(0)}(\tau)) \quad (3.69)$$
$$r^{II}(\tau) = \epsilon^2 A_I^2(a^X(\tau) - \gamma_I a^{I\,(0)}(\tau)) \quad (3.70)$$
$$r^{EI}(\tau) = r^{IE}(\tau) = \epsilon^2 A_E A_I a^X(\tau). \quad (3.71)$$

Eqs. 3.61-3.65 were derived keeping fixed the value of $\omega = \omega_0$, taking the limit $N \to \infty$ and preserving the leading order terms. We have then repeated the process for all values of ω. The product $\tilde{R}^\alpha(\omega)\tilde{j}_{syn}(\omega)$ is, thus, $O(1)$. Notice that $\tilde{j}_{syn}(\omega) \to 0$ when

[7] In homogeneous networks the afferent currents and the neuronal dynamics do not depend on the population the post-synaptic neurons belong to

$\omega \to \infty$ and $\tilde{R}^{\alpha}(\omega)$ tends to a constant value in the case the synaptic noise is colored [Fourcaud and Brunel, 2002]. Thus, $\tilde{R}^{\alpha}(\omega)\tilde{j}_{syn}(\omega) \to 0$ when $\omega \to \infty$. Notice that, in practice, one deals with a finite network of a given size N_c. In such a case, there is a frequency ω_c, such as for $\omega >> \omega_c$, $\tilde{R}^{\alpha}(\omega)\tilde{j}_{syn}(\omega_c) << 1/\sqrt{N_c}$, and one can wonder if the predictions derived assuming $\tilde{R}^{\alpha}(\omega)\tilde{j}_{syn}(\omega) \sim O(1)$ are still valid even when finite networks are employed. Figs. 3.4b,c,d. show the cross-spectra, $|\tilde{r}^{\alpha\alpha'}(\omega)|^2$. At finite N, the theory predicts well the low frequency limit but for high ω the prediction is no longer accurate. The peak in the cross-spectra calculated directly from the simulation gives us the value of ω where the discrepancy between theory and simulation is maximal. Notice, that it moves to large values of ω with N, i.e., for $N \to \infty$ the maximum occurs at $\omega \to \infty$.

In the time domain, this fact appears in the following way. First notice that $a^E(\tau)$ and $a^I(\tau)$ have almost no structure apart from the peak at $\tau = 0$, ($|\tilde{a}^{\alpha}(\omega)|^2$ are rather flat (fig. 3.4a)). The fast time-scale ($O(\epsilon)$) at finite value of N of spike train cross-covariance functions described in *Results* (section 2.3.2) should be understood as the convergence to the delta-shaped limit implicit in eqs. 3.67-3.71 given the shape of, $a^{\alpha}(t)$.

Notice that equations 3.61-3.65 were derived in the case when all the synaptic filters are identical. However, for a fixed value of $\omega = \omega_0$ one can rescale the values of the synaptic couplings:

$$\tilde{j}^{\,\alpha\beta}(\omega_0) \to \tilde{j}^{\alpha\beta}_{syn}(\omega_0) j^{\alpha\beta}, \tag{3.72}$$

where we denote by $\tilde{j}^{\alpha\beta}_{syn}(\omega)$ the population-averaged synaptic filter of the connection between a pre-synaptic neuron in population β with a post-synaptic neuron in population α. Thus, for a fixed value of $\omega = \omega_0$ formally identical equations to eqs. 3.61-3.65 hold true.

$$\begin{aligned}
\tilde{r}^{XE\,(2)}(\omega_0) &= \tilde{A}'_E(\omega_0)\tilde{a}^X(\omega_0) && (3.73)\\
\tilde{r}^{XI\,(2)}(\omega_0) &= \tilde{A}'_I(\omega_0)\tilde{a}^X(\omega_0) && (3.74)\\
\tilde{r}^{EE\,(2)}_{+}(\omega_0) &= \tilde{A}'_E(\omega_0)^2\tilde{a}^X(\omega_0) - \tilde{a}^{E\,(0)}(\omega_0) && (3.75)\\
\tilde{r}^{II\,(2)}_{+}(\omega_0) &= \tilde{A}'_I(\omega_0)^2\tilde{a}^X(\omega_0) - \gamma_I\tilde{a}^{I\,(0)}(\omega_0) && (3.76)\\
\tilde{r}_{+}{}^{E}I\,(2)(\omega_0) &= \tilde{r}^{IE\,(2)*}_{+}(\omega_0) \;=\; \tilde{A}'^{*}_E(\omega_0)\tilde{A}'_I(\omega_0)\tilde{a}^X(\omega_0). && (3.77)
\end{aligned}$$

where $\tilde{A}'_E(\omega_0)$ and $\tilde{A}'_I(\omega_0)$ are defined analogously to A_E and A_I but using the values $j'^{\alpha\beta}(\omega_0)$ given by eq. 3.72. ($\tilde{A}'^*_\alpha(\omega_0)$ denotes the complex conjugate of $\tilde{A}'_\alpha(\omega_0)$)

3-A4. Cancellation of the total current cross-covariance

As mentioned before, in the limit $N \to \infty$, eqs. 3.61-3.65 are valid for all values of ω. In that case, one can prove that the total current cross-covariance functions, $\tilde{c}^{\alpha\alpha'}(\omega)$, cancel for all the values of ω. Assuming that the synaptic filters are the same for all types of synapses, using the expression of the total pre-synaptic current, $I_i^\alpha(t)$, (eq. 3.44) and the definition $\gamma_\alpha \equiv \frac{N}{N_\alpha}$, one can easily write, in the frequency domain:

$$\begin{aligned}\tilde{c}^{\alpha\alpha'}(\omega) &= p^2 \sum_\beta \gamma_\beta^{-1} j^{\alpha\beta} j^{\alpha'\beta} \tilde{\phi}_{syn}(\omega)\tilde{a}^\beta(\omega) + p^2 \sum_{\beta\beta'} N \bar{\jmath}^{\alpha\beta} \bar{\jmath}^{\alpha'\beta'} \tilde{\phi}_{syn}(\omega)\tilde{r}^{\beta\beta'}(\omega) \;= \\ &= p^2 \sum_\beta \gamma_\beta^{-1} j^{\alpha\beta} j^{\alpha'\beta} |\tilde{\jmath}_{syn}(\omega)|^2 \tilde{a}^\beta(\omega) + p^2 \sum_{\beta\beta'} N \bar{\jmath}^{\alpha\beta} \bar{\jmath}^{\alpha'\beta'} |\tilde{\jmath}_{syn}(\omega)|^2 \tilde{r}^{\beta\beta'} \quad (3.78)\end{aligned}$$

where we have made use of:

$$\tilde{\phi}(\omega) \equiv \mathcal{F}[\phi(\tau)] = \tilde{\jmath}^*_{syn}(\omega)\tilde{\jmath}_{syn}(\omega) = |\tilde{\jmath}_{syn}(\omega)|^2. \quad (3.79)$$

Inserting the expressions for $\tilde{r}^{\beta\beta'}(\omega)$, given by eqs. 3.61-3.65, in eq. 3.78 we obtain that the right hand side cancels to leading order. Thus, $\tilde{c}^{\alpha\alpha'}(\omega)$ is at most $O(\epsilon)$. Notice, however, that one can write eq. 3.78 in terms of the cross-covariance of the current components, $\tilde{c}^{\alpha\alpha'}_{\mathcal{I};\beta\beta'}(\omega)$, as:

$$\tilde{c}^{\alpha\alpha'}(\omega) = \sum_{\beta\beta'} \tilde{c}^{\alpha\alpha'}_{\mathcal{I};\beta\beta'}(\omega) \qquad (\beta\beta') = (E, I, X) \quad (3.80)$$

where:

$$\tilde{c}^{\alpha\alpha'}_{\mathcal{I};\beta\beta'}(\omega) = p^2 \gamma_\beta^{-1} j^{\alpha\beta} j^{\alpha'\beta} \tilde{\phi}_{syn}(\omega)\tilde{a}^\beta(\omega)\delta_{\beta\beta'} + p^2 N \bar{\jmath}^{\alpha\beta} \bar{\jmath}^{\alpha'\beta'} \tilde{\phi}_{syn}(\omega)\tilde{r}^{\beta\beta'}(\omega) \quad (3.81)$$

Substituting the values of $\tilde{r}^{\beta\beta'}(\omega)$ (Fourier transform of eqs. 3.67-3.71) previously found in eq. 3.81 one finds that they are $O(1)$. Thus, the cancellation of the leading order in eq. 3.78 comes from the sum of the current components cross-covariances and not from their small values.

The integral of $\tilde{c}^{\alpha\alpha}(\omega)$ gives $c^{\alpha\alpha'}(0)$. Specifically:

$$c^{\alpha\alpha'}(0) = \frac{1}{2\pi}\int_{-\infty}^{\infty} \tilde{c}^{\alpha\alpha'}(\omega)\mathrm{d}\omega \tag{3.82}$$

Because of the linearity of the integral, we conclude that $c^{\alpha\alpha'}(0)$ is $O(\epsilon)$ at most. Our simulation shows that $c^{\alpha\alpha'}(0) = O(\epsilon)$ and a fast time-scale of the same order appears so that the integral of the cross-covariance function is $O(\epsilon^2)$.

If the synaptic filters depend on the type of synapses, one can still prove that a similar cancellation occurs using eqs. 3.73-3.77. However, fig. 3.10c shows that the zero-lag cross-covariance of the total current is small but does not decay with N. As we have already mentioned, for a finite network our theory is expected to work well at low frequencies, so it should not be surprising that the scaling behavior of the peak of the cross-covariance function is not well predicted (although in the case with identical synaptic filters for all the synapses it worked well, see fig. 3.2h). Fig. 3.10d shows that the cross-covariance of membrane potentials exhibits a cancellation $O(\epsilon^2)$. In Appendix 3-B, we explain that the cross-covariance function of the membrane potential can be calculated from the cross-covariance function of the total current convolved with an exponential kernel. This operation implies the integration of the cross-covariance function of the total current, which is related to the low frequency values of its Fourier transform. Then, although the zero-lag cross-covariance function of the total current does not show the expected cancellation, magnitudes related to the integral of this function do reflect it.

Analogously, one can show that $\tilde{\mathcal{A}}^{X\alpha}(\omega) \equiv [< \delta y_j^X(t)\delta I_i^\alpha(t+\tau) >]$ $(\alpha = E, I)$ also cancels to leading order.

Notice that we have recovered the starting point in chapter 2: the cancellation of total current cross-covariances. We have shown that an asynchronous state exists so the conclusions derived in chapter 2 apply in this case.

3-A5. Special case: Homogeneous networks

In this section we will study the case of homogeneous networks. Homogeneous networks are characterized by statistically equivalent afferent couplings of recurrent

neurons, no matter the population the post-synaptic neuron belongs to. The characteristic membrane time and refractory time are also statistically equivalent for all the populations. Thus, we have:

$$\bar{\jmath}^{IX} = j^{EX} \equiv j^X \tag{3.83}$$
$$\bar{\jmath}^{II} = j^{EI} \equiv j^I \tag{3.84}$$
$$\bar{\jmath}^{IE} = j^{EE} \equiv j^E \tag{3.85}$$
$$\tilde{R}^I(\omega) = \tilde{R}^E(\omega) \equiv \tilde{R}(\omega) \tag{3.86}$$

The last identity arises because the linear response kernel depends only on the properties of the membrane filter and on the afferent currents' statistics, which can be trivially proved to be independent of the neuron's population given the values of the synaptic couplings. In such circumstances, the magnitudes A_E and A_I previously defined diverge. Notice that, these magnitudes appeared when one calculates the balanced firing rates (eq. 2.77, Appendix 2-A), and one solves the uncoupled systems of equations that determine the cross-covariance functions (eqs. 3.57 and 3.60). The divergence occurred because the inverse matrix of $\bar{\jmath}^{\alpha\beta}$ does not exist. This is a sign that the system of equations is degenerated and some other technique must be used.

First, we calculate the firing rates as we did in Appendix 2-A. If the afferent currents and the neurons' parameter are identical the firing rates of excitatory and inhibitory neurons must be identical: $\nu^I = \nu^E \equiv \nu$. Thus, from eq. 2.77:

$$\nu = -\frac{\bar{\jmath}^X}{(\bar{\jmath}^E + \bar{\jmath}^I)}\, \nu^X \tag{3.87}$$

where we have defined $\bar{\jmath}^\alpha \equiv \frac{N_\alpha}{N} j^\alpha$. Last equation imposes that $|\bar{\jmath}^I| > \bar{\jmath}^E$ in order for ν to have physically plausible values.
For the case of spike trian cross-covariance functions, we start by solving the case of external-recurrent cross-covariances, $r^{X\alpha}(\omega)$. Eq. 3.60 allows us to write:

$$\tilde{r}^{X\alpha}(\omega) = \tilde{R}(\omega)\tilde{\jmath}_{syn}(\omega) p\Big\{ \tfrac{\bar{\jmath}^X}{\sqrt{N}} \tilde{a}^X(\omega) + \sqrt{N}(\bar{\jmath}^E \tilde{r}^{XE}(\omega) + \bar{\jmath}^I \tilde{r}^{XI}(\omega)) \Big\}. \tag{3.88}$$

Notice that the right-hand side of the last equations does not depend on α. Thus $\tilde{r}^{XE}(\omega) = \tilde{r}^{XI}(\omega)$. Using this relationship reduces the system of two equations to one unique equation. At a fixed value of $\omega = \omega_0$ one can solve it at leading order by

proposing Taylor series expansion of the form $\tilde{r}^{XI}(\omega_0) = \tilde{r}^{XE}(\omega_0) = \sum_n \tilde{r}^{XE\,(n)}(\omega_0)\epsilon^n$, where $\epsilon \equiv 1/\sqrt{N}$:

$$\tilde{r}^{XE}(\omega_0) = \tilde{r}^{XI}(\omega_0) = -\epsilon^2 \frac{j^X}{j^E + \gamma_I^{-1} j} a^X(\omega_0) \tag{3.89}$$

For the cross-covariance functions $\tilde{r}^{EE}(\omega)$, $\tilde{r}^{EI}(\omega)$, $\tilde{r}^{II}(\omega)$ and $\tilde{r}^{IE}(\omega)$ eq. 3.57 also represents a degenerated system of equations in the case of homogeneous networks. We write explicitly eq. 3.57 for a homogeneous network:

$$\tilde{r}_+^{EE}(\omega) = \tilde{R}(\omega)\tilde{\jmath}_{syn}(\omega)p\Big\{\frac{j^E}{\sqrt{N}}\tilde{a}^E(\omega) + \sqrt{N}\Big(\bar{\jmath}^X\tilde{r}^{EX}(\omega) + \bar{\jmath}^E\tilde{r}_+^{EE}(\omega) + \bar{\jmath}^I\tilde{r}_+^{EI}(\omega)\Big)\Big\} \tag{3.90}$$

$$\tilde{r}_+^{II}(\omega) = \tilde{R}(\omega)\tilde{\jmath}_{syn}(\omega)p\Big\{\frac{j^I}{\sqrt{N}}\tilde{a}^I(\omega) + \sqrt{N}\Big(\bar{\jmath}^X\tilde{r}^{IX}(\omega) + \bar{\jmath}^E\tilde{r}_+^{IE}(\omega) + \bar{\jmath}^I\tilde{r}_+^{II}(\omega)\Big)\Big\} \tag{3.91}$$

$$\tilde{r}_+^{EI}(\omega) = \tilde{R}(\omega)\tilde{\jmath}_{syn}(\omega)p\Big\{\frac{j^E}{\sqrt{N}}\tilde{a}^E(\omega) + \sqrt{N}\Big(\bar{\jmath}^I\tilde{r}^{EX}(\omega) + \bar{\jmath}^E\tilde{r}_+^{EE}(\omega) + \bar{\jmath}^I\tilde{r}_+^{EI}(\omega)\Big)\Big\} \tag{3.92}$$

$$\tilde{r}_+^{IE}(\omega) = \tilde{R}(\omega)\tilde{\jmath}_{syn}(\omega)p\Big\{\frac{j^I}{\sqrt{N}}\tilde{a}^I(\omega) + \sqrt{N}\Big(\bar{\jmath}^X\tilde{r}^{IX}(\omega) + \bar{\jmath}^I\tilde{r}_+^{II}(\omega) + \bar{\jmath}^E\tilde{r}_+^{IE}(\omega)\Big)\Big\} \tag{3.93}$$

Notice that one can write:

$$\tilde{r}_+^{EI}(\omega) + \tilde{r}_+^{IE}(\omega) = \tilde{r}_+^{EE}(\omega) + \tilde{r}_+^{II}(\omega) \tag{3.94}$$

Using this identity one can reduce the previous system of four dependent equations to three independent ones. Besides one has, by construction, $\tilde{r}_+^{EI}(\omega) = \tilde{r}_+^{IE\,*}(\omega)$. Performing the perturbative method explained before one can see that at leading order $\tilde{r}_+^{EI}(\omega)$ necessarily has to be real, i.e., $\tilde{r}_+^{EI}(\omega) = \tilde{r}_+^{IE}(\omega)$. Using this identity and after some algebra we arrive to:

$$\tilde{r}_+^{II}(\omega_0) = \epsilon^2\,\frac{\tilde{a}^X(\omega_0)j^{X\,2} - \tilde{a}^{(0)}(\omega_0)(\gamma_I^{-1}j^{I\,2} - j^{E\,2} + 2j^E j^I)}{(j^E + \gamma_I^{-1}j^I)^2} \tag{3.95}$$

$$\tilde{r}_+^{EE}(\omega_0) = \epsilon^2\,\frac{\tilde{a}^X(\omega_0)j^{X\,2} - \tilde{a}^{(0)}(\omega_0)(j^{E\,2} - \gamma_I^{-1}j^{I\,2} + 2j^E j^I)}{(j^E + \gamma_I^{-1}j^I)^2} \tag{3.96}$$

$$\tilde{r}_+^{EI}(\omega_0) = \tilde{r}_+^{IE}(\omega_0) = \epsilon^2\frac{\tilde{a}_X(\omega_0)j^{X\,2} - 2\tilde{a}^{(0)}(\omega_0)j^E j^I}{(j^E + \gamma_I^{-1}j^I)^2} \tag{3.97}$$

where $\tilde{a}^{(0)}(\omega_0) \equiv \tilde{a}^{E\,(0)}(\omega_0) = \tilde{a}^{I\,(0)}(\omega_0)$ in a homogeneous network. One can easily prove that these expressions for the cross-covariance functions do not imply the tracking of the external firing rate that we mentioned before. One must take into account that this is a very marginal case and, thus, it is not biophysically relevant. Conclusions derived using these networks do not extrapolate to the more typical case of heterogeneous networks.

3-A6. Finite-size solution

In this section we explain a method to solve the system of equations eqs. 3.57 and 3.60 assuming N is finite. The solution provides information about how the asymptotic limit described by eqs. 3.67-3.71 is reached. As we explained in section 3.4, an approximation for the function $\tilde{R}^\alpha(\omega)\tilde{j}_{syn}(\omega)$ must be made in order for the system to be analytically tractable. We approximate $\tilde{R}^\alpha(\omega)\tilde{j}_{syn}(\omega)$ similarly to Ostojic et al., 2009:

$$\tilde{R}^\alpha(\omega)\tilde{j}_{syn}(\omega) \simeq \frac{k^\alpha}{\bar{\tau}_\alpha^{-1} + i\omega} \tag{3.98}$$

As explained in Ostojic et al., 2009, this approximation consists in taking the first term of the Laurent series of the function $\tilde{R}^\alpha(\omega)\tilde{j}_{syn}(\omega)$. Besides, we assume that we are in the parameter region in which no resonance for the function $\tilde{R}^\alpha(\omega)\tilde{j}_{syn}(\omega)$ appears, i.e., $\bar{\tau}_\alpha$ is real. This is the case provided the synaptic noise is large enough [Ostojic et al., 2009]. Notice also that eq. 3.98 reads in the time domain as $(R^\alpha * j_{syn})(\tau) = \Theta(\tau)k^\alpha e^{-\frac{\tau}{\bar{\tau}_\alpha}}$, as in Tetzlaff et al., 2012.

$\tilde{R}^\alpha(\omega)$ is a function of the afferent current statistics. These depend on N. Thus, one should calculate $\tilde{R}^\alpha(\omega)$ for a given N and solve the equation for each value of N. However, as we have already pointed out, if N is large enough the incoming current can be considered a Gaussian variable whose mean and standard deviation almost do not vary with N (see figs. 3.2b,c). Thus, $\tilde{R}^\alpha(\omega)$ can be considered independent of N, provided N is large enough.

We start by solving the equation for $\tilde{r}^{X\alpha}(\omega)$. With the previous approximation, eq. 3.60 reads as:

$$\tilde{r}^{X\alpha}(\omega) = \frac{k^\alpha}{\bar{\tau}_\alpha^{-1} + i\omega} p\Big\{\frac{j^{\alpha X}}{\sqrt{N}}\tilde{a}^X(\omega) + \sum_{\alpha' \in E,I} \sqrt{N}\bar{j}^{\alpha\alpha'}\tilde{r}^{X\alpha'}(\omega)\Big\}. \tag{3.99}$$

$$i\omega\tilde{r}^{X\alpha}(\omega) = -\bar{\tau}_\alpha^{-1}\tilde{r}^{X\alpha}(\omega) + k^\alpha p\Big\{\frac{j^{\alpha X}}{\sqrt{N}}\tilde{a}^X(\omega) + \sum_{\alpha' \in E,I} \sqrt{N}\bar{j}^{\alpha\alpha'}\tilde{r}^{X\alpha'}(\omega)\Big\}. \tag{3.100}$$

We propose an Ansatz for $\tilde{r}^{X\alpha}(\omega)$:

$$\tilde{r}^{X\alpha}(\omega) = \Big\{C_0\frac{u^\alpha}{-\lambda + i\omega} + C_1\frac{u^{\alpha\,*}}{-\lambda^* + i\omega}\Big\}k^\alpha p\frac{j^{\alpha X}}{\sqrt{N}}\tilde{a}^X(\omega) \tag{3.101}$$

where u^α, $u^{\alpha\,*}$ are the complex eigenvectors of the matrix $\Lambda^{\alpha\alpha'} \equiv \sqrt{N}pk^\alpha \bar{j}^{\alpha\alpha'} - \bar{\tau}_\alpha^{-1}\delta_{\alpha\alpha'}$, λ, λ^*, are the associated complex eigenvalues and C_0, C_1 are some constants to be determined. We have assumed that $\Lambda^{\alpha\alpha'}$ has eigenvalues with non-null imaginary and real parts. Inserting the Ansatz in eq. 3.100 and after some algebra one finds that:

$$1 = C_0 u^\alpha + C_1 u^{\alpha\,*}. \tag{3.102}$$

Since the eigenvectors are orthogonal, and thus linearly independent, this system of equations univocally determine the values of C_0 and C_1. It is also easy to see that $C_1 = C_0^*$.

Taking into account that $a^X(\tau) = \nu^X \delta(\tau)$, and assuming $\mathrm{Re}(\lambda) < 0$, eq. 3.101 in the time space reads as:

$$r^{X\alpha}(\tau) = \Theta(\tau)\nu^X \frac{j^{\alpha X}}{\sqrt{N}} e^{-v\sqrt{N})\tau}\Big\{2\mathrm{Re}(C_0 u^\alpha)\cos(w\sqrt{N}\tau) - 2\mathrm{Im}(C_0 u^\alpha)\sin(w\sqrt{N}\tau)\Big\} \tag{3.103}$$

with $v\sqrt{N} \equiv \mathrm{Re}(\lambda)$ and $w\sqrt{N} \equiv \mathrm{Im}(\lambda)$. Notice that the amplitude of $r^{X\alpha}(\tau)$ is $O(\epsilon)$, the frequency of the oscillation is $O(\epsilon^{-1})$ and the damping characteristic time is $O(\epsilon)$. Last equation can be written as:

$$\begin{aligned} r^{XE}(\tau) &= \Theta(\tau)\Gamma^E \nu^X k^E p \frac{j^{EX}}{\sqrt{N}} e^{-(v\sqrt{N})\tau}\cos(w\sqrt{N}\tau + \phi^E) && (3.104)\\ r^{XI}(\tau) &= \Theta(\tau)\Gamma^I \nu^X k^I p \frac{j^{IX}}{\sqrt{N}} e^{-(v\sqrt{N})\tau}\cos(w\sqrt{N}\tau + \phi^I) && (3.105)\\ & && (3.106) \end{aligned}$$

where the constants Γ^α and ϕ^α can be calculated from C_0 and u^α. Notice that they do not depend on N:

$$\begin{aligned} \Gamma^\alpha &\equiv \sqrt{(2\mathrm{Re}(C_0 u^\alpha))^2 + (2\mathrm{Im}(C_0 u^\alpha))^2} && (3.107)\\ \phi^\alpha &\equiv \tan^{-1}\Big(\frac{\mathrm{Im}(C_0 u^\alpha)}{\mathrm{Re}(C_0 u^\alpha)}\Big) && (3.108) \end{aligned}$$

For the case of $\tilde{r}^{\alpha\alpha'}(\omega)$, $(\alpha, \alpha') = (E, I)$, we use the same approximation for the function $\tilde{R}^\alpha(\omega)\tilde{j}_{syn}(\omega)$, eq. 3.57. Eq. 3.98 reads as:

$$\tilde{r}_+^{\alpha\beta}(\omega) = \frac{k^\beta}{\bar{\tau}_\beta^{-1} + i\omega} p\Big\{\frac{j^{\beta\alpha}}{\sqrt{N}}\tilde{a}^\alpha(\omega) + \sqrt{N}\Big(\bar{j}^{\beta X}\tilde{r}^{\alpha X}(\omega) + \sum_{\alpha' \in E,I} \bar{j}^{\beta\alpha'}\tilde{r}_+^{\alpha\alpha'}(\omega)\Big)\Big\}, \tag{3.109}$$

Notice that this last equation is formally identical to the case $\tilde{r}^{X\alpha}(\omega)$, eq. 3.99, but now the role of $\tilde{a}^X(\omega)$ is played by a linear combination of $\tilde{a}^\alpha(\omega)$ and $\tilde{r}^{\beta X}(\omega)$. We propose an Ansatz of the form:

$$\tilde{r}_+^{\alpha\beta}(\omega) = \Big(D_0\frac{u^\beta}{-\lambda+i\omega} + D_1\frac{u^{\beta\,*}}{-\lambda^*+i\omega}\Big)k^\alpha p\Big(\frac{j^{\beta\alpha}}{\sqrt{N}}\tilde{a}^\alpha(\omega) + \sqrt{N}\bar{j}^{\beta X}\tilde{r}^{\alpha X}(\omega)\Big) \tag{3.110}$$

where D_0 and D_1 are constants to be determined. It is trivial to show that this is the correct form of the solution. We skip the details of the calculation because they are very similar to the previous case. We approximate the auto-covariances functions $a^\alpha(\tau) \simeq \nu^\alpha\delta(\tau)$, where ν^α is the firing rate obtained with the balanced equations in Appendix 2-A. Notice that ν^α is calculated at leading order in N. Strictly, $a^\alpha(\tau)$ is a function of N. However, as we discussed previously for the case of $\tilde{R}^\alpha(\omega)$, $\tilde{a}^\alpha(\omega)$ is a finite magnitude and in practice, one can neglect the $O(\epsilon)$ corrections if N is large enough (see fig. 3.4a). Proceeding like this, we arrive to the following result:

$$\begin{aligned} r^{EE}(\tau) &= k^E p\Gamma^E\Big(\nu^E\frac{j^{EE}}{\sqrt{N}}\cos(w\sqrt{N}|\tau|+\phi^E) + \frac{\Gamma^E}{\sqrt{N}}\nu^X j^{EX}\bar{j}^{EX}k^E p(\Upsilon\cos(w\sqrt{N}|\tau|+2\phi^E+\Phi)+\frac{1}{4v}\cos(w\sqrt{N}|\tau|))\Big) \\ &\times\ e^{-v\sqrt{N}|\tau|} \end{aligned} \tag{3.111}$$

$$\begin{aligned} r^{II}(\tau) &= k^I p\Gamma^I\Big(\nu^I\frac{j^{II}}{\sqrt{N}}\cos(w\sqrt{N}|\tau|+\phi^I) + \frac{\Gamma^I}{\sqrt{N}}\nu^X j^{IX}\bar{j}^{IX}k^I p(\Upsilon\cos(w\sqrt{N}|\tau|+2\phi^I+\Phi)+\frac{1}{4v}\cos(w\sqrt{N}|\tau|))\Big) \\ &\times\ e^{-v\sqrt{N}|\tau|} \end{aligned} \tag{3.112}$$

$$r^{IE}(\tau) = \begin{cases} k^I p\Gamma^I\Big(\nu^E\frac{j^{IE}}{\sqrt{N}}\cos(-w\sqrt{N}\tau+\phi^I) \\ \quad + \frac{\Gamma^E}{\sqrt{N}}\nu^X j^{EX}\bar{j}^{IX}k^E p(\Upsilon\cos(-w\sqrt{N}\tau+\phi^I+\phi^E+\Phi)+\frac{1}{4v}\cos(-w\sqrt{N}\tau+\phi^I-\phi^E))\Big)\times\ e^{v\sqrt{N}\tau}, & \tau\le 0 \\ k^E p\Gamma^E\Big(\nu^I\frac{j^{EI}}{\sqrt{N}}\cos(w\sqrt{N}\tau+\phi^E) \\ \quad + \frac{\Gamma^I}{\sqrt{N}}\nu^X j^{IX}\bar{j}^{EX}k^I p(\Upsilon\cos(w\sqrt{N}\tau+\phi^I+\phi^E+\Phi)+\frac{1}{4v}\cos(w\sqrt{N}\tau+\phi^E-\phi^I))\Big)\times\ e^{-v\sqrt{N})\tau}, & \tau>0 \end{cases} \tag{3.113}$$

where:

$$\begin{aligned} \Phi &\equiv \tan^{-1}\Big(\frac{v}{w}\Big) \\ \Upsilon &\equiv \frac{1}{4\sqrt{v^2+w^2}} \end{aligned} \tag{3.114}$$

3-A7. Comparison with binary networks

We show that the formalism presented here for LIF neurons can be directly compared with the techniques in binary neurons, [Renart et al., 2010]. To show this, let us suppose a simplified example in which the synaptic function $j_{syn}(t)$ is just an exponential function, which in the frequency domain can be written:

$$\tilde{j}_{syn} = \frac{1}{\tau_s^{-1} + i\omega}. \tag{3.115}$$

We start with equation 3.58 and substitute the value of $\tilde{j}_{syn}(\omega)$:

$$\tilde{r}_{ij}^{X\alpha}(\omega) = \tilde{R}_j^{\alpha}(\omega)\frac{1}{\tau_s^{-1} + i\omega}\Big\{m_{ji}^{\alpha X} J_{ji}^{\alpha X} \tilde{a}_i^X(\omega) + \sum_{\substack{(k,\beta)\\ k\neq i}} J_{jk}^{\alpha\beta}\tilde{r}_{ik}^{X\beta}(\omega)\Big\}, \tag{3.116}$$

$$i\omega\tilde{r}_{ij}^{X\alpha}(\omega) = -\tau_s^{-1}\tilde{r}_{ij}^{X\alpha}(\omega) + \tilde{R}_j^{\alpha}(\omega)\Big\{m_{ji}^{\alpha X} J_{ji}^{\alpha X} \tilde{a}_i^X(\omega) + \sum_{\substack{(k,\beta)\\ k\neq i}} J_{jk}^{\alpha\beta}\tilde{r}_{ik}^{X\beta}(\omega)\Big\} \tag{3.117}$$

Taking the Fourier inverse transform and multiplying by τ_s^{-1} one gets:

$$\tau_s\frac{d}{d\tau}r_{ij}^{X\alpha}(\tau) = -r_{ij}^{X\alpha}(\tau) + \Big(R_j^{\alpha} * \Big\{m_{ji}^{\alpha X} J_{ji}^{\alpha X} a_i^X + \sum_{\substack{(k,\beta)\\ k\neq i}} J_{jk}^{\alpha\beta} r_{ik}^{X\beta}\Big\}\Big)(\tau). \tag{3.118}$$

This equation is formally identical to the one in [Renart et al., 2010](SOM, non-numbered equation above eq. (19)) when τ =0. Similarly one can show the analogy for recurrent-recurrent cross-correlations in binary and LIF networks.

Appendix 3-B. Linking current and membrane potential correlations

Here we will obtain a relationship between membrane potential and total current cross-covariances.

In the LIF model the input current and the membrane potential of one neuron in which the spike mechanism is disabled are related via a convolution.

$$V_i^\alpha(t) \quad = \quad (f_{VI} * I_i^\alpha)(t), \tag{3.119}$$

where $f_{VI}(t) = \Theta(t)\tau_m^{-1}e^{-\frac{t}{\tau_m}}$. We have seen that the decorrelation of the membrane potentials of spiking neurons is very similar to the one of non-spiking ones (fig. 3.2k), so we can describe membrane potential cross-covariances by using formulae obtained for neurons that do not fire. The cross-covariance between the membrane potentials of neurons (i, α) and (k, β) can be expressed in terms of the cross-covariance of the total currents afferent to those neurons (for more details see [Tetzlaff et al., 2008])

$$c_{V,\,ik}^{\alpha\alpha'}(\tau) \quad = \quad < \delta V_i^\alpha(t)\delta V_k^{\alpha'}(t+\tau) >= (\phi_{VI} * c_{ik}^{\alpha\alpha'})(\tau), \tag{3.120}$$

where $\phi_{VI}(\tau) = \int f_{VI}(\tau)f_{VI}(\tau + s)\mathrm{d}s$, i.e.

$$\phi_{VI}(\tau) \quad = \quad \frac{e^{-\frac{|\tau|}{\tau_m}}}{2\tau_m} \tag{3.121}$$

Averaging eq. 3.120 over neurons in populations α and α', we obtain:

$$c_V^{\alpha\alpha'}(\tau) \quad = \quad (\phi_{VI} * c^{\alpha\alpha'})(\tau) \tag{3.122}$$

At $\tau = 0$, c_V is, by definition, the population-averaged zero-lag cross-covariance of the membrane potentials between neurons in populations α and α'. Under the parameterization in eq. 3.33, one obtains the membrane potential zero-lag cross-covariance in terms of the parameters A_N, ω_N and τ_N.

$$CC_V \propto A_N \frac{\tau_m + \tau_N}{\tau_m^2 \tau_N \omega_N^2} \left(1 + \left(\frac{\tau_m + \tau_N}{\omega_N \tau_N \tau_m}\right)^2\right)^{-1}, \tag{3.123}$$

which is eq. 3.34 in the *Results* section.

Appendix 3-C. Linking membrane potential and spike-count cross-correlation coefficients

The description employed in Appendix 3-A, explains in a self-consistent way how spike-counts and total currents of pairs of neurons are decorrelated. The reason why the behaviour of membrane potentials are not needed in the self-consistent theory previously explained is the following. By using the linear response approximation in eq. 3.50, we link the effect of incoming currents to the generation of spike trains bypassing the effect of the membrane filter. Just for completeness, we will explain here how the cross-correlations in the membrane potentials are transmitted to the spike-counts. It is not the intention of this appendix to explain this in a rigorous mathematical way, but to qualitatively show that the cross-correlation coefficients of both magnitudes should have the same scaling. Here we use a statistical model proposed by [Dorn and Ringach, 2003] to relate membrane potential and spike-count cross-correlation coefficients. To make the exposition clearer, we use a notation different from the one used in the *Results* section.

The model assumes that the joint distribution of the membrane potentials $V_i^\alpha \equiv a$ and $V_j^\beta \equiv b$ of cells (i,α) and (j,β) can be written, at a fixed time, as

$$g(a,b) \;=\; \frac{1}{2\pi mq\sqrt{1-c^2}} e^{-\frac{1}{2(1-c)}\left(\frac{(a-<a>)^2}{m}+\frac{(b-<b>)^2}{q}-\frac{2c(a-<a>)(b-<b>)}{mq}\right)} \qquad (3.124)$$

where $\nu_i^\alpha \equiv m$ and $\nu_j^\beta \equiv q$ are the cells' firing rates and $c \equiv \overline{CC}_V$). The probability of finding both a and b above V_{th} is denoted as P and interpreted as the probability of both neurons firing together in a small window. This probability is

$$\begin{aligned} P &= \frac{1}{2\pi\sqrt{1-c^2}} \int_{a'_{th}}^{\infty}\int_{b'_{th}}^{\infty} e^{-\frac{1}{2(1-c)}(a'^2+b'^2-2ca'b')}\mathrm{d}a'\mathrm{d}b' = \\ &= M(a'_{th})M(b'_{th}) + \frac{c}{2\pi}\, e^{-\frac{a'^2_{th}+b'^2_{th}}{2}} + O(c^2) \end{aligned} \qquad (3.125)$$

where $M(a'_{th})$ and $M(b'_{th})$ are the firing probability of the two neurons

$$M(a'_{th}) = \frac{1}{2}\mathrm{erfc}\left(\frac{a'_{th}}{\sqrt{2}}\right) \quad ; \quad M(b'_{th}) = \frac{1}{2}\mathrm{erfc}\left(\frac{b'_{th}}{\sqrt{2}}\right) \qquad (3.126)$$

Besides, $a' \equiv (a- < a >)/m$, $b' \equiv (b- < b >)/q$, $a'_{th} = (V_{th}- < a >)/m$, $b'_{th} = (V_{th}- < b >)/q$ and $\mathrm{erfc}(x) = \frac{2}{\sqrt{\pi}}\int_x^\infty e^{-t^2}\mathrm{d}t$.

The spike-count correlation coefficient, $\overline{CC}_{sc}(T)$, can be obtained form P, $M(a'_{th})$ and $M(b'_{th})$ (see details in [Dorn and Ringach, 2003])

$$\overline{CC}_{sc}(T) \;=\; M(a'_{th}, b'_{th})\; c \tag{3.127}$$

where $M(a'_{th}, b'_{th})$ is

$$M(a'_{th}, b'_{th}) \;\equiv\; \frac{1}{2\pi} \frac{e^{-\frac{{a'_{th}}^2 + {b'_{th}}^2}{2}}}{\sqrt{M(a'_{th})(1 - M(a'_{th}))M(b'_{th})(1 - M(b'_{th}))}}. \tag{3.128}$$

Let us see how eq. 3.127 determines the scaling of $\overline{CC}_{sc}(T)$ with network size. Parameters $a'_{th} \equiv (V_{th} - < V_i^{\alpha} >)/\nu_i^{\alpha}$ and $b'_{th} \equiv (V_{th} - < V_j^{\beta} >)/\nu_j^{\beta}$ do not depend on network size. To see this, remember that the firing rates are $O(1)$ (fig. 3.2a). As long as the input current does not depend on N (fig. 3.2b), the mean membrane potentials are also $O(1)$. Thus, $M(a'_{th}, b'_{th})$ in eq. 3.127, which only depends on these parameters, does not scale with network size. Therefore, $\overline{CC}_{sc}(T)$ scales in the same way as $c \equiv \overline{CC}_V$.

Eqs. 3.127-3.128 also give the dependence of the cross-correlation coefficient of the spike-count on the average value of the membrane potentials. Expanding $M(a'_{th})$ and $M(b'_{th})$ in powers of a'_{th} and b'_{th} respectively, we arrive to the relationship:

$$\overline{CC}_{sc}(T) \;\simeq\; \frac{2}{\pi}\left(1 - \frac{\pi - 2}{2\pi}\left(a'^2_{th} + b'^2_{th}\right)\right)\; c, \tag{3.129}$$

This last relationship shows that when the temporal-averaged membrane potentials get far from the spiking threshold, the transmission of correlations to spiking activity is less efficient. This is in agreement with previous studies [de la Rocha et al., 2007, Cohen and Kohn, 2011]. It is important to note that the scaling of the spike-count cross-correlation coefficients is not affected by this effect.

Appendix 3-D. Estimating the function $(R^\alpha * j_{syn})(t)$

In this appendix we focus on estimating the function $K^\alpha(\omega) \equiv (R^\alpha * \tilde{j}_{syn})(t)$ that appears in the computation of spike train cross-covariance functions (see Appendix 3-A). More specifically, we will determine the parameters k^α and $\bar{\tau}^\alpha$ assuming the approximation in eq. 3.98. To do this, we look at the firing rate of a neuron when a small current $(j_{syn} * Y)(t)$ is applied. In the linear response approximation the firing rate of the neuron is:

$$\begin{aligned} \nu_i^\alpha(t) &= \nu_i^{\alpha\,(0)} + \Big(R_i^\alpha * (j_{syn} * Y)\Big)(t) \\ &= \nu_i^{\alpha\,(0)} + \Big((R_i^\alpha * j_{syn}) * Y\Big)(t) \\ &= \nu_i^{\alpha\,(0)} + \Big(K_i^\alpha * Y\Big)(t) \end{aligned} \tag{3.130}$$

where $\nu_i^{\alpha\,(0)}$ is the firing rate of the neuron evoked by the background noise. Averaging over neurons one has:

$$\nu^\alpha(t) = \nu^{\alpha\,(0)} + \Big(K^\alpha * Y\Big)(t) \tag{3.131}$$

If one assumes that the approximation in eq. 3.98 remains valid and takes $Y = X_0\cos(\omega t)$, it is easy to show that:

$$\nu^\alpha(t) = \nu^{\alpha\,(0)} + \Psi^\alpha(\omega)\cos(\omega t + \rho^\alpha(\omega)) \tag{3.132}$$

with:

$$\Psi^\alpha(\omega) = \frac{k^\alpha}{\sqrt{(\bar{\tau}^\alpha)^{-2} + \omega^2}} X_0 \tag{3.133}$$

$$\tan(\rho^\alpha(\omega)) = -\bar{\tau}^\alpha \omega \tag{3.134}$$

Last equations suggest a possible way to compute the parameters k^α and $\bar{\tau}^\alpha$: we first filter a small perturbation of the form $Y = X_0\cos(\omega t)$ through the synaptic kernel, inject the resulting current to a set of neurons and measure the amplitude and the phase of their fluctuating population-averaged firing rate. Doing this in a network as the one we have been studying is, however, technically difficult. The first problem comes from the fact that one needs an ensemble of neurons over which one can average their firing responses. Besides, because the firing rates of the neurons are low, one finds that, in

order to get enough data to estimate $\nu^\alpha(t)$, very large simulation times are needed, which is computationally very costly, especially for large networks. As we have seen, the firing activity of neurons in the network is almost Poisson. Besides, the neurons fire almost independently. We thus, propose an alternative way to estimate the parameters k^α and $\bar{\tau}^\alpha$. We simulate a two layer feedworward network. In the first layer we have $pN = pN_E = pN_X$ external and excitatory and pN_I inhibitory neurons firing in an independent Poissonian way with the corresponding average firing rates obtained when simulating the recurrent network (fig. 3.2a). Neurons in the second layer are excitatory and inhibitory units of the LIF type. They have the same parameters as the ones for the recurrent network described in *Methods*. All the neurons in the first layer connect to each of the neurons in the second one. The synaptic couplings are drawn from the same distributions described in *Methods*. Neurons in the second layer do not connect to each other. We now inject the small current $(j_{syn} * Y)(t)$ to the neurons in the second layer and look at their population-averaged firing rate [8] Notice that, although we still need to average over a set of neurons, the computational cost is much smaller than before, because of the fact that we deal with a feedforward network.

For a given value of ω we superimpose the different cycles of the resulting fluctuating population-averaged firing rate and average them. The resulting function is finally fitted to $\nu^\alpha(t) = \nu^{\alpha\,(0)} + \Psi^\alpha(\omega)\cos(\omega t + \rho^\alpha(\omega))$ and k^α and $\bar{\tau}^\alpha$ are calculated from the plots of $\Psi^\alpha(\omega)$ and $\rho^\alpha(\omega)$ (see details in the caption of fig. 3.11)

[8] In order for the linear approximation to be valid, the current $(j_{syn} * Y)(t)$ has to be small. We have chosen the parameter X_0 such that the peak value of $(j_{syn} * Y)(t)$ is much smaller than the mean and the standard deviation of the total current arriving to each of the neuron in the second layer. Besides, we verified that when increasing the values of X_0, the amplitude of the resulting fluctuating firing rate increases linearly.

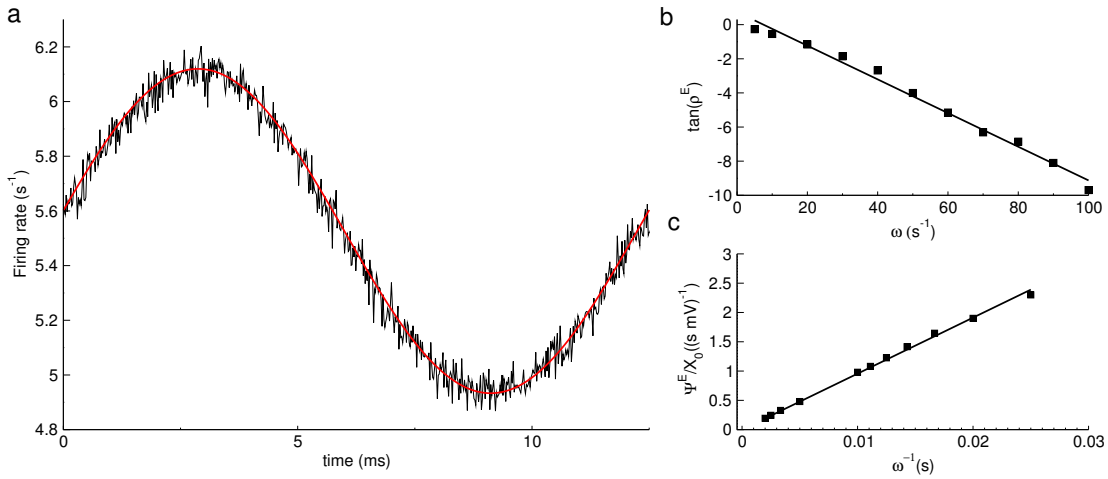

Figure 3.11: **Estimate of the function $\tilde{K}^{\alpha}(\omega)$. Computation of the parameters k^E and $\bar{\tau}^E$ in eq. 3.38. a)** Black: Population-averaged firing rate when a perturbation $Y = X_0\cos(\omega t)$ is applied (ω= 80 Hz). Red line corresponds to a least squares fit to eq. 3.132. **b)** Computation of $\bar{\tau}^{\alpha}$ from the slope of the function $\tan(\rho^E(\omega))$. The black line corresponds to the linear regression computed with the data from the feedforward network simulation (squares). **c)** Computation of k^E. From eq. 3.133, $\Psi^E(\omega)/X_0 \simeq \frac{k^E}{\omega}$ for large values of ω. The black line corresponds to the linear regression computed with the data from the feedforward network simulation (squares). The slope of this function gives the value of k^E . **Details of the simulation**: Simulation time = 200 s, X_0 = 1 mV , # LIF cells = 10000 , # Poisson cells: $pN = pN_X = pN_E$ excitatory and external cells and $pN_I = \frac{pN}{4}$ inhibitory cells (N = 32000). The values of the firing rates of Poisson neurons are given by the average firing rates in fig. 3.2a for this value of N.

Appendix 3-E. Cancellation of common input correlations by recurrent feedback

Here we explicitly show that the negative correlations generated by the network dynamics reduce the positive correlations induced by the common inputs. We calculate the cross-covariance functions of networks on which we could isolate the effect of the shared input and of the recurrent feedback. We follow a procedure introduced in Renart et al., 2010.

To isolate the effect of common inputs, we simulate a feedforward two-layer network. In the first layer, neurons of each type (E, I, X) fire as independent Poisson processes with the firing rates in fig. 3.1b. The number of these neurons are in the same ratio as in the original recurrent network we have studied ($N \equiv N_X = N_E = 4N_I$). Neurons in the second layer have the same dynamics as the original network and do not connect to each other. Neurons in the first layer project to neurons in the second layer following the same probabilistic rule as the external neurons did for the previously simulated networks. In this way, the only source of correlation in neurons from the second layer comes from the amount of shared input. As we see in fig. 3.12 (dashed line), the cross-covariance function of neurons in second layer is positive and its peak value is big.

To study the correlations induced by the recurrent dynamics, we simulate two read-out populations. Neurons in each population receive inputs exclusively from one half of the neurons in the original recurrent network. The external population is also divided into two subpopulations which neurons projects only to one of the these read-out populations. Thus, by construction, neurons in different read-out populations do not share any input. We calculate the cross-covariance function of neurons in different read-out populations, which will reflect the correlations induced only by the recurrent network dynamics. Fig. 3.12 (dashed-dotted line) shows that cross-covariance induced by the dynamics of the network are negative.

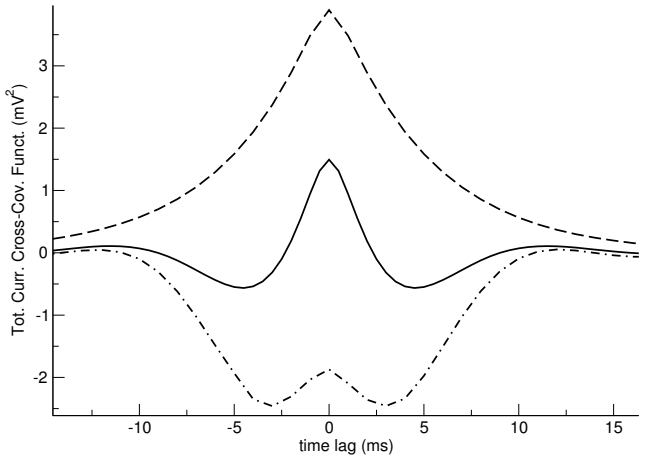

Figure 3.12: **Cancellation of common input correlations by recurrent dynamics.** Population-averaged cross-covariance functions of the total incoming current to an excitatory-excitatory pair of neurons when they receive only feedforward inputs with some common currents (dashed line) and when they do not receive any common input (dashed-dotted line) ($N = 8000$). Solid line corresponds to the total current cross-covariance function in fig. 3.3a ($N = 8000$).

Appendix 3-F. A study on the *sparse* scaling

In the literature, the sparse limit of randomly connected networks is very often employed to analyze the network spiking activity [van Vreeswijk and Sompolinsky, 1996, 1998]. In such a limit, the number of inputs afferent to a neuron remains fixed as the network size increases, so the probability of connection decays as $p = \frac{p_0}{N}$, p_0 being $O(1)$. In order to preserve the mean and standard deviation of the total afferent current to a neuron, the synaptic efficacies J's have to remain constant as N varies. In this appendix we study this regime by means of simulations and analytical tools.

In the sparsely connected regime, neural activities cross-correlations behave as $O(1/N)$ by construction (fig. 3.13a) in contrast to the densely connected case, where cross-correlations decrease with N as a consequence of a dynamical phenomenon consisting in the tracking of excitatory fluctuations by the inhibitory activity. Notice that total current and current components zero-lag cross-covariances and cross-correlation coefficients scale in the same way ($O(1/N)$)(figs. 3.13b,c).

It is easy to see that no fast time-scales are generated in the sparse limit. To see this analytically, notice that eqs.3.56 and 3.59 for the spike train cross-covariance functions are still valid because to deduce them we only assumed a weak degree of cross-correlation, which, by construction, also occurs in this limit. Replacing p by p_0/N and $J^{\beta\alpha}$ by $j^{\beta\alpha}$ ($\bar{j}^{\beta\alpha} = \frac{N_\alpha}{N}$) in eqs. 3.56 and 3.59 we arrive to:

$$\tilde{r}_+^{\alpha\beta}(\omega) = \tilde{R}^\beta(\omega)\tilde{j}_{syn}(\omega)p_0\Big\{\frac{j^{\beta\alpha}}{N}\tilde{a}^\alpha(\omega) + \Big(\bar{j}^{\beta X}\tilde{r}^{\alpha X}(\omega) + \sum_{\alpha'\in E,I}\bar{j}^{\beta\alpha'}\tilde{r}_+^{\alpha\alpha'}(\omega)\Big)\Big\}, \quad (3.135)$$

$$\tilde{r}^{X\alpha}(\omega) = \tilde{R}^\alpha(\omega)\tilde{j}_{syn}(\omega)p_0\Big\{\frac{j^{\alpha X}}{N}\tilde{a}^X(\omega) + \sum_{\alpha'\in E,I}\bar{j}^{\alpha\alpha'}\tilde{r}^{X\alpha'}(\omega)\Big\} \quad (\alpha,\beta = E,I) \quad (3.136)$$

For the sake of simplicity, we focus now on eq. 3.136. Assuming the same approximation for $\tilde{R}^\alpha(\omega)\tilde{j}_{syn}(\omega)$ that we used in *Results*, section 3.4 ($\tilde{R}^\alpha(\omega)\tilde{j}_{syn}(\omega) = \frac{k^\alpha}{\bar{\tau}_\alpha + i\omega}$) we have:

$$i\omega\tilde{r}^{X\alpha}(\omega) = -\bar{\tau}_\alpha^{-1}\tilde{r}^{X\alpha}(\omega) + k^\alpha p_0\Big\{\frac{j^{\alpha X}}{N}\tilde{a}^X(\omega) + \sum_{\alpha'\in E,I}\bar{j}^{\alpha\alpha'}\tilde{r}^{X\alpha'}(\omega)\Big\}. \quad (3.137)$$

To solve the last equation, we employ a similar technique to the one described in Appendix 3-A6. We propose an Ansatz of the form:

$$\tilde{r}^{X\alpha}(\omega) = \Big\{C_0\frac{u^\alpha}{-\lambda + i\omega} + C_1\frac{u^{\alpha\,*}}{-\lambda^* + i\omega}\Big\}k^\alpha p_0\frac{j^{\alpha X}}{N}\tilde{a}^X(\omega) \quad (3.138)$$

where u^α, $u^{\alpha\,*}$ are now the eigenvectors of the matrix $\Lambda^{\alpha\alpha'} \equiv p_0 k^\alpha \bar{J}^{\alpha\alpha'} - \bar{\tau}_\alpha^{-1}\delta_{\alpha\alpha'}$ and λ, λ^* the associate eigenvalues [9]. Notice that λ and λ^* are $O(1)$. Proceeding as explained for the case of densely connected networks (see Appendix 3-A6) one can find the values of C_0 and C_1 (as before, it turns out that $C_1 = C_0^*$). Finally, one can show that in the time domain the spike train cross-covariance functions read as:

$$r^{XE}(\tau) = \Theta(\tau)\Gamma^E \nu^X k^E p \frac{j^{\alpha E}}{N} e^{-v\tau}\cos(w\tau + \phi^E) \tag{3.139}$$

$$r^{XI}(\tau) = \Theta(\tau)\Gamma^I \nu^X k^I p \frac{j^{\alpha I}}{N} e^{-v\tau}\cos(w\tau + \phi^I) \tag{3.140}$$

where u and v are the real and imaginary parts of λ and $\Gamma^\alpha \equiv \sqrt{(2\mathrm{Re}(C_0 u^\alpha))^2 + (2\mathrm{Im}(C_0 u^\alpha))^2}$ and $\phi^\alpha \equiv \tan^{-1}\left(\frac{\mathrm{Im}(C_0 u^\alpha)}{\mathrm{Re}(C_0 u^\alpha)}\right)$. Notice the overall factor $1/N$ in eqs. 3.139 and 3.140 and the fact that no fast time-scale appears. One can show, analogously, that $r^{\alpha\beta}(\tau)$ $(\alpha, \beta = E, I)$ are also weighted by an overall $1/N$ factor and that no fast time-scale appears. Consequently, the population-averaged total current cross-covariance functions do not present any fast time-scale either. To show this, we fitted them in the same way as in the densely connected limit, eq. 3.33 (fig. 3.13c). The parameters τ_N and ω_N remain constant (fig.3.13 d,e) as N increases. This has consequences on the way the scaling of cross-correlations is transmitted from synaptic currents to membrane potentials. In dense networks, the different scaling of total current and membrane potential zero-lag cross-covariances can be explained by the shape transformation of the cross-covariance functions,eq. 3.34. The effect of this change can be summarized by the presence of the characteristic time $(\tau_N \omega_N^2) \sim N^{-0.45}$ in that equation. On the other hand, in the sparse limit, zero-lag cross-covariances of both currents and membrane potentials decay as $O(1/N)$ (fig. 3.13b,c) so the transformation from current to membrane potential zero-lag cross-covariances does not require the existence of a fast characteristic time constant.

Finally, we consider it worth to focus on the scaling employed in Ginzburg and Sompolinsky, 1994. There, the probability of connection p does not depend on N and the synaptic couplings scale as $\sim 1/N$. Notice that in eqs. 3.56 and 3.59 the probability of connection p and the synaptic couplings $J^{\beta\alpha}$ always appear as a product $pJ^{\beta\alpha}$. Thus, the conclusions established before for the sparse limit also apply for this case.

[9] We have assumed, as in Appendix 3-A6, that the eigenvalues have non-null real and imaginary parts

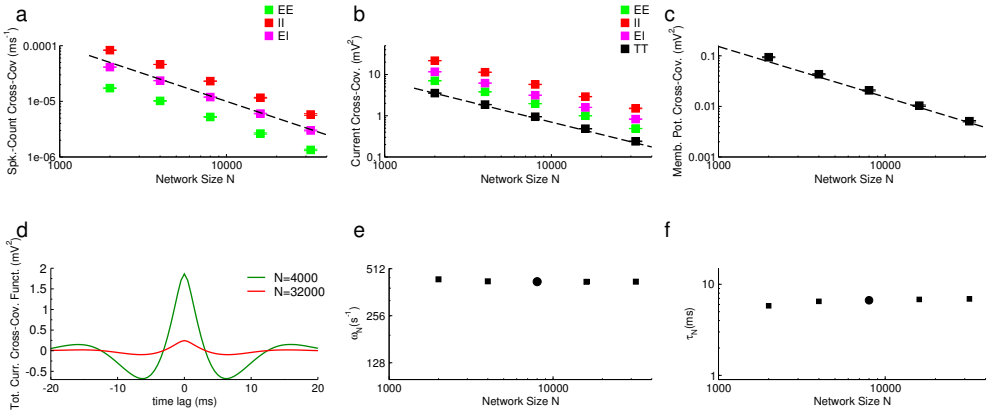

Figure 3.13: **Sparsely connected networks.** The results in this figure correspond to simulations in which the neuron parameters are the same as the one described in *Methods* section, except synaptic couplings that do not scale with N and p that scales as $p = \frac{p_0}{N}$. J's and p_0 are chosen such that the network with $N = 4000$ is the same as the one of the same size in figure 3.2. **a)** Population-averaged cross-covariances of the spike-count ($T = 80$ ms). **b)** Absolute value of the population-averaged zero-lag cross-covariances between the current components and between the total currents afferent to a pair of excitatory neurons. **c)** Absolute value of the population-averaged correlation coefficients between the current components and between the total currents afferent to a pair of excitatory neurons. Same color conventions as in figure 3.2. **d)** Population-averaged total current cross-covariance function for two network sizes. **e)** Dependence of ω_N and **f)** τ_N with network size. Circle stands for a network with the same values of synaptic couplings as the one of the same size in figure 3.2.

Appendix 3-G. Computing spike-count cross-covariances in different time windows

We have measured spike-count cross-covariances in different time windows. For small time windows (T=0.25 ms) (fig. 3.14a) the spike-count cross-covariances decay approximately as $O(\epsilon)$. For time windows $T \geq 20$ ms the scaling is $O(\epsilon^2)$ and the theoretical limit is asymptotically achieved (fig. 3.14b,c). As explained in Appendix 3-A, the theory is exact in the limit of $N \to \infty$. Dealing with networks of finite size the theory is only valid for slow frequencies of $\tilde{r}^{\alpha\alpha'}(\omega)$. Notice that $\tilde{r}^{\alpha\alpha'}(0)$ corresponds to the integral of $r^{\alpha\alpha'}(\tau)$ for all the values of τ, a magnitude closely related to the spike-count cross-covariances in infinite time windows. Because cross-correlations are concentrated at small time scales, the computation of infinite integrals can be accurately predicted from time windows of the order of $T \geq 20$ ms (fig. 3.14d). The limit $T \geq$20 ms should not be thought of as one fundamental time-scale of the problem. In fact, because spike train cross-covariance functions present a fast time-scale that increase with N one can conclude that as the networks get larger estimations of spike-count cross-covariance for smaller values of T will be well predicted.

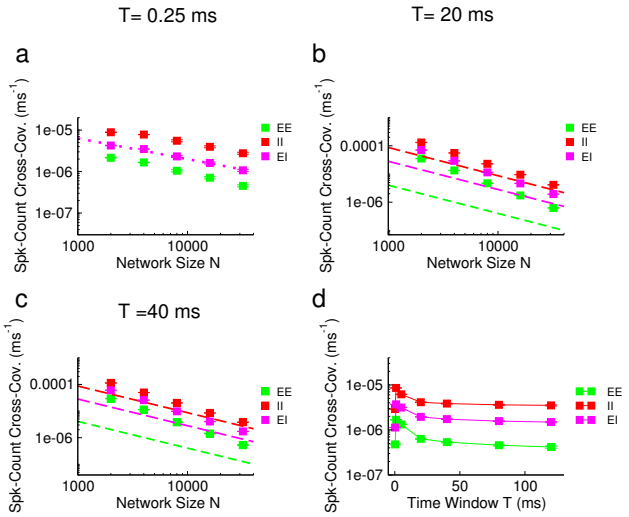

Figure 3.14: **Spike-count cross-covariances vs T. a,b,c.** Scaling of the population-averaged cross-covariances of the spike-count for different values of the time window T. **a)** $T = 0.25$ ms. **b)** $T = 5$ ms. **c)** $T = 40$ ms **d)** Dependence of spike-count cross-covariances on the time window for a network with $N = 32000$ neurons. Same color code as in fig. 3.2.

Chapter 4

Decorrelation in LIF networks with slow synaptic kinetics

4.1 Introduction

In the previous chapter we have shown how decorrelation in a neural network of LIF neurons with current-based synapses can occur. In biological networks, the transmission of a spike to a cell produces a change in its conductance. In this situation, the effective membrane time constant is dramatically reduced when the number of incoming inputs is large [Bernarder et al., 1991, Pare et al., 1998, Hirsch et al., 1998, Borg-Graham et al., 1998, Destexhe et al., 1999, Anderson et al., 2000b, Destexhe et al., 2001, Kuhn et al., 2004, Moreno-Bote and Parga, 2005, Léger et al., 2005]. In that scenario, our previous model, in which the synaptic time constants are faster than the membrane potential characteristic time, may not be accurate.

An alternative consists in imposing membrane time constants smaller than synaptic time constants, to mimic the effect of large number of inputs [Moreno-Bote and Parga, 2004]. This is the perspective we will adopt throughout this chapter. In the analytical calculations we will employ an adiabatic approximation [Moreno-Bote and Parga, 2004, 2006, 2010] which describes the regime in which the synaptic time constant is comparable or larger than the membrane time constant.

In this case, we will discuss a recurrent network containing only inhibitory neurons although the theory presented here is easy to extend to recurrent networks of excitatory and inhibitory neurons. The study is biologically relevant because networks of inhibitory neurons can be found in the basal ganglia, where spiking cross-correlations have been reported to be small [Nini et al., 1995, Raz et al., 2000, Bar-Gad et al., 2003,

Magill et al., 2000].

4.2 Methods

4.2.1 Model

4.2.1.1 Network model

The network consists of two modules, fig. 4.1a: a recurrent population, with N inhibitory (I) leaky integrate-and-fire neurons (LIF) and a population of external excitatory neurons of the same size. N will be varied in order to perform a scaling analysis. Neurons in the recurrent network are randomly connected with connection probability p= 0.2. External afferents are connected to cells in the network with the same probability p. This probability will be kept fixed as N varies (from 1050 to 32000) in order to work in the regime of *densely* connected networks.

4.2.1.2 External neuron model

Each external neuron fires independently with Poisson statistics and a mean firing rate of 2.5 Hz. The firing rate of the external neurons is kept constant except in section 4.3.3 *Effect of weakly correlated external neurons*. In that section, cross-correlations in the activity of external neurons are generated by means of an identical fluctuating firing rate that evolves according to an Ornstein-Uhlenbeck process of the form:

$$\tau_{OU}\frac{d\nu^X(t)}{dt} = \nu^X - \nu^X(t) + \sigma_{OU;N}\sqrt{\frac{2}{\tau_{OU}}}\zeta(t), \tag{4.1}$$

where $\nu^X \equiv < \nu^X(t) > = 2.5$ Hz is the temporal average of the external firing rate, $\tau_{OU} = 15.9$ ms is the correlation time, $\sigma_{OU;N}$ is the standard deviation of the rate and $\zeta(t)$ is a white noise with unit variance and zero mean. In order for the variance of the external current not to be arbitrarily large, we need to scale $\sigma^2_{OU;N} \equiv \frac{\sigma^2_{OU}}{N}$. We take $\sigma_{OU;N} = 0.8$ Hz for a network with $N = 32000$.

4.2.1.3 Recurrent neuron model

Recurrent neurons are modeled as follows. Below a critical value, V_{Th}, the membrane potential of neuron i in population I, V_i^I, evolves according to the following equation:

$$\tau_m \frac{dV_i^I(t)}{dt} = -(V_i^I(t) - V_L) + I_i^I(t), \tag{4.2}$$

where $I_i^I(t)$ is the pre-synaptic current to neuron (i, I) due to the presence of the other pre-synaptic neurons. When $V_i^I(t)$ reaches the value V_{Th} a spike is emitted and the membrane potential is reset to the value $V_i^I = V_{Reset}$, where it remains for a time τ_{ref}. The parameters employed for the simulation are, unless explicitly mentioned: $\tau_m = 2.5$ ms, V_L =10 mV, V_{Reset} =16 mV , V_{Th} =20 mV.

4.2.1.4 Synaptic currents

The spike train emitted by neuron (i, α) $(\alpha = X, I)$, denoted as $y_i^\alpha(t)$, is

$$y_i^\alpha(t) = \sum_k \delta(t - t_i^{\alpha,k}), \tag{4.3}$$

where $t_j^{\alpha,k}$ is the spike time of the k-th action potential fired by the neuron. Spike trains are filtered through synapses as:

$$\tau_s \frac{ds_i^\alpha(t)}{dt} = \tilde{\tau} y_i^\alpha(t) - s_i^\alpha(t), \tag{4.4}$$

where $s_i^\alpha(t)$ is the filtered spike train, τ_s= 20 ms is the synaptic decay time constant and the factor $\tilde{\tau}$= 1 ms ensures that the area under $s(t)$ is constant regardless of the value of τ_s. The dynamics defined by eq. 4.4 is equivalent to:

$$s_i^\alpha(\tau) = \int_{-\infty}^{\infty} \mathrm{d}t j_{syn}(t) y_i^\alpha(\tau - t), \tag{4.5}$$

where $j_{syn}(t) = \frac{\tilde{\tau}}{\tau_s}\Theta(t)e^{-\frac{t}{\tau_s}}$ ($\Theta(t)$ is the Heaviside step function). The current generated by a spike can be calculated as the product of the filtered spike and the synaptic coupling. The total pre-synaptic current afferent to a cell (i, I) is then:

$$I_i^I(t) = \sum_{(j,\alpha)} m_{ij}^{I\alpha} J_{ij}^{I\alpha} s_j^\alpha(t), \tag{4.6}$$

where the synaptic efficacies, $J_{ij}^{I\alpha}$, have average values: $J^{IX} = \frac{j^{IX}}{\sqrt{N}} = \frac{437.4}{\sqrt{N}}$ mV and $J^{II} = \frac{j^{II}}{\sqrt{N}} = -\frac{416.6}{\sqrt{N}}$ mV. Notice that for a network of $N = 10000$ neurons the magnitudes of the amplitudes of IPSPs and EPSPs are some tenths of mV. Synaptic efficacies

take their values from Gaussian distributions. The standard deviations of these distributions are half of the value of their mean but they were truncated at two standard deviations in order to prevent changes of sign. We will denote by $J^{(2)\,\alpha\alpha'}$ the second moment of the distributions of synaptic efficacies:

$$\begin{aligned} J^{(2)\,\alpha\alpha'} &\equiv [(J_{ij}^{\alpha\alpha'})^2] \\ &= \frac{1}{J^{\alpha\alpha'}}\sqrt{\frac{2}{\pi}}\int_{-J^{\alpha\alpha'}}^{J^{\alpha\alpha'}} x^2 e^{-2\frac{(x-J^{\alpha\alpha'})^2}{(J^{\alpha\alpha'})^2}}\,\mathrm{d}x. \end{aligned} \tag{4.7}$$

It is easy to show that $J^{(2)\,\alpha\alpha'} \sim O(1/N)$. We find it useful to define the $O(1)$ magnitude $j^{(2)\,\alpha\alpha'}$:

$$J^{(2)\,\alpha\alpha'} \equiv \frac{j^{(2)\,\alpha\alpha'}}{N} \tag{4.8}$$

4.2.2 Parameter values

In the following table we summarize the default values of all the model parameters:

τ_m	2.5 ms
τ_s	20 ms
τ_{ref}	1 ms
V_L	10 mV
V_{Th}	20 mV
V_{Reset}	16 mV
j^{II}	-416.6 mV
j^{IX}	437.4 mV
ν^X	2.5 Hz
p	0.2

Table 4.1: Values of the parameters

4.2.3 Current and spiking statistics

Statistical measures were defined in chapter 2.

4.2.4 Jittered spike trains

Jittered spike trains were constructed by adding to each spike time an independent random variable drawn from a uniform distribution in the interval [-0.5, 0.5] s. By doing this one eliminates the cross-correlations between them in time scales shorter than 0.5 s. As we will see, in the networks we simulate cross-correlations are concentrated at time-scales of the order of some tens of ms, thus, jittered spike trains generated in this way are uncorrelated.

For each simulation, we generated 100 surrogate data sets where spike trains were jittered in the described way. The histogram of spike-count cross-covariances of jittered spike trains in fig. 4.5b (grey lines) was computed by averaging the corresponding histograms obtained for each of the surrogate data sets of a given simulation.

4.2.5 Simulation

Equations for the evolution of the membrane potential (eq. 4.2) and pre-synaptic currents (eq. 4.4) were integrated using Euler's method, with an integration time step $\mathrm{d}t = 0.05$ ms. Simulated network sizes were (N = Number of external neurons=Number of inhibitory neurons: $N = 1050, 2000, 4000, 8000, 16000, 32000$.

For each run, simulation time was $S = 500$ s. We recorded the pre-synaptic current traces of 40 inhibitory neurons for the last 200 s. We also recorded the spike times of 1000 neurons in each population during the whole simulated time, except for the networks with $N = 16000$ and $N = 32000$, in which the number of neurons was 2000. Population-averaged magnitudes were computed with these data. Figures showing the scaling of certain magnitudes with N were computed by averaging over 20 simulations with different realizations of the connectivity matrix. Error bars correspond to the standard errors.

Simulation and data analysis were performed with custom codes written in C and Matlab. Spectral analysis was performed with the Chronux toolbox.

4.3 Results

Under *in vivo* conditions the effective membrane integration time is rather short [Pare et al., 1998, Borg-Graham et al., 1998, Hirsch et al., 1998, Destexhe et al., 1999,

2001, Anderson et al., 2000b, Léger et al., 2005] in comparison with characteristic times of synaptic filtering. Input integration at a timescale shorter than that of synaptic filtering has some interesting consequences [Moreno-Bote and Parga, 2004, 2006, 2010]. In order to study the decorrelation mechanisms in networks with this kind of filters, we have simulated a recurrent network of $N = 32000$ inhibitory neurons receiving input from an external population of the same size (fig. 4.1a). External neurons connect to recurrent neurons and recurrent neurons connect to each other in a random way with mean connectivity $p = 0.2$, which results in the same fraction of common inputs. Notice that common inputs come both from the external and recurrent connections. The values of the synaptic and membrane time constant mimic the experimental situation (see section 4.2, *Methods*, for more details). Notice that, during the timescale of the membrane dynamics, the slowly evolving input currents can be considered *frozen* at a constant value (fig. 4.1b). This gives rise to rather irregular firing patterns consisting in bursts of spikes, occurring when the input current becomes sufficiently large (see rasters in fig. 4.1c and membrane potential traces in fig. 4.1d).

Fig. 4.1a illustrates another important feature of the network: the balance between the recurrent and external currents. Although, external (blue) and recurrent (red) input currents take large values, the total incoming current (black) is small. This results in a very irregular activity pattern characterized by a large CV of the ISIs (fig. 4.1e) and a long-tailed distribution of firing rates across the inhibitory population (fig. 4.1f).

Notice that the firing patterns of different neurons seem quite independent (figs. 4.1c). One can think that this could be due to a very small amount of common input. To discard this idea we have simulated networks with different values of the mean connectivity (fig. 4.1g). We have calculated the cross-correlation coefficients of the current afferent to pairs of neurons. We find it relevant to decompose the current into its external (excitatory) and inhibitory components. Current components cross-correlation coefficients are of the same order as the mean connectivity. However, the cross-correlation coefficients of the total incoming currents are two orders of magnitude smaller, which shows that the decorrelation phenomenon is not an artifact of the small amount of common inputs.

In the following sections we will explain the decorrelation mechanism that leads to an *asynchronous* state as the one in fig. 4.1. Because the synaptic characteristic time is large (compared to the membrane potential time scale) and currents are *frozen* at time scales of the order of τ_m, we will employ the adiabatic approximation [Moreno-Bote

and Parga, 2004, 2006, 2010] to calculate firing rates and cross-covariance functions. Briefly, this technique takes advantage of the fact that current fluctuations are slow compared to the evolution of the membrane potential, so the instantaneous effect of them on post-synaptic cells can be well approximated assuming their value is constant and averaging over their distribution.

As we will see in the following sections, the network in fig. 4.1 is in an *asynchronous* state, thus, the conclusions derived in chapter 2 apply[1]. The structure of this chapter is the following: first, we will characterize some variables, such as input currents and firing rates, proving that the adiabatic approximation is appropriate. We will continue by showing the predictions concerning pairwise cross-correlations. Finally, we will show some predictions about macroscopic magnitudes for large size networks. We omit most of the mathematical derivations postponing them to the appendices at the end of this chapter.

4.3.1 Self-consistent scheme

Recurrent activity in a neural network has to obey self-consistent equations. These are presented and explained in the next subsections. We will first characterize the afferent current to a neuron in terms of the activity of the pre-synaptic neurons. We will close the self-consistent loop by calculating the effect of those currents on the activity of the neurons by means of the adiabatic approximation.

4.3.1.1 Characterizing input currents in terms of neuronal activity

If the number of pre-synaptic cells is large enough, the currents arriving to the recurrent neurons can be described as Gaussian variables. In that limit, they are fully characterized by their mean and variance. We have tested this hypothesis by means of a numerical simulation (fig. 4.2b). Let us denote by $I_i^I(t)$ the synaptic current that reaches neuron (i, I). It has mean μ_i^I and variance $\sigma_i^{I\ 2}$ given by:

$$\begin{aligned} \mu_i^I &\equiv < I_i^I(t) > = < \sum_{(k,\alpha)} m_{ik}^{I\alpha} J_{ik}^{I\alpha} s_k^\alpha(t) > \\ \sigma_i^{I\ 2} &\equiv < (\delta I_i^I(t))^2 > = < \sum_{(k,\alpha)} m_{ik}^{I\alpha} J_{ik}^{I\alpha} \delta s_k^\alpha(t) \sum_{(l,\alpha')} m_{il}^{I\alpha'} J_{il}^{I\alpha'} s_l^{\alpha'}(t) >, \end{aligned} \tag{4.9}$$

[1]The mathematical proof can be found in Appendix 4-A

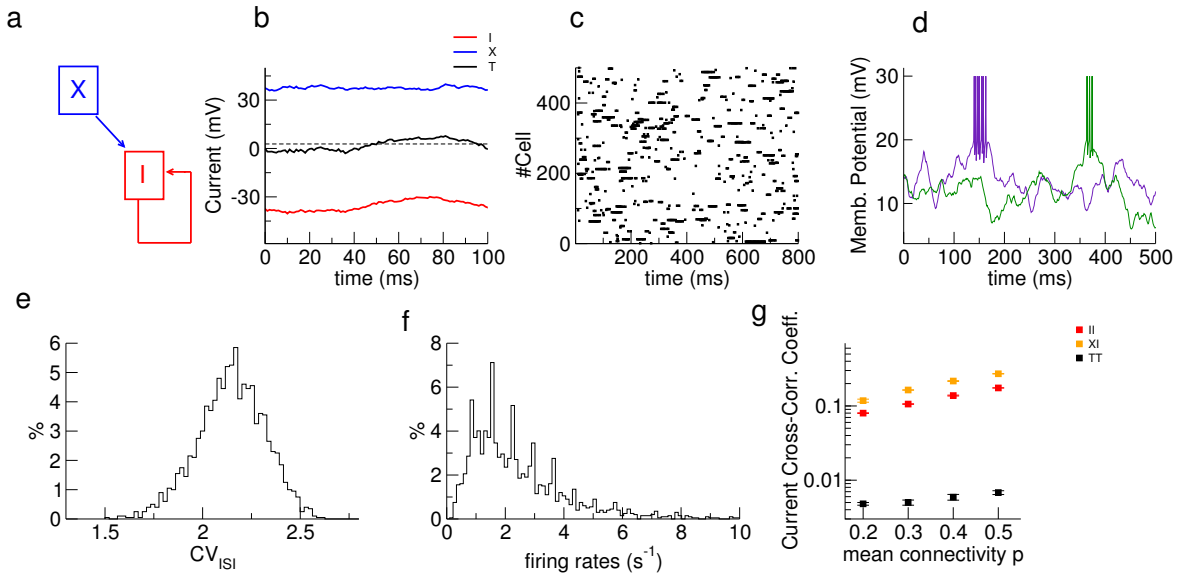

Figure 4.1: **Model architecture and characterization of the asynchronous state. a)** Network architecture. **b)** Rastergram of 500 recurrents cells ($N = 32000$). **c)** Pre-synaptic currents to a random cell ($N = 32000$). Color convention: red, inhibitory current component; blue, external; black, total current. Dashed line is the temporal-averaged value of the total current. **d)** Dependence of the input cross-correlations on mean connectivity p. Color convention: black, total current-total current; red, inhibitory-inhibitory current components; orange, external-inhibitory current components. **e)** Traces of the membrane potential of two recurrent neurons. **f)** Distribution of the CV of the ISIs of 2000 neurons. **g)** Distribution of the firing rates of 2000 neurons. All panels except panel **d)** correspond to the same network with $N = 32000$. See other parameter values in *Methods*. Squares in panel **d)** correspond to averages over 20 networks of size N =32000 and the same parameters as in the others panels (except the connection probability).

where $m_{ab}^{I\alpha}$ is the connectivity matrix and the sums run over all neurons. Averaging eqs. 4.9 over the neurons in the population we obtain:

$$\mu^I \equiv [\mu_i^I] = \sum_\alpha NpJ^{I\alpha}G\nu^\alpha \tag{4.10}$$

$$\sigma^{I\ 2} \equiv [\sigma_i^{I\ 2}] = \sum_\alpha Np(1-p)J^{(2)\ I\alpha}[< (\delta s_i^\alpha(t))^2 >] + c^{II}(0), \tag{4.11}$$

where $G = \int_{-\infty}^{\infty} j_{syn}(t)\mathrm{d}t$. As we will see, the zero-lag cross-covariance of the total current $c^{II}(0)$ vanishes as $O(1/\sqrt{N})$, so to leading order, $\sigma^{I\ 2}$ is:

$$\sigma^{I\ 2} \simeq [\sigma_i^{I\ 2}] = \sum_\alpha Np(1-p)J^{(2)\ I\alpha}[< (\delta s_i^\alpha(t))^2 >]. \tag{4.12}$$

4.3.1.2 Characterizing neuronal activity in terms of the input currents

The firing rate of a neuron that receives input currents filtered through slow synapses is well described by the adiabatic approximation [Moreno-Bote and Parga, 2004]. In this approximation, one calculates the mean rate of a neuron, $\nu_i^I \equiv < y_i^I(t) >$, assuming the pre-synaptic current $I_i^I(t)$, afferent to neuron (i, I) at a given time t is constant, calculating the *instantaneous* firing rate induced by this value of the current, $\nu_{R;i}(I_i^I)$, and averaging over all the possible values of the current:

$$\nu_i^I = \int \mathrm{d}P(I_i^I, \mu_i^I, \sigma_i^{I\ 2})\nu_{R;i}^I(I_i^I), \tag{4.13}$$

where $\mathrm{d}P(I_i^I, \mu_i^I, \sigma_i^{I\ 2})$ is the probability distribution of having the current I_i^I given the average synaptic current and its variance are μ_i^I and $\sigma_i^{I\ 2}$. Current distributions can be evaluated from the different values the current takes over time. An important interpretation of eq. 4.13 is that the adiabatic approximation allows us to substitute temporal averages by averages over the distribution of *frozen* input currents. Notice that, in [Moreno-Bote and Parga, 2004] eq. 4.13 was derived assuming a white noise input current. In our case, external neurons fire according to Poisson processes but recurrent neurons have, at this point, unknown statistics. Nevertheless, we hypothesize that the net effect of spiking cross- and auto-correlations can be taken into account just by including them in the current variance, $\sigma_i^{I\ 2}$, defined in eq. 4.11. The reason for this assumption is that, in such a theory, the *important* variable for the neurons is the incoming current. At each moment neurons see *frozen* currents, no matter the precise way these currents arise. In such a case eq. 4.13 reads as:

$$\nu_i^I = \int_{V_{Th}-V_L}^{\infty} \frac{\mathrm{d}I_i^I}{\sqrt{2\pi}\sigma_i^I} e^{-\frac{(I_i^I-\mu_i^I)^2}{2\sigma_i^{I\,2}}} \nu_{R;i}^I(I_i^I, \mu_i^I, \sigma_i^{I\,2}), \tag{4.14}$$

with:

$$(\nu_{R;i}^I)^{-1}(I_i^I, \mu_i^I, \sigma_i^{I\,2}) = \tau_{ref} + \tau_m \ln\Big(\frac{I_i^I - (V_{Reset} - V_L)}{I_i^I - (V_{Th} - V_L)}\Big) \tag{4.15}$$

for $I_i^I > (V_{Th} - V_L)$ and zero otherwise. Notice that $\nu_{R;i}^I(I_i^I, \mu_i^I, \sigma_i^{I\,2})$ is the firing rate of a leaky-integrate-and-fire neuron receiving a constant current I_i^I. Eq. 4.14 can be rewritten in terms of the current fluctuation around its mean value $z_i^I \equiv \frac{I_i^I - \mu_i^I}{\sigma_i^I}$.

$$\nu_i^I = \int_{\hat{V}_{Th}\sqrt{\frac{\tau_s}{\tau_m}}}^{\infty} \frac{\mathrm{d}z_i^I}{\sqrt{2\pi}} e^{-(z_i^I)^2/2} \nu_{(0);i}^I(z_i^I, \mu_i^I, \sigma_i^{I\,2}) \tag{4.16}$$

where:

$$\hat{V}_{Reset} \equiv \sqrt{\tau_m/\tau_s}(V_{Reset} - V_L - \mu_i^I)/\sigma_i^I \tag{4.17}$$

$$\hat{V}_{Th} \equiv \sqrt{\tau_m/\tau_s}(V_{Th} - V_L - \mu_i^I)/\sigma_i^I \tag{4.18}$$

$$\nu_{(0);i}^I(z_i^I, \mu_i^I, \sigma_i^{I\,2}) = \tau_{ref} + \tau_m \ln\Big(\frac{\hat{V}_{Reset} - \sqrt{\frac{\tau_m}{\tau_s}} z_i^I}{\hat{V}_{Th} - \sqrt{\frac{\tau_m}{\tau_s}} z_i^I}\Big) \tag{4.19}$$

In the following, we will omit the dependence on μ_i^I and σ_i^I in $\nu_{(0);i}^I(z_i^I, \mu_i^I, \sigma_i^{I\,2}) \equiv \nu_{(0);i}^I(z_i^I)$, unless explicitly mentioned.

Fig. 4.2a shows the firing rate of 25 randomly chosen inhibitory neurons computed directly from the rastergrams (black squares) and with eq. 4.14 (red squares), with the values of μ_i^I and σ_i^I computed from the simulation, indicating a good agreement. [2]

In the adiabatic limit, the spike cross-covariance function of two neurons can be described by the following equation [Moreno-Bote and Parga, 2010]:

$$< \delta y_j^I(t) \delta y_i^I(t+\tau) > = \int \mathrm{d}P_c(z_j^I, z_i^I; \tau) \nu_{(0);j}^I(z_j^I) \nu_{(0);i}^I(z_i^I) - \nu_i^I \nu_j^I. \tag{4.20}$$

[2] Notice that there is a systematic bias between the prediction of the theory and the actual value of the firing rates in fig. 4.2a. This was expected because the adiabatic approximation is only exact in the limit $\tau_m/\tau_s \to 0$, and it is reasonable to think that the convergence to the asymptotic values is achieved monotonically (see fig. 2 in Moreno-Bote and Parga, 2004).

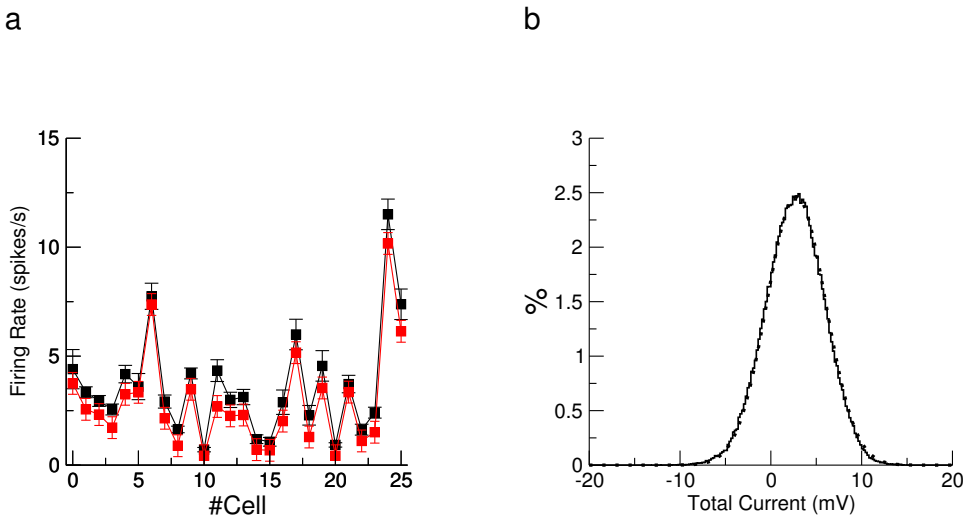

Figure 4.2: **Prediction of the single-neuron firing rates with the adiabatic approach. a)** Firing rates of 25 neurons in a simulation with $N = 32000$ neurons. Red squares were computed from the rastergrams, while black squares are the values obtained using eq. 4.14. Error bars were estimated dividing the simulation time in five intervals, computing the rate for each one and calculating the standard error of this measurements. **b)** Histogram of the total synaptic current to a random neuron in a simulation with $N = 32000$ neurons (solid line). Dashed line is a fit to a Gaussian with mean 2.8 mV and s.d. 3.2 mV

$\mathrm{d}P_c(z_j^I, z_i^I; \tau)$ is the joint probability of having a fluctuation of the current arriving to neuron (j, I) at a given time with value z_j^I and a fluctuation arriving to neuron (i, I) with a delay τ with value z_i^I (we assume stationary conditions). The distribution of z's can be evaluated from the different values they take over time. Thus, eq. 4.20 implies that one can calculate the spike cross-covariance function by computing the *instantaneous* firing rates induced by the different values of the current fluctuations reaching a pair of neurons and averaging over the joint distribution of these fluctuations. Eq. 4.20 will be our starting point for the self-consistent theory explained in Appendix 4-A.

4.3.2 Scaling analysis of the network properties

In Appendix 4-A we present a self-consistent theory that shows that for this kind of networks an *asynchronous* state as the one defined in chapter 2 exists. In this section we will present numerical and analytical results, while explaining in a qualitative way their different implications. On the way, we will explain some of the techniques employed for the analytical calculations presented in Appendix 4-A.

We start by showing some features of *densely* connected networks of *strongly* coupled inhibitory neurons in the large N limit. First, we show that population-averaged rates (fig. 4.3a) and mean currents (fig. 4.3b) behave asymptotically as predicted (dashed lines, see Appendix 2-A, in chapter 2). Notice that the input current components increase as $\sim \sqrt{N}$ but their sum remains finite, a typical feature of the balanced regime described in van Vreeswijk and Sompolinsky, 1996. We also show that for large enough networks, the population-averaged variance of the input currents and membrane potentials also reach constant values (fig. 4.3c) that are biologically realistic (s.d.$\sim$ 3 mV) [Stern et al., 1997, Anderson et al., 2000a].

Once we have shown that the prediction for single-neuron statistics are well understood, we go on describing pairwise magnitudes. In Appendix 4-A we derive the self-consistent equations for the population-averaged spike train cross-covariance functions, $r^{II}(\tau)$ and $r^{XI}(\tau)$, starting from the microscopic equations 4.16 and 4.20. Those equations are solved using a perturbative technique in the parameter $1/\sqrt{N}$. Here we give their final expressions:

$$r^{II}(\tau) = \frac{1}{N}(A^2 a^X(\tau) - a^{I\,(0)}(\tau)) \quad (4.21)$$

$$r^{XI}(\tau) = \frac{1}{N} A a^X(\tau), \quad (4.22)$$

where $A \equiv \frac{j^{IX}}{|j^{II}|}$ and $a^\alpha(\tau)$ is the population-averaged auto-covariance functions of neurons in population $\alpha = X, I$. These equations are the same as the ones we presented in chapter 2 for decorrelated networks (eqs. 2.54-2.55). In Appendix 4-B we show that the auto-covariance function $a^{I\,(0)}(\tau)$ is $O(1)$, i.e., at leading order it does not depend on N. *Balance equations* 4.21 and 4.22 contain some relevant predictions. First, spike-cross-covariance functions are small, $O(1/N)$. Second, they can be calculated from the auto-covariance functions of the external and recurrent populations. Fig. 4.4a shows $r^{II}(\tau)$ for some values of N, reflecting the modulation by the overall factor $1/N$. Fig. 4.4b shows $r^{II}(\tau)$ for a network of $N = 32000$ neurons calculated from rastergrams (red line) and via eq. 4.21, with $a^{I\,(0)}(\tau)$ and $a^X(\tau)$ numerically computed (black dashed line), confirming our prediction. Spike train cross-covariance functions in fig. 4.4 show a delta peak at $\tau = 0$, arising from the sum of the delta peaks present both in $a^{I\,(0)}(\tau)$ and $a^X(\tau)$ [3], and a slow decay for $|\tau| > \tau_{ref}$ inherited from the shape of the $a^{I\,(0)}(\tau)$ (these functions are shown in Appendix 4-B, fig. 4.8).

The population-averaged spike-count cross-covariances defined over a time window of size T, $CC^{\alpha I}_{sc}(T)$, can be obtained from $r^{\alpha I}(\tau)$ [Tetzlaff et al., 2008]:

$$CC^{\alpha I}_{sc}(T) = \int_{-T}^{T} r^{\alpha I}(\tau)\frac{T - |\tau|}{T}\mathrm{d}\tau \quad (4.23)$$

Their balance expressions are analogous to eqs. 4.21 and 4.22:

$$CC^{II}_{sc}(T) = \frac{1}{N}(A^2\, AC^X_{sc}(T) - AC^{I\,(0)}_{sc}(T)) \quad (4.24)$$

$$CC^{XI}_{sc}(T) = \frac{1}{N} A\, AC^X_{sc}(T), \quad (4.25)$$

where $AC^\alpha_{sc}(T) = \int_{-T}^{T} a^\alpha(\tau)\frac{T-|\tau|}{T}\mathrm{d}\tau$ is the population-averaged auto-covariance of the spike-count in population α. This prediction is similar to those for networks of binary neurons [Renart et al., 2010] and LIF neurons with fast synaptic kinetics (see

[3] Working with a finite temporal resolution, bin ,the delta-peak at $\tau = 0$ is reflected in the value of the maximun. In the inset of fig. 4.4b) the value of this maximum varies inversely to the temporal resolution 1/bin . Red squares corresponds to the simulation while the black ones correspond to the theoretical prediction, eq. 4.21

previous chapter). Figs. 4.3d,e show the scaling of these magnitudes and the comparison with theoretical predictions. For small networks, $CC^{II}_{sc}(T)$ ($T = 70$ ms) has positive values (not shown), while eq. 4.25 predicts negative ones. However, a good agreement is accomplished for larger networks ($N > 1000$). Closely related to the cross-covariance, the pairwise spike-count cross-correlation coefficients (figs. 4.3g,h) also show the same behaviour at large values of N. With regards to synaptic current, zero-lag cross-covariances between the current components are high and constant (fig. 4.3f). Their cross-correlation coefficients (fig. 4.3i) reflect the intrinsic correlation degree due to the fraction of shared inputs. In contrast, the population-averaged zero-lag cross-covariance of the total current, $c^{II}(0)$, decreases with N (fig. 4.3f, black squares). Our theory predicts that the leading order of the total current zero-lag cross-covariances necessarily has to be a power $\lambda \geq 1$ of $1/\sqrt{N}$ (see Appendix 4-A for more details). Simulation results in fig. 4.3f show that $c^{II}(0) \sim 1/\sqrt{N}$ (dashed line) and similarly for the cross-correlation coefficients (fig. 4.3i, dashed line), although the integral of these functions in large time windows decay as $\sim 1/N$ (see Appendix 4-C). In Appendix 4-A we also show that the magnitude $\mathcal{A}^{XI}(\tau) \equiv [< \delta y^X_j(t)\delta I^I_i(t+\tau) >]$ also vanishes. Notice that this was the definition of asynchronous state we gave in chapter 2. As we explained there, the tracking of external (excitatory) fluctuations by inhibitory activity precisely allows them to cancel, similarly to the case in binary neurons [Renart et al., 2010] and in LIF neurons with faster synaptic filters (see previous chapter). This effect is shown in fig. 4.5a: inhibitory current tracks the external (excitatory) one with a small delay. Another typical feature of these networks is that the distribution of spike-count cross-covariances is wide (fig. 4.5b).

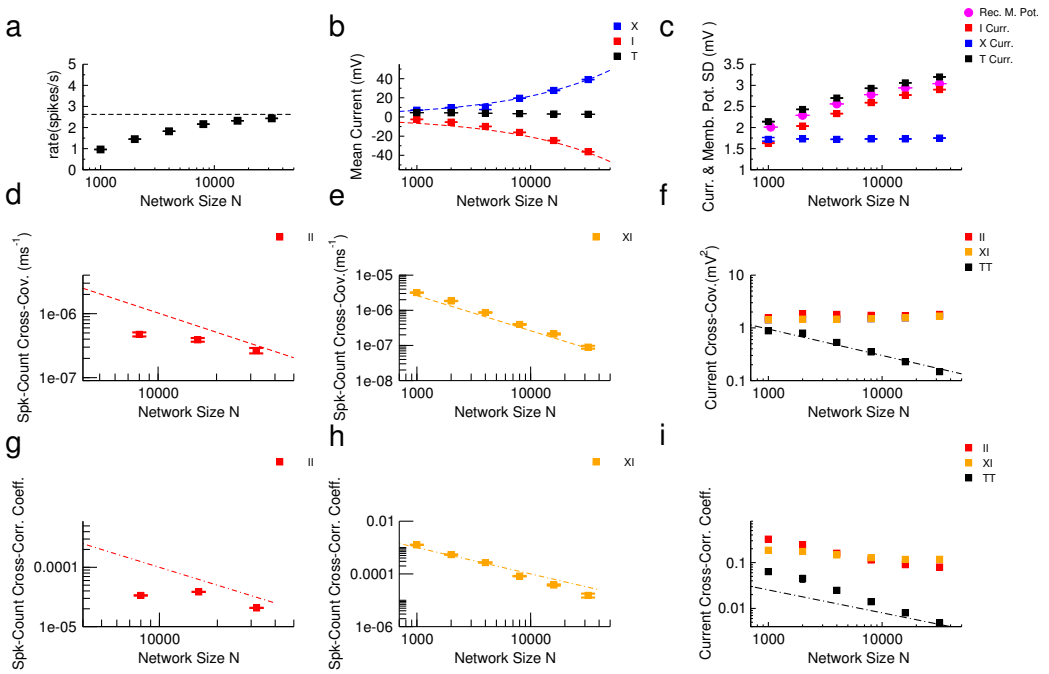

Figure 4.3: **Scaling of first- and second-order statistical magnitudes. a)** Population-averaged mean rates of the recurrent neurons for different network sizes (black squares). Dashed line corresponds to the asymptotic limit (eq. 2.88 in Appendix 2-A in chapter 2). **b)** Population-averaged mean currents afferent to recurrent neurons. Same color convention as in fig. 4.1c. Dashed line corresponds to their theoretical value (see Appendix 2-A).**c)** Population-averaged standard deviation of the afferent current components and total current (squares) and standard deviation of the membrane potential of an inhibitory neuron (circle). **d)** Absolute values of the population-averaged spike-count cross-covariances of inhibitory pair of neurons. Dashed line corresponds to the theoretical prediction given by the absolute value of eq. 4.25 where the value of $AC_{sc}^{I\,(0)}$ was estimated numerically from the largest network ($N = 32000$). The values represented had originally negative signs. **e)** Population-averaged spike-count cross-covariances for an external-inhibitory pair of neurons. Dashed line corresponds to the theoretical prediction in eq. 4.25. **f)** Absolute values of the population-averaged zero-lag cross-covariances of the afferent total currents and current components to a neuron pair. Same color conventions as in fig. 4.1d. Population-averaged cross-covariances of excitatory-inhibitory current components have negative sign while the others are positive. The dash-dotted line represents a $O(1/\sqrt{N})$ scaling. **g)** Absolute values of the population-averaged cross-correlation coefficients between spike-counts of inhibitory-inhibitory pairs. The dash-dotted line corresponds to a $O(1/N)$ scaling. The values represented have negative signs. **h)** Population-averaged cross-correlation coefficients of the spike-count of external-inhibitory pairs. Dash-dotted line corresponds to a $O(1/N)$ scaling. **i)** Absolute values of the population-averaged cross-correlation coefficients of the afferent total currents and current components to a neuron pair. Same color conventions as in fig. 4.1e. Population-averaged cross-correlation coefficients of external-inhibitory current components have negative sign while the others are positive. Dash-dotted line represents a $O(1/\sqrt{N})$ scaling. Spike-count in panels **d, e, g, h** were computed for $T = 70$ ms. Similar agreement between theoretical prediction and simulation is found for different values of T.

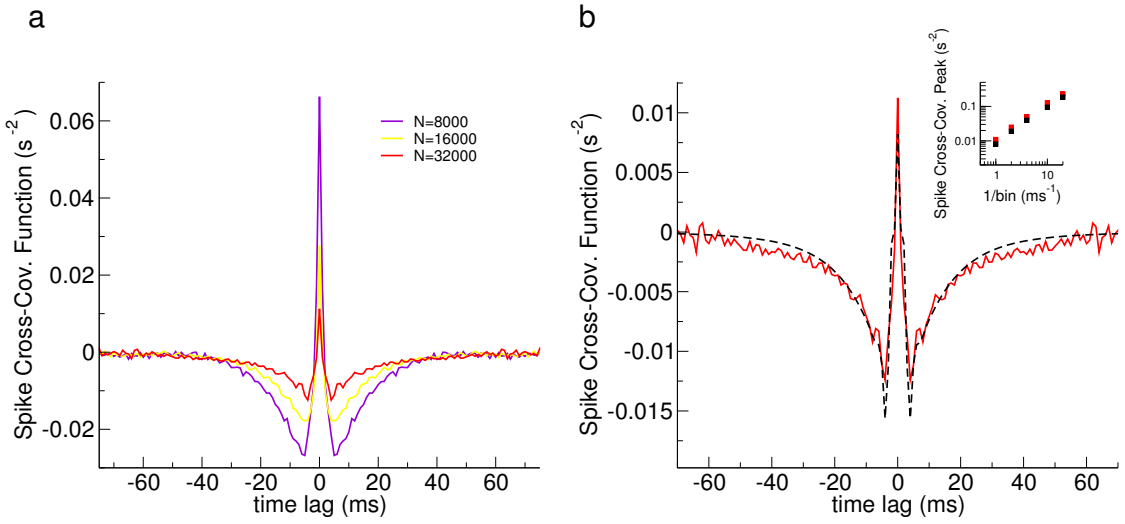

Figure 4.4: **Spike train cross-covariance functions of recurrent neurons.** **a)** Population-averaged spike trains cross-covariance functions for different network sizes: $N = 8000$ (violet), $N = 16000$ (yellow), $N = 32000$ (red). **b)** Population-averaged spike trains cross-covariance function for the largest network ($N = 32000$) computed from the rastergrams (red line) and through eq. 4.57 (black line), with $a^X(\tau)$ and $a^{I\ (0)}(\tau)$ calculated also with the rastergrams at 1 ms resolution. **Inset** Value of the population-averaged spike trains cross-covariance function at zero-lag for different temporal resolution (bin). Red squares correspond to the simulation while the black ones correspond to the theoretical prediction.

4.3.3 Effect of correlated external neurons

As we have seen, the cancellation of spiking cross-correlations leads to formulae that relate the population-averaged spike train cross-covariance function with the population-averaged spike train auto-covariance functions, which are single neuron magnitudes. Those equations were derived when the correlation from external neurons comes only from the shared external input. One can wonder if decorrelation also occurs if external neurons themselves are also correlated. As an example, we focus on the case in which external neurons' firing rates are identical and fluctuate in time according to an Ornstein-Uhlenbeck process:

$$\tau_{OU}\frac{\nu^X(t)}{dt} = \nu^X - \nu^X(t) + \sigma_{OU;N}\sqrt{\frac{2}{\tau_{OU}}}\zeta(t), \tag{4.26}$$

where τ_{OU} and $\sigma_{OU;N}$ are the correlation time and the standard deviation of the Ornstein-Uhlenbeck process and $\zeta(t)$ is a white noise process with zero mean and

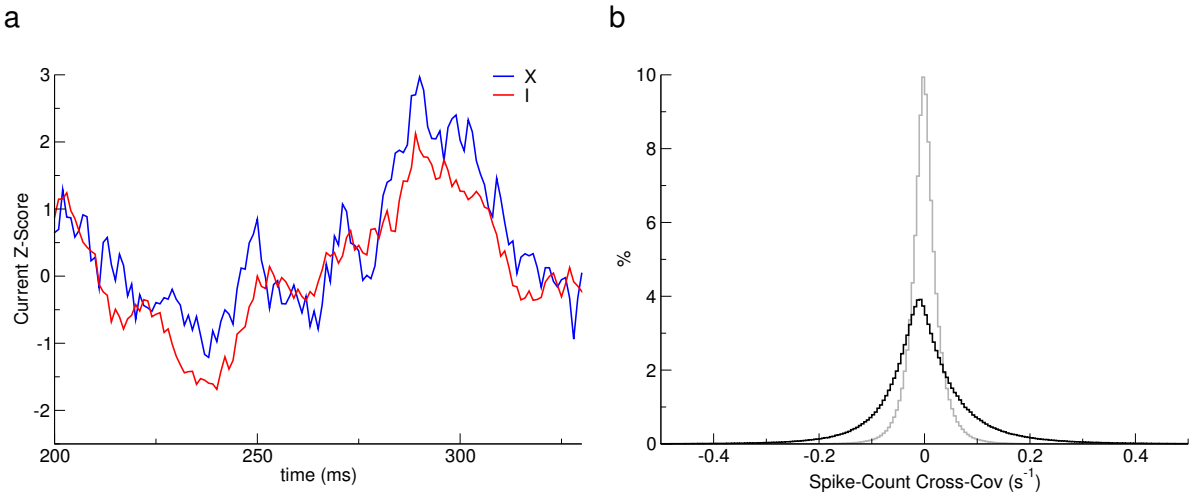

Figure 4.5: **Tracking of excitatory fluctuations and wide distribution of spike-count cross-correlation coefficients. a)** Z-score of the external (excitatory)(blue) and inhibitory (red) current components afferent to a random neuron ($N = 32000$). **b)** Distribution of pairwise spike-count cross-covariances of recurrent neurons (black) for a given network ($N = 32000$, $T = 70$ ms). Grey histogram represents the same distribution for jittered spike trains (see *Methods*, section 4.2.4.

unit variance (see section 4.2.1.2 in *Methods* for further details). The variance of the external current afferent to a recurrent neuron can be written as:

$$< (\mathcal{I}^X(t))^2 > = \int_{-\infty}^{\infty} \Big(p^2 (j^{(2)\,IX}) \phi_{syn}(\tau) a^X(\tau - t) + p^2 N (j^{IX})^2 \phi_{syn}(\tau) r^{XX}(\tau - t) \Big) \, \mathrm{d}t \quad (4.27)$$

Notice that, in order for this variance to be $O(1)$, $r^{XX}(\tau)$ has to scale as $1/N$, i.e. $r^{XX}(\tau) \equiv \frac{1}{N} r^{XX\,(2)}(\tau)$. It is easy to show that $r^{XX}(0) = \sigma^2_{OU;\,N}$ (see Appendix 4-D), so $\sigma^2_{OU;\,N}$ has to be $O(1/N)$ in order for the input variance not to be arbitrarily large. Notice that although cross-covariance functions $r^{XX}(\tau)$ are small ($O(1/N)$), their net effect on magnitudes such as $< (\mathcal{I}^X(t))^2 >$ rests finite.

Proceeding as we did before, but keeping the terms $r^{XX}(\tau)$, we arrive to the following balance equations for cross-covariance functions:

$$r^{II}(\tau) = \frac{1}{N} (A^2 (a^{X\,(0)}(\tau) + r^{XX\,(2)}(\tau)) - a^{I\,(0)}(\tau)) \quad (4.28)$$

$$r^{XI}(\tau) = \frac{1}{N} A (a^{X\,(0)}(\tau) + r^{XX\,(2)}(\tau)) \quad (4.29)$$

Notice that, although a common fluctuating external firing rate induces both auto- and cross-correlations in the firing activity of recurrent neurons, if the cofluctuations are

weak enough ($\sigma^2_{OU;\,N} = O(1/N)$) their effect on the cross-covariance of the recurrent network is $O(1/N)$. We have tested eqs. 4.28 and 4.29 by running simulations in which external neurons' firing rate evolves according to the Ornstein-Uhlenbeck process in eq. 4.26. Simulation and theory are compared in fig. 4.6 ($N = 32000$). The parameters employed for these simulations are such that $r^{XX}(\tau)$) is considerably bigger than $a^I(\tau)$ and $a^X(\tau)$, which is reflected in $r^{II}(\tau)$ according to our prediction. The systematic difference between the theory and the simulation comes from the fact that eq. 4.28 has to be interpreted as the asymptotic limit for $N \to \infty$. For $N = 32000$ the prediction is close to this limit, although the convergence is not complete.

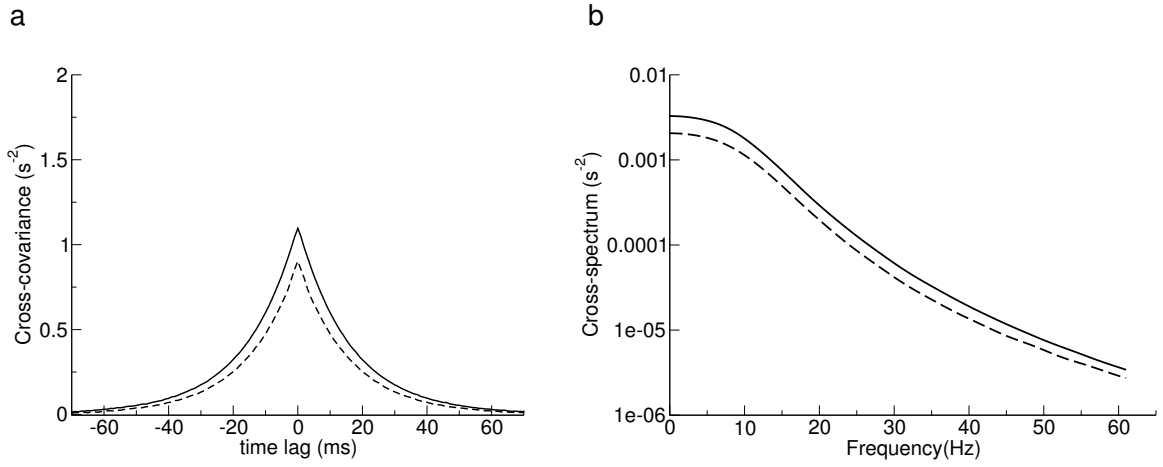

Figure 4.6: **Decorrelation when external neurons are weakly correlated.** Population-averaged cross-covariance functions **(a)** and cross-spectra **(b)** of II pairs when the external output rate follows an Ornstein-Uhlenbeck process which causes a non-zero cross-covariance of the external neurons. Solid lines: Simulation. Dashed lines: Theory, leading order(eq. 4.28)

4.3.4 Prediction on macroscopic properties

Measuring pair-wise cross-correlations the firing activity of neuronal pairs is technically difficult. In Ecker et al., 2010 some of the problems found in the experiments are described (see chapter 1, section 1.3). One of them, is the difficulty to isolate the spikes generated by each cell. Analyzing macroscopic signals such as LFP or MUA require simpler techniques. One can wonder how the balance equations 4.28 and 4.29 manifest in such macroscopic signals. To address this issue, we will calculate the auto-covariance function of the MUA of an ensemble of N' neurons in the network with correlated external neurons. First we define the MUA, $\bar{\nu}^I(t)$:

$$\bar{\nu}^I(t) \equiv \sum_{(i,I)}^{N'} \nu_i^I(t) \tag{4.30}$$

The sum runs over the spike trains of the N' neurons recorded by the electrode ($N' \leq N$). We calculate its auto-covariance as:

$$\begin{aligned} < \delta\bar{\nu}^I(t)\delta\bar{\nu}^I(t+\tau) > &= \sum_{\substack{(i,I)\\(j,I)}}^{N'} < \nu_i^I(t)\nu_j^I(t+\tau) > \simeq \sum_{\substack{(i,I)\\(j,I)}}^{N'} < y_i^I(t)y_j^I(t+\tau) > \\ &= \Big(\sum_{(i,I)}^{N'} < y_i^I(t)y_i^I(t+\tau) > + \sum_{\substack{(i,I)\\(j,I)\\i\neq j}}^{N'} < y_i^I(t)y_j^I(t+\tau) > \Big) \\ &= N'a^I(\tau) + N'(N'-1)r^{II}(\tau) \end{aligned} \tag{4.31}$$

Substituting the balance equation for $r^{II}(\tau)$ we find:

$$< \delta\bar{\nu}^I(t)\delta\bar{\nu}^I(t+\tau) > = N'\Big(\Big(1 - \frac{N'-1}{N}\Big)a^I(\tau) + A^2\frac{N'-1}{N}(a^X(\tau) + r^{XX\ (2)}(\tau))\Big) \tag{4.32}$$

$$\simeq N'a^I(\tau). \tag{4.33}$$

where the last identity holds if $N' << N$. This is usually the case, provided the estimated number of neurons around the electrode's tip is of the order of hundreds of neurons. Fig. 4.7a shows the MUA auto-covariance function computed for a population $N' = 200$ neurons directly form the simulation (solid blak line), and through eqs. 4.32 (dashed black line) and 4.33 (dashed blue line) for a network of $N = 32000$. The fact that the main contribution to MUA auto-covariance is basically the auto-covariance function of single cells weighted by a factor N' can be interpreted as follows. It is easy to show that the MUA cross-covariance function of N' neurons which population-averaged spiking cross-correlations are strictly zero is $N'a^I(\tau)$ (to see this, just neglect the second sum in the second line of the calculation in eq. 4.31). Our theory predicts small (but non-zero) values of the population-averaged spike-trains cross-correlations. Being these correlations $O(1/N)$ their effect is, more noticeable when $N' \sim N$; however, neurons can be considered *virtually* uncorrelated for calculations which require summing over a small subpopulation. Fig. 4.7b shows the MUA auto-covariance function computed for a population of $N' = N = 32000$. In this case, the first term on the right side in eq. 4.32 cancels to leading order and all the contribution comes

from the second one. Notice that, although one could think that the contribution of cross-correlations to MUA auto-covariance function should be $O(N^2)$ (due to the sum over N^2 pairs) population averaged spiking cross-correlations being $O(1/N)$ results in $< \delta\bar{\nu}^I(t)\delta\bar{\nu}^I(t+\tau) >= O(N)$.

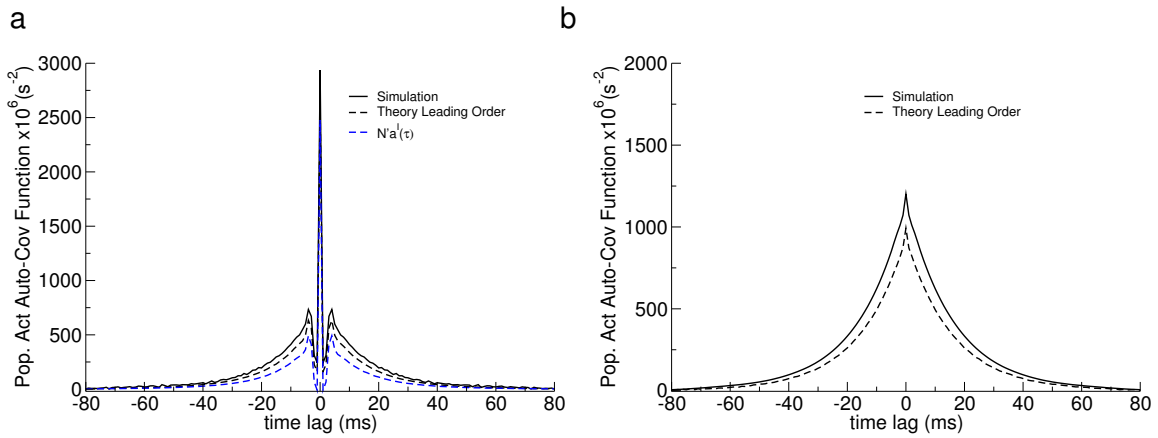

Figure 4.7: **Macroscopic signals. a)** Auto-covariance function of the MUA of $N' = 200$ neurons computed with the simulation (black solid line) and through eqs. 4.32 (black dashed line) and 4.33 for a network with $N = 32000$ neurons. **b)** Auto-covariance function of the MUA of $N' = N = 32000$ neurons computed with the simulation (solid line) and through eq. 4.32 (dashed line) for a network with $N = 32000$ neurons

4.4 Discussion

We have shown that decorrelation in the activity of integrate and fire cells can occur in the case of slow synaptic filters. This regime describes properly the limit of large number of inputs, which effectively translates into a decrease of the membrane time constant [Bernarder et al., 1991, Pare et al., 1998, Hirsch et al., 1998, Borg-Graham et al., 1998, Destexhe et al., 1999, Anderson et al., 2000b, Destexhe et al., 2001, Kuhn et al., 2004, Moreno-Bote and Parga, 2005, Léger et al., 2005]. Similar equations to the ones found for faster filters were derived using the adiabatic approximation. Equations were solved with the same perturbative technique that we used previously. As in that case, we find that population-averaged spike-count cross- covariances decrease with the network size as $1/N$, while zero-lag population-averaged current cross-covariances do as $1/\sqrt{N}$. Although the present study only considers a recurrent population of inhibitory cells, it is straightforward to show that similar equations can be predicted for the case of a recurrent network of inhibitory and excitatory cells. The phenomenon of tracking of external (excitatory) fluctuations by the recurrent (inhibitory) population is also present.

An alternative to the model presented here could be a conductance-based one. The reason for not studying such a model is that there is not a straightforward way of using the scaling scheme we have presented. A naive intuition would lead us to scale unitary conductances in the same way as we did with the unitary currents. However, one can show that by doing so, the variance of the synaptic current vanishes in the limit of large networks, due to the fact that effective membrane time constants tend to zero when the number of input tends to infinity [Kuhn et al., 2004, Renart et al., 2007]. This situation is not biological plausible and consequently is not a good scenario.

The network presented here can model structures formed by inhibitory neurons such as basal ganglia. Basal ganglia are important in the regulation of voluntary motor tasks [Hikosaka et al., 2000] and has a critical role in neurological diseases such as Parkinson [Wichmann and DeLong, 1996]. In Magill et al., 2000 small correlations in the globus pallidus of rats during spontaneous activity states were found. The authors suggest that asynchrony might arise from a hardwire design that assures that cells receive very different inputs. Here we show that even if the currents afferent to neurons are similar, the dynamics of the recurrent network can decorrelate the activity of the neurons. Low activity correlations were also found in the globus pallidus of awake monkeys performing visual-motor tasks [Nini et al., 1995, Raz et al., 2000, Bar-Gad

et al., 2003]. In this last paper, the shape of the spike trains cross-covariance functions at long time scales was very similar to the one in fig. 4.4, although the time constant of the functions was larger, suggesting even a slower synaptic dynamics, which would make the adiabatic approximation even more accurate. Although in this work it was just mentioned as a curiosity, the authors pointed out a relation between spike train auto- and cross-covariance functions in perfect agreement with the one given by the balance relation in eq. 4.21.

High degree of spiking cross-correlation has been reported in data of basal ganglia of anesthetized songbirds[Kimpo et al., 2003, Doupe et al., 2005]. In such systems cross-correlations could be transmitted from layer to layer, suggesting a plausible spike-timing code. Transmission of strong cross-correlations was explained by models as the one in Diesmann et al., 1999. This model consits of a feed-forward structure formed by layers of neurons receiving common input only from previous layers and can sustain activity in form of synfire chains [Abeles, 1991]. Our study, thus, shed some light on the differences between the basal ganglia of the different animals suggesting that the presence/absence of recurrent inhibiton in the layers can determine the presence/absence of cross-correlated activity.

Pair-wise cross-correlations (or the lack of them) in neuronal activities are reflected in macroscopical signals such as MUA or the LFP. We have shown that our framework allows for calculations of auto-covariance functions and power spectra of MUA, suggesting an indirect way of experimentally testing our theory. Another macroscopic signal commonly studied is the LFP in networks with excitatory neurons. An approximation of this signal can be obtained by considering the sum of the absolute values of the excitatory and inhibitory currents [Mazzoni et al., 2008]. Because currents can be decomposed into the sum of filtered spike trains, it should be possible to reduce the calculation of LFP power spectrum in a similar way as we did for the MUA.

Appendix 4-A. Cross-correlations self-consistent theory

4-A1. Self-consistent equations

Recurrent-recurrent pairs

In this section we will calculate self-consistently the population-averaged cross-covariance function between a pair of neurons in the recurrent network. The starting point is 4.20:

$$< \delta y_j^I(t)\delta y_i^I(t+\tau) >= \int \mathrm{d}P_c(z_j^I, z_i^I;\tau)\nu^I_{(0);j}(z_j^I, \mu_j^I, {\sigma_j^I}^2)\nu^I_{(0);i}(z_i^I, \mu_i^I, {\sigma_i^I}^2) - \nu_i^I\nu_j^I. \quad (4.34)$$

where $\mathrm{d}P_c(z_j^I, z_i^I;\tau)$ is the joint probability of having a fluctuation of the current arriving to neuron (j, I) at a given time with value z_j^I and a fluctuation arriving to neuron (i, I) with a delay τ with value z_i^I (we assume stationary conditions) and $\nu^I_{(0);i}(z_i^I, \mu_i^I, {\sigma_i^I}^2)$ has been previously defined (eq. 4.19) and is the firing rate of a neuron receiving a constant current $I_i^I = \mu_i^I + \sigma_i^I\, z_i^I$ (see more details in section *Self-consistent scheme*).

One can estimate the distribution of z's from a temporal sampling. Eq. 4.34 tells us that to calculate the cross-covariance of spike trains one can calculate the instantaneous firing rates induced in each neuron by their respective incoming current fluctuations and average over the probability of those fluctuations. Notice that fluctuations univocally determine the instantaneous firing rate. Thus, one can perform a change of variable and calculate the integral over the distribution of the instantaneous firing rates. Performing this change of variables for neuron, (j, I), we have the following identities (we denote by ${\nu_j^I}^{(*)}$ the value of the firing rate of neuron (j, I) induced by fluctuation z_j^I):

$$\begin{aligned} < \delta y_j^I(t)\delta y_i^I(t+\tau) > &= \int \mathrm{d}P'_c({\nu_j^I}^{(*)}, z_i^I;\tau)\ \nu^I_{(0);i}(z_i^I)\ {\nu_j^I}^* - \nu_i^I\nu_j^I \\ &= \int \mathrm{d}P'_c({y_j^I}^{(*)}, z_i^I;\tau)\ \nu^I_{(0);i}(z_i^I, \mu_i^I, {\sigma_i^I}^2)\ {y_j^I}^* - \nu_i^I\nu_j^I, \quad (4.35) \end{aligned}$$

where ${y_j^I}^{(*)}$ denotes the value of the spike train induced by the fluctuation z_j^I [4]. $\mathrm{d}P'_c({y_j^I}^{(*)}, z_i^I;\tau)$ denotes the joint probability distribution that at a given time the spike train of neuron $(j, I))$ is ${y_j^I}^{(*)}$ and that the fluctuation of the τ-delayed input

[4] It can be shown that the substitution of ${\nu_j^I}^{(*)}$ by ${y_j^I}^{(*)}$ in eq. 4.35 is allowed and the identity is valid. Compare eq. 16 in Moreno-Bote and Parga, 2006 and eq. 2.7 in Moreno-Bote and Parga, 2010

current to neuron (i, I) is z_i^I.

$y_j^{I\,(*)}$, in general, will depend on $\nu_i^I(z_i^I)$ and, thus, it will depend indirectly on z_i^I. However, in the following we will not consider the effect of the spikes emitted by neuron (i, I) on neuron (j, I). This is equivalent to restricting ourselves to the case $\tau \geq 0$. To calculate the cross-covariance function for $\tau < 0$ one can reverse the role of neurons i and j. In fact, symmetry arguments lead to $r_{ji}^{II}(-\tau) = r_{ij}^{II}(\tau)$. We find it useful to decompose the joint probability distribution $\mathrm{d}P_c'(y_j^{I\,(*)}, z_i^I; \tau)$ in terms of the probability distribution over z_i^I conditioned to the value of the spike train, $\mathrm{d}P(z_i^I; \tau | y_j^{I\,(*)})$, and the probability distribution of the spike train values $y_j^{I\,(*)}$, $\mathrm{d}P''(y_j^{I\,(*)})$:

$$\begin{aligned} &< \delta y_j^I(t) \delta y_i^I(t+\tau) > = \\ &\quad = \int \mathrm{d}P''(y_j^{I\,(*)}) \int \mathrm{d}P(z_i^I; \tau | y_j^{I\,(*)})\ \nu_{(0);i}^I(z_i^I, \mu_i^I, {\sigma_i^I}^2) y_j^{I\,(*)} - \nu_i^I \nu_j^I \end{aligned} \tag{4.36}$$

Notice that $y_j^{I\,(*)}$ can take only two possible values: 0 when there is not a spike and $\delta(0)$ if the neuron fires. This allows us to write the last equation as:

$$\begin{aligned} < \delta y_j^I(t) \delta y_i^I(t+\tau) > &= (\int \mathrm{d}P''(y_j^{I\,(*)}) y_j^{I\,(*)}) (\int \mathrm{d}P(z_i^I; \tau | y_j^{I\,(*)} = \delta(0))\ \nu_{(0);i}^I(z_i^I, \mu_i^I, {\sigma_i^I}^2)) - \nu_i^I \nu_j^I \\ &= \nu_j^I \int \mathrm{d}P(z_i^I; \tau | y_j^{I\,(*)} = \delta(0))\ \nu_{(0);i}^I(z_i^I, \mu_i^I, {\sigma_i^I}^2) - \nu_i^I \nu_j^I; \end{aligned} \tag{4.37}$$

where we have used the definition of $\nu_j^I \equiv < y_i^I(t) > = \int \mathrm{d}P''(y_j^{I\,(*)}) y_j^{I\,(*)}$. We use the notation $r_{+,\,ji}^{II}(\tau)$ to explicitly indicate that the function is the cross-covariance function $r_{ji}^{II}(\tau)$ for $\tau \geq 0$. We denote by $\bar{\mu}_i^I(\tau)$ and by $(\bar{\sigma}_i^I(\tau))^2$ the average and variance of I_i^I a time τ after neuron (j, I) has emitted one spike.

$$r_{+,\,ji}^{II}(\tau) = \nu_j^I \int \mathrm{d}P(z_i^I)\ \nu_{(0);i}^I(z_i^I, \bar{\mu}_i^I(\tau), {\bar{\sigma}_i^I}^2(\tau)) - \nu_i^I \nu_j^X. \tag{4.38}$$

where, for completeness, we have written down explicitly the dependence of the instantaneous firing rate on the current moments. We have to calculate the magnitude $\nu_{(0);i}^I(I_i^I, \bar{\mu}_i^I(\tau), {\bar{\sigma}_i^I}^2(\tau))$. The technique we use is similar to the one employed in Renart et al., 2010 for networks of binary units. We start by calculating $\bar{\mu}_i^I(\tau)$:

$$\begin{aligned} \bar{\mu}_i^I(\tau) &= < I_i^I > + \tfrac{1}{\nu_j^I} < \delta y_j^I(t) \delta I_i^I(t+\tau) > \\ &= \mu_i^I + \frac{\mathcal{A}_{ji}^{II}(\tau)}{\nu_j^I}, \end{aligned} \tag{4.39}$$

with:

$$\mathcal{A}^{II}_{ji}(\tau) \equiv < \delta y^I_j(t)\delta I^I_i(t+\tau) > . \tag{4.40}$$

Analogously, one can prove that:

$$(\bar{\sigma}^I_i(\tau))^2 = \sigma_i^{I\ 2} + \frac{\mathcal{B}^{II}_{ji}(\tau)}{\nu^I_j} - \Big(\frac{\mathcal{A}^{II}_{ji}(\tau)}{\nu^I_j}\Big)^2, \tag{4.41}$$

where $\mathcal{B}^{II}_{ji}(\tau)$ is:

$$\mathcal{B}^{II}_{ji}(\tau) \equiv < \delta y^I_j(t)(\delta I^I_i(t+\tau))^2 > . \tag{4.42}$$

Inserting eqs. 4.39, 4.41 into eq. 4.38, we arrive to:

$$r^{II}_{+,\,ji}(\tau) = \nu^I_j \int \mathrm{d}P(z^I_i)\nu^I_{(0);i}(z^I_i, \mu^I_i + \frac{\mathcal{A}^{II}_{ji}(\tau)}{\nu^I_j}, \sigma_i^{I\ 2} + \frac{\mathcal{B}^{II}_{ji}(\tau)}{\nu^I_j} - \Big(\frac{\mathcal{A}^{II}_{ji}(\tau)}{\nu^I_j}\Big)^2) - \nu^I_j\nu^I_i. \tag{4.43}$$

As explained in Renart et al., 2010, in asynchronous states the population average of the magnitudes $\mathcal{A}^{II}_{ji}(\tau)/\nu^I_j$ and $\mathcal{B}^{II}_{ji}(\tau)/\nu^I_j - \mathcal{A}^{II}_{ji}(\tau)/\nu^I_j$ must be $O(1/N)$ at most. Thus, one can expand $\nu^I_{(0);i}$ in these variables and keep only the first order terms. Precisely, we expand $\nu^I_{(0);i}$ in powers of $\mathcal{A}^{II}_{ji}(\tau)$ and neglect terms $O((\mathcal{A}^{II}_{ji}(\tau))^2)$ and $O(\mathcal{B}^{II}_{ji}(\tau))$ [5] [6]:

$$\nu^I_{(0);i}\Big(\mathcal{A}^{II}_{ji}(\tau)\Big) = \nu^{I\ (0)}_{(0);i} + \nu^{I\ (1)}_{(0);i}\mathcal{A}^{II}_{ji}(\tau) + O((\mathcal{A}^{II}_{ji}(\tau))^2) + O(\mathcal{B}^{II}_{ji}(\tau)), \tag{4.44}$$

where:

$$\begin{aligned} \nu^{I\ (0)}_{(0);i} &= \nu^I_{(0);i}(z^I_i, \mu^I_i, \sigma^I_i) \equiv \nu^I_{(0);i} \\ \nu^{I\ (1)}_{(0);i} &= \frac{\partial \nu^I_{(0);i}\Big(\mathcal{A}^{II}_{ji}(\tau)\Big)}{\partial \mathcal{A}^{II}_{ji}(\tau)}\Big|_{\mathcal{A}^{II}_{ji}(\tau)=0} = \frac{1}{\nu^I_j}\frac{\partial \nu^I_{(0);i}\Big(\mathcal{A}^{II}_{ji}(\tau)\Big)}{\partial \mu^I_i}\Big|_{\mathcal{A}^{II}_{ji}(\tau)=0}. \end{aligned} \tag{4.45}$$

Substituting the expansion in eq. 4.44 into eq. 4.43 we arrive to the result:

[5] To simplify the notation we do not write the dependence of $\nu^I_{(0);i}$ on $(z^I_i, \mu^I_i + \frac{\mathcal{A}^{II}_{ji}(\tau)}{\nu^I_j}, \sigma_i^{I\ 2} + \frac{\mathcal{B}^{II}_{ji}(\tau)}{\nu^I_j} - \Big(\frac{\mathcal{A}^{II}_{ji}(\tau)}{\nu^I_j}\Big)^2)$

[6] We are assuming that $\mathcal{B}^{II}_{ji} << \mathcal{A}^{II}_{ji}$, similar to Renart et al., 2010.

$$r^{II}_{+,\,ji}(\tau) = < \frac{\partial \nu^I_{(0);i}}{\partial \mu^I_i} > \mathcal{A}^{II}_{ji}(\tau) - \nu^I_j \nu^I_i. \tag{4.46}$$

Using the definition of $\mathcal{A}^{II}_{ji}(\tau)$ and averaging over neurons, eq. 4.46 becomes:

$$r^{II}_{+}(\tau) = L \int_{-\infty}^{\infty} \mathrm{d}t j_{syn}(t) \Big\{ pJ^{II} a^I(\tau - t) + NpJ^{II} r^{II}_{+}(\tau - t) + NpJ^{IX} r^{IX}(\tau - t) \Big\}, \tag{4.47}$$

where $L \equiv [< \frac{\partial \nu^I_{(0);i}}{\partial \mu^I_i} \Big|_{A^{II}_{ji}(\tau)=0} >]$ and we have assumed that the dynamical properties of a neuron and the synaptic weight with which it connects to the others are independent magnitudes [Renart et al., 2010]. To make explicit the dependence on N we write the last equation in terms of the $O(1)$ synaptic efficacies, $j^{\alpha\alpha'}$:

$$r^{II}_{+}(\tau) = L \int_{-\infty}^{\infty} \mathrm{d}t j_{syn}(t) \Big\{ \frac{pj^{II}}{\sqrt{N}} a^I(\tau - t) + \sqrt{N} pj^{II} r^{II}_{+}(\tau - t) + \sqrt{N} pj^{IX} r^{IX}(\tau - t) \Big\}. \tag{4.48}$$

External-recurrent pairs

In the previous derivation, one can assume that neuron j belongs to the population X and proceed exactly in the same way to calculate $r^{XI}(\tau)$ from eq. 4.35. We arrive to the following equation:

$$r^{XI}(\tau) = L' \int_{-\infty}^{\infty} \mathrm{d}t j_{syn}(t) \Big\{ \frac{pj^{IX}}{\sqrt{N}} a^X(\tau - t) + \sqrt{N} pj^{II} r^{XI}(\tau - t) \Big\}. \tag{4.49}$$

where:

$$L' \equiv [< \frac{\partial \nu^I_{(0);i}}{\partial \mu^I_i} \Big|_{\mathcal{A}^{XI}_{ji}(\tau))=0} >] \tag{4.50}$$

$$\mathcal{A}^{XI}_{ji}(\tau) \equiv < \delta y^X_j(t) \delta I^I_i(t + \tau) > . \tag{4.51}$$

Notice that in this case the activity of (i, I) has no impact over neuron (j, X). Thus eq. 4.49 is valid for all values of τ.

4-A2. Leading-order solution

In this section we will solve eqs. 4.48 and 4.49 in the limit $N \to \infty$ keeping the leading order terms. We find it useful to define the perturbative parameter as $\epsilon = 1/\sqrt{N}$. Solving eqs. 4.48 and 4.49 to leading order means that all the quantities have to be evaluated at leading order. Notice, for example, that to leading order L and

L' should be calculated considering $r^{\alpha I}(\tau) = 0$. This is what we will implicitly assume in the next derivations. We start by solving eq. 4.49. After Fourier transforming it, it reads:

$$\tilde{r}^{XI}(\omega) = L'\tilde{j}_{syn}(\omega)\Big\{pj^{IX}\tilde{a}^X(\omega) + \epsilon^{-2}pj^{II}\tilde{r}^{XI}(\omega)\Big\}, \tag{4.52}$$

where, $\tilde{j}_{syn}(\omega) \equiv \frac{1}{\tau_s^{-1}+i\omega}$ is the Fourier transform of $j_{syn}(\tau)$. We now propose a Taylor expansion of the form $\tilde{r}^{XI}(\omega) = \sum_n \tilde{r}^{XI\,(n)}(\omega)$. Keeping $\omega = \omega_0$ when taking the limit $N \to \infty$ we obtain that, to leading order:

$$\tilde{r}^{XI}(\omega_0) = \epsilon^2 A\tilde{a}^X(\omega_0), \tag{4.53}$$

where $A \equiv \frac{j^{IX}}{|j^{II}|}$. Notice that this is the same constant that relates the population-averaged mean firing rates of external and recurrent neurons (see Appendix 2-A eq. 2.88, in chapter 2). As explained in the previous chapter, one can proceed like this for all values of ω and take the Fourier inverse transform to obtain:

$$r^{XI}(\tau) = \epsilon^2 A a^X(\tau) \tag{4.54}$$

We now solve the leading order for $\tilde{r}_+^{II}(\omega)$. We first Fourier transform eq. 4.48 and obtain:

$$\tilde{r}_+^{II}(\omega) = L\tilde{j}_{syn}(\omega)\Big\{\frac{pj^{II}}{\sqrt{N}}\tilde{a}^I(\omega) + \sqrt{N}pj^{II}\tilde{r}_+^{II}(\omega) + \sqrt{N}pj^{IX}\tilde{r}^{IX}(\omega)\Big\}. \tag{4.55}$$

In Appendix 4-B we will show that $a^I(\tau)$ is $O(1)$. Using the result for $\tilde{r}^{XI}(\omega_0)$ in eq. 4.53 and proposing an analogous Taylor expansion for $\tilde{r}^{II}(\omega_0) = \sum_n \epsilon^n \tilde{r}^{II\,(n)}(\omega_0)$, from eq. 4.55 we obtain:

$$\tilde{r}_+^{II}(\omega_0) = \epsilon^2(A^2\tilde{a}^{X\,(0)}(\omega_0) - \tilde{a}^{I\,(0)}(\omega_0)), \tag{4.56}$$

Proceeding like this for all the values of ω_0 we can recover the cross-covariance function in time domain. Taking into account the symmetry $r^{II}(-\tau) = r^{II}(\tau)$ we have:

$$r^{II}(\tau) = \epsilon^2(A^2 a^X(\tau) - a^{I\,(0)}(\tau)). \tag{4.57}$$

Eqs. 4.52 and 4.57 were derived for a value $\omega = \omega_0$, taking the limit $N \to \infty$ and keeping the leading order terms. $\tilde{j}_{syn}(\omega)$ is, thus, $O(1)$. But as mentioned in the previous chapter, in practice, one deals with a finite network of a given size N_c. In such

a case, being $\tilde{j}_{syn}(\omega)$ a decreasing function there is a critical frequency ω_c, such as for $\omega >> \omega_c$, $\tilde{j}_{syn}(\omega_c) << 1/\sqrt{N_c}$, and one can wonder if the predictions derived assuming $\tilde{j}_{syn}(\omega) \sim O(1)$ are still valid even when finite networks are employed. For the largest simulated network ($N = 32000$) eq. 4.57 predicts very well the cross-covariance function as can be seen in fig. 4.4b.

4-A3. Total current cross-covariances cancellation

As it happened in the case of binary neurons [Renart et al., 2010] and LIF neurons with faster filters (see chapter 3), the cancellation of spike-count cross-covariances implies the cancellation of total current zero-lag cross-covariances. In fact, working in frequency domain, one can show that a similar cancellation occurs for all values of ω (and, consequently, for all the values of τ), provided we take the $N \to \infty$ limit as we explained before (see discussion after eq. 4.57). The expression for $\tilde{c}^{II}(\omega)$ was derived in chapter 2 (eq. 2.35):

$$\begin{aligned}\tilde{c}^{II}(\omega) &= \tilde{\phi}_{syn}(\omega)p^2\left(\sum_{\alpha}(j^{I\alpha})^2\tilde{a}^{\alpha}(\omega) + N\sum_{\alpha\alpha'}j^{I\alpha}j^{I\alpha'}\tilde{r}^{\alpha\alpha'}(\omega)\right)\mathrm{d}t \\ &= \tilde{\phi}_{syn}(\omega)p^2\left(\sum_{\alpha}(j^{I\alpha})^2\tilde{a}^{\alpha}(\omega) + N\sum_{\alpha\alpha'}j^{I\alpha}j^{I\alpha`}\tilde{r}^{\alpha\alpha'}(\omega)\right). \qquad (4.58)\end{aligned}$$

Substituting the expression of $\tilde{r}^{\alpha\alpha'}(\omega)$ from eqs. 4.53 and 4.56 we obtain that the left hand side cancels at $O(1)$. Thus, the leading order of $\tilde{c}^{II}(\omega)$ is necessarily $O(\epsilon^{\gamma})$ with $\gamma \geq 1$.

Analogously, one can show that $\tilde{\mathcal{A}}^{XI}(\omega)$ also cancels to leading order:

$$\begin{aligned}\tilde{\mathcal{A}}^{XI}(\omega) &\equiv [\tilde{\mathcal{A}}^{XI}_{ij}(\omega)] \\ &= p\tilde{j}_{syn}(\omega)(\frac{j^{IX}}{\sqrt{N}}\tilde{a}^{X}(\omega) + \sqrt{N}j^{IX}\tilde{r}^{XI}(\omega)) \qquad (4.59)\end{aligned}$$

We have just shown that an asynchronous state characterized by a cancellation of the leading order of $\tilde{c}^{II}(\omega)$ and $\tilde{\mathcal{A}}^{XI}(\omega)$ exists. This is the definition of asynchronous state we presented in chapter 2. Thus, all the results and conclusions derived there apply for this case.

4-A4. Decorrelation when external inputs are weakly correlated

In the previous derivation of $r^{\alpha I}(\tau)$, we have supposed that neurons in the external population fire in a decorrelated way and their only contribution to recurrent correlations comes from projecting common inputs to the inhibitory neurons. One can extend the theory to non-zero but small correlations in the external spike trains, $r^{XX}(\tau) = \epsilon^2 r^{XX\,(2)}(\tau)$. We assume that the source of correlation is a common fluctuating external rate whose standard deviation is $\sigma_{OU;N}$. The adiabatic approximation is also valid, provided the currents afferent to a pair of neurons can be considered 'frozen' due to the large time constant of the synaptic filters. Besides, since $\sigma_{OU;N}$ is small ($O(\epsilon)$), the fluctuations around the finite mean value of ν_X will be negligible in the limit of large N. Thus, the assumption of stationarity of the current fluctuations probability distribution is, at first approximation, also valid in this case. Proceeding as we did before, but keeping the terms $r^{XX}(t)$, one arrives to the following balance equations:

$$r^{XI}(\tau) = \epsilon^2 A(a^{X\,(0)}(\tau) + r^{XX\,(2)}(\tau)) \tag{4.60}$$

$$r^{II}(\tau) = \epsilon^2 (A^2(a^{X\,(0)}(\tau) + r^{XX\,(2)}(\tau)) - a^{I\,(0)}(\tau)). \tag{4.61}$$

One can easily show that the tracking of external fluctuations by inhibitory ones also occurs in this case. Besides, the cancellation of the leading order of $\tilde{c}^{II}(\omega)$ and $\tilde{\mathcal{A}}^{XI}(\omega)$ is also obtained. Thus, we have proved that an asynchronous state as the one described in chapter 2 exists.

Appendix 4-B: Fit of the auto-covariance functions

In this appendix we study the spike auto-covariance functions. Fig. 4.8a shows these functions for the three largest simulated networks. Their shape and magnitude are similar, no matter the size of the network. Thus, they can be considered $O(1)$. In fig. 4.8b we fit the function for $N = 32000$ to an exponential function for $\tau > \tau_{ref}$. After the refractory time, the fit is reasonably good.

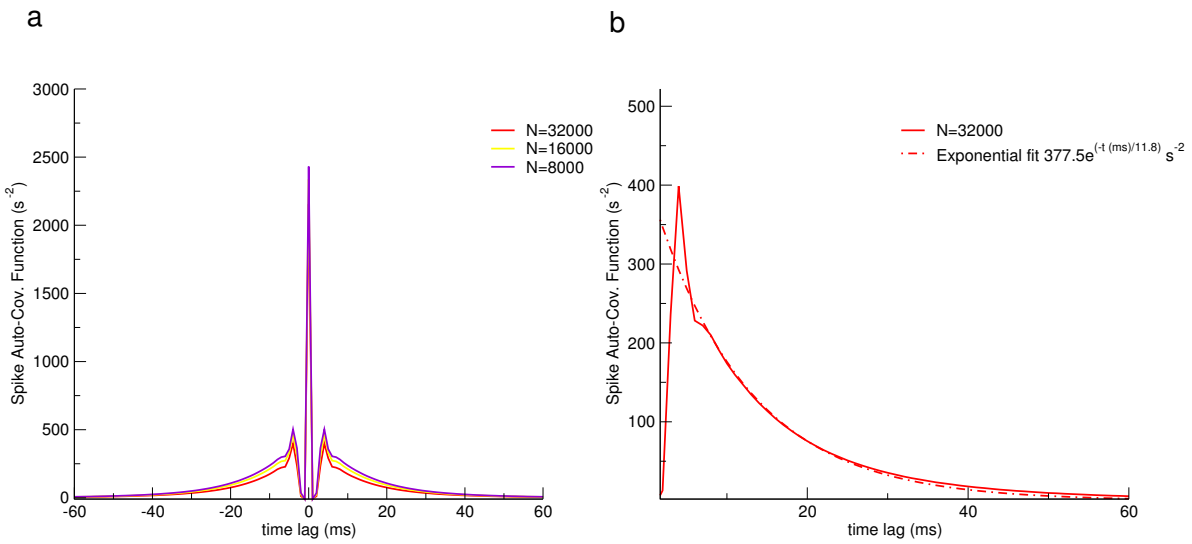

Figure 4.8: **Spike auto-covariance functions.** **a)** Population-averaged spike auto-covariance functions for different network sizes. $N = 8000$ (violet), 16000 (yellow), 32000 (red). **b)** Fit of the auto-covariance function (solid line) to an exponential (dash-dotted line) ($N = 32000$).

Besides, for $\tau_{ref} \geq \tau \geq 0$ it is easy to show by using the definition that the auto-covariance function is:

$$a^I(\tau) = \nu^I \delta(\tau) - \nu^I{}^2 \qquad \tau_{ref} \geq \tau \geq 0. \tag{4.62}$$

Thus, we conclude that we can fit the auto-covariance functions by:

$$a^I(\tau) = \begin{cases} \nu^I \delta(\tau) - \nu^I{}^2, & |\tau| \leq \tau_{ref} \\ 377.5 e^{-\frac{|\tau|}{11.8}} (s^{-2}), & |\tau| > \tau_{ref} \end{cases} \tag{4.63}$$

where we have also made use of the symmetry of $a^I(\tau)$.

Appendix 4-C. About the scaling of spike-count and total current cross-covariances

We have seen that spike-count and total current zero-lag cross-covariances follow different scalings ($O(\epsilon^2)$ vs $O(\epsilon)$). How is it possible that input correlations are different from output correlations? In the case of fast filters we have explained the phenomenon according to the shape of the cross-covariance functions. In this case we also do. Fig. 4.9a shows the cross-covariance functions of the total input currents obtained from simulations. These functions present a peak close to $\tau = 0$ which apparently gets narrower with N. Currents are filtered by the cells' membrane and, as explained in the previous chapter, this process makes the relevant magnitude for spike train decorrelation not to be the zero-lag cross-covariance of the input currents, but the integral of the whole function, which scales as $O(1/N)$ (fig 4.9b).

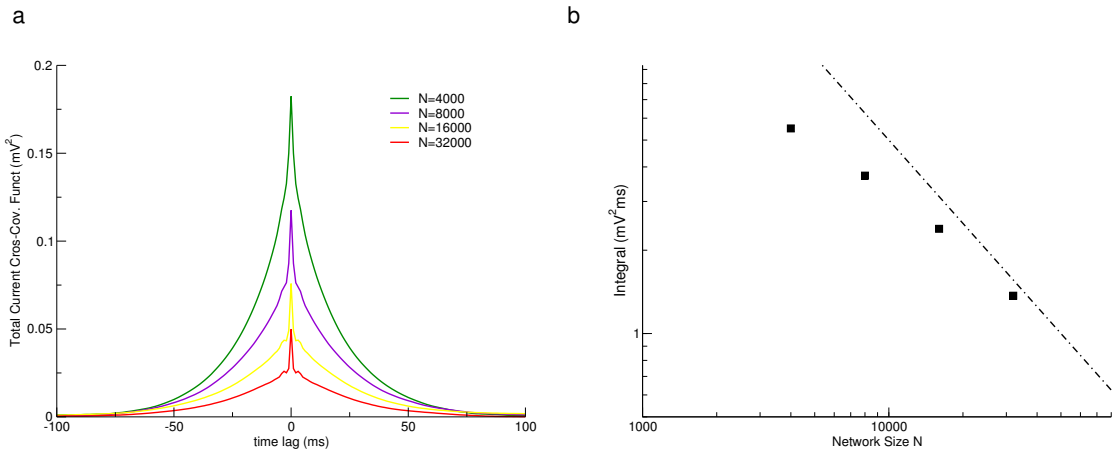

Figure 4.9: **Total Current Cross-Covariance Functions. a)** Population-averaged total current cross-covariance functions for $N = 4000$ (green), 8000 (violet), 16000 (yellow), 32000 (red).**b)** Scaling of the integral of this functions. Dash-dotted line is $\sim 1/N$.

Appendix 4-D: Common fluctuating external firing rate

In this appendix, we will calculate the cross-covariance of neurons that fire in a Poissonian way with a common and fluctuating firing rate. The process of firing is a doubly stochastic process (Cox process). As we will see, even if for a fixed firing rate the neurons fire in an independent way, the fact of sharing a common fluctuating rate induces some degree of correlation.

For the sake of simplicity, we are going to calculate the zero-lag cross-covariance of two spike trains given by a Cox process. The result is easily generalizable to delayed cross-covariances. As an example of Cox process, we will use the one mentioned in section 4.2.1.2, in which the firing rate of the external population of neurons varies according to an Ornstein-Uhlenbeck process of variance $\sigma^2_{OU;\,N}$. For a given value of the firing rate, the neurons fire independently. The law of total covariance states that if $y_i^X(t)$, $y_j^X(t)$, and $\nu^X(t)$ are random variables, then:

$$\begin{aligned} < \delta y_i^X(t)\delta y_j^X(t) > &= [< (\delta y_i^X(t)\delta y_j^X(t))|\nu^X(t) >]_{\nu^X} \\ &+ [\delta(< y_i^X(t)|\nu^X(t) >)\delta(< y_j^X(t)|\nu^X(t)) >]_{\nu^X}. \end{aligned} \tag{4.64}$$

where the symbol $[.]_{\nu^X}$ stands for an average over the possible values of $\nu^X(t)$. The first term on the right hand side of the last equation denotes the time-averaged value of the zero-lag cross-covariance calculated at a given value of the firing rate. This is, by hypothesis, zero. The second term is the cross-covariance of the time-averaged values of the spike trains conditioned to a given value of the firing rate. We realize that:

$$\begin{aligned} < \delta y_i^X(t)\delta y_j^X(t) > &= [\delta(< y_i^X(t)|\nu^X(t) >)\delta(< y_j^X(t)|\nu^X(t) >)]_{\nu^X} \\ &= < \delta\nu^X(t)\delta\nu^X(t) > \\ &= \sigma^2_{OU;\,N}. \end{aligned} \tag{4.65}$$

Thus, the common and fluctuating firing rate induces a finite value of the spike-count cross-covariance equal to the variance of the stochastic process that governs it.

Chapter 5

A model on slow oscillations: role of $GABA_B$ receptors

5.1 Introduction

To complete our study, in this chapter we will present an example of correlated activity in the form of slow oscillations. The aim of this study is to explain the role of $GABA_B$ receptors in the generation of Up/Down states. A computational model is employed to test some hypothesis about how $GABA_B$ can induce variability in the duration of the cycles. Model predictions are compared with experiments on ferret slices carried out by M.V. Sánchez-Vives' lab members [Sanchez-Vives et al., 2010].

Spontaneous activity during slow wave sleep or in anesthetized animals is characterized by the emergence of cycles of high and low activity, referred to as Up and Down states, respectively [Steriade et al., 1993a,b,c, Lampl et al., 1999]. Such transitions can also be recorded in vitro in slices of ferrets [Sanchez-Vives and McCormick, 2000] and mice [Cossart et al., 2003]. The biophysical mechanisms by which activity organizes in such a way are not well understood, but some reasonable hypothesis can be found in the literature which merge the effect of cortical interactions [Cossart et al., 2003, Metherate and Ashe, 1993, Sanchez-Vives and McCormick, 2000, Seamans et al., 2003, Wilson and Kawaguchi, 1996] with neuronal intrinsic features [Crunelli et al., 2005, Mao et al., 2001, Sanchez-Vives and McCormick, 2000]. Modeling studies have focused on some plausible mechanisms responsible for the transitions from Up to Down states, such as firing rate adaptation [Compte et al., 2003], $GABA_B$ inhibition [Parga and Abbott, 2007] and short-term synaptic depression [Timofeev et al., 2000, Melamed et al., 2008]. Probably these mechanisms are not exclusive and several of them participate in some degree in the generation of the rhythms, being the whole set of the experimentally

observed features determined by their combined effect.
Here we will study the role of $GABA_B$ receptors in slow oscillations generation. Motivated by the results by M. Sánchez Vives lab on the blockade of receptors [Sanchez-Vives et al., 2010], which we briefly introduce in the *Results* section, we will present a network model based on Parga and Abbott, 2007. We will study the specific role of $GABA_B$ receptors in the neural dynamics, especially its role in cycle duration and duration variability.

5.2 Methods

5.2.1 Model

We have simulated networks of IF neurons, with the addition of a nonlinear membrane current, receiving synaptic input composed of slow and fast excitatory and inhibitory conductances. These networks consist of random connections with finite range. Each neuron is described by its membrane potential V which, below its threshold value, evolves according to the equation:

$$\tau_m \frac{dV}{dt} = -g_L(V - V_L) - g_a(V - V_a) - I_{syn,E} - I_{syn,I} - I_{noise} - I_{nl}\,. \qquad (5.1)$$

Here τ_m is the membrane time constant, g_L is the leak conductance and V_L is the leak reversal potential. The adaptation current, $g_a(V - V_a)$, affects only the excitatory neurons. Its conductance, g_a, decays exponentially with a time constant t_a, until a spike is fired. When this happens, it is augmented by an amount Δg_a. $I_{syn,E}$ and $I_{syn,I}$ are the excitatory and inhibitory synaptic currents. I_{noise} is an external noise. I_{nl} describes a nonlinear property of the neuron (see below). A neuron fires whenever its membrane potential $V(t)$ reaches the spike generation threshold V_{th}. At that point, an action potential is discharged, and the potential $V(t)$ is reset and kept at a value V_{reset} during a refractory period τ_{ref}. Two excitatory (AMPA, NMDA), and two inhibitory ($GABA_A$, $GABA_B$) synaptic currents, are included as:

$$\begin{aligned} I_{syn,E}(t) &= g_{AMPA}(V(t) - V_{AMPA}) + g_{NMDA}(V(t) - V_{NMDA}) \\ I_{syn,I}(t) &= g_{GABA_A}(V(t) - V_{GABA_A}) + g_{GABA_B}(V(t) - V_{GABA_B})\,. \end{aligned}$$

When a neuron fires an action potential, the synaptic conductances of its post-synaptic neurons are modified by an amount Δg_X for X = AMPA, NMDA and $GABA_A$, $GABA_B$. Otherwise, the synaptic conductances decay exponentially, with synaptic time constant τ_X. Nonlinearities characterizing NMDA and the $GABA_B$ receptors are not included,

because the emphasis is on their timescales not their voltage dependencies.

The nonlinear membrane current pretends to take account for some of the ions fluxes (Ca^{2+}, K^{+}...) not included in the leakage term. It is described by:

$$I_{nl}(t) = c(V(t) - V_1)(V(t) - V_2)(V(t) - V_3)$$

where $V_1 < V_2 < V_3$ and c is a parameter that determines the strength of the current. In the absence of noise, I_{nl} induces three fixed points, one of them being unstable. Fluctuations induced by the noise term and by the synaptic currents allow the neuron membrane potential not to be indefinitely stuck to the fixed point values, but to alternate in a bistable way[Parga and Abbott, 2007].

Each neuron receives independent noise I_{noise} consisting of two Poisson trains, one excitatory and one inhibitory. These Poisson trains can be described by their unitary conductances($\Delta g_{syn,E}$ and $\Delta g_{syn,I}$) and their rates. This noise is exponentially filtered with slow synaptic time constants (i.e. τ_{NMDA} and τ_{GABA_B}).

5.2.2 Parameter values

We have simulated several networks in order to reproduce the experimentally observed data. These networks differ in parameters related to synaptic and adaptation properties. We firstly present the parameters common to all the networks and then we will proceed to give the parameter values which are different for each of them.

5.2.2.1 Network parameters

Networks contain 4000 neurons of which 17% are inhibitory and the rest excitatory. Each neuron is connected with a probability of 2% to other neurons contained within a disk centered about its location and containing about 31% of the total number of neurons. This results in each neuron, on average, connecting to 25 other neurons. The network size is 50×80, with periodic boundary conditions.

5.2.2.2 Neuron parameters

All the neurons have a membrane time constant of 20 ms and a refractory time $\tau_{refr} = 5$ ms. Other passive properties are distributed uniformly. The membrane

threshold, V_{th}, takes values in the interval -45 ± 2 mV, the reset potential V_{reset} in the interval -55 ± 1 mV, and the leak potential V_L in the interval -68 ± 1 mV. The parameters of the nonlinear current are $c = 0.03$ mV^{-2}, $\tilde{V}_1 = -72 \pm 2$ mV, $\tilde{V}_2 = -58 \pm 2$ mV and $\tilde{V}_3 = -44 \pm 2$ mV.

5.2.2.3 Synaptic parameters

$AMPA$ and $NMDA$ currents are present in all excitatory synapses. Similarly, we assigned $GABA_A$ receptors to 100% of the inhibitory synapses but $GABA_B$ receptors only to 70% of them.

Here we present the parameter values for the network that is referred to as 'typical'. The synaptic time constants are $\tau_{AMPA} = 2$ ms, $\tau_{NMDA} = 100$ ms, $\tau_{GABA_A} = 10$ ms, and $\tau_{GABA_B} = 200$ ms. The leak conductance of excitatory neurons has the value $g_{E,L} = 10nS$. All unitary conductances are measured in units of $g_{E,L}$. $\Delta g_{E,AMPA} = 0.54$, $\Delta g_{E,NMDA} = 0.04$, $\Delta g_{E,GABA_A} = 1.00$, $\Delta g_{E,GABA_B} = 0.18$. For inhibitory neurons, $\Delta g_{I,AMPA} = 0.38$, $\Delta g_{I,NMDA} = 0.04$, $\Delta g_{I,GABA_A} = 0.02$, $\Delta g_{I,GABA_B} = 0.017$ and $g_{I,L} = 1.4$. In addition, for excitatory neurons $\Delta g_a = 0.03$, $V_a = -80$ mV and $\tau_a = 1900$ ms. The reversal potentials for the inhibition, V_{GABA_B} and V_{GABA_A} fall uniformly within the intervals -90 ± 2 mV and -80 ± 2 mV, respectively. V_{AMPA} and V_{NMDA} are both set to zero.

5.2.2.4 Other networks

The network which is called 'atypical' differs from the 'typical' one only in the unitary conductance $\Delta g_{I,AMPA}$, and the adaptation characteristic time τ_a which now take the value $\Delta g_{I,AMPA} = 0.57$ and $\tau_a = 2500$ ms respectively.

5.2.2.5 Parameters of the noise model

The parameters of the noise model were: $\Delta g_{syn,E} = 0.09$, $\Delta g_{syn,I} = 0.18$ for the conductances and $\nu_{syn,E} = 66.66$ Hz, $\nu_{syn,I} = 24.31$ Hz for the firing rates.

5.2.3 Up and Down transitions detection algorithm

Up states detection algorithm

The algorithm employed to identify the Up-Down transitions is the same as that used by Peyrache et al., 2009 based on Luczak et al., 2007, though other parameter values are needed in this context in order not to miss any of the transitions which take place.

This algorithm provides criteria for determining when the network moves from one state to another. These criteria can be summarized as follows:
Up-to-Down transitions: At a given time, the number of spikes of each neuron in a window of 60 ms is measured. If every cell fires less than two spikes the transition to the Down state takes place.

Down-to-Up transitions: If the percentage of neurons that fire in windows of 60 and 100 ms is, at least 10% and 30%, respectively, then the transition to the Up state occurs.

5.2.4 Correlation Functions and CV

We have calculated spike train cross-correlation functions for a pair of neurons i,j as follows:

$$r_{i,j}(\tau) = \frac{\int y_i(t) y_j(t-\tau) \mathrm{d}t}{\nu_i \nu_j}, \tag{5.2}$$

$y_{i(j)}(t)$ and $\nu_{i(j)}$ being the spike trains and the rate of neuron $i(j)$ respectively, and τ the time lag. In the figures we plot the average of this magnitude over 19900 pairs.

Cross-correlation functions of the currents were computed as:

$$c_{\tilde{I}_\alpha, \tilde{I}_\beta}(\tau) = \int \tilde{I}_\alpha(t) \tilde{I}_\beta(t-\tau) \mathrm{d}t, \tag{5.3}$$

where $\tilde{I}_{\alpha,(\beta)}$ stands for the population averaged currents $I_{\alpha,(\beta)}$. Both $r_{i,j}(\tau)$ and $c_{\tilde{I}_\alpha, \tilde{I}_\beta}(\tau)$ were normalized to their value at their respective peaks. Notice that here we are not interested in the scaling of the cross-covariance function, so in order to better plot and compare the normalization employed is more adequate.

CVs of the duration of the states were calculated in the standard way:

$$CV_{duration} = \frac{SD_{duration}}{mean_{duration}} \tag{5.4}$$

5.2.5 Simulation

Simulation times were typically 1200 s. Differential equations were integrated using the Euler method with an integration step of $\Delta t = 0.1$ ms. All codes were written in C and run under the Linux operating system.

5.3 Results

5.3.1 Summary of the experimental results

The effect of $GABA_B$ synaptic receptors in the generation and properties of slow waves was studied in slices of ferrets. $GABA_B$ receptors blocker CGP 35348 was employed. Experiments were carried out by M.V. Sánchez-Vives' lab members [Sanchez-Vives et al., 2010].

The most relevant information of the experimental results is summarized in tables 5.1 and 5.2. We have classified networks as typical (n=28) and atypical (n=9) according to the behaviour of the duration of the Down states and the cycle when the $GABA_B$ receptors were blocked. In typical networks, Down state and cycle duration became large when $GABA_B$ receptors were blocked while in atypical ones the situation was reversed. Variability of the duration of Down states decreased and an enlargement in the duration of the Up states was observed for both kind of networks when CGP was applied.

Typical Networks

	CGP/Control
Average Up duration	1.85
Average Down duration	1.6
Average Up duration CV	0.6
Average Down duration CV	0.7
Average Cycle duration CV	0.65

Table 5.1: Typical networks relevant features. Data from Sanchez-Vives et al., 2010

Atypical Networks

	CGP/Control
Average Up duration	1.8
Average Down duration	0.7
Average Up duration CV	1.1
Average Down duration CV	0.65
Average Cycle duration CV	0.5

Table 5.2: Atypical networks relevant features. Data from Sanchez-Vives et al., 2010

5.3.2 The model: description of its basic properties

First we present the basic features of the slow oscillations generated with the model. We generated two example networks, responding to the $GABA_B$ receptor blockade in a typical/atypical situation. We next explored a mechanistic explanation of the most remarkable features of the effects of the $GABA_B$ receptors described in the previous section: modulation of the duration of the Up states and modulation of the regularity of the oscillations.

We generated several sample networks with a fixed connectivity but differing in the precise realization of the connectivity matrix and in the value of some parameters (see Methods for details). Two examples networks (typical and atypical) are shown in figs. 5.1a and 5.1b respectively. The duration of the Up and Down states in both networks correspond to values characteristic of the experimentally studied slices. In both cases blocking the $GABA_B$ receptors did not suppress the slow oscillation and the duration of the Up state became longer, a feature present in all the generated samples and in all the slices recorded in the experiments. For the network in fig. 5.1a the average duration of the Down states increased as it did in the typical experimental cases. As it has been described in sectin 4.3.1, the Down states of atypical slices were instead shortened, as occurs with the example presented in fig. 5.1b. Notice that for the two networks the histogram of the duration of Down states (figs. 5.1a.2, a.5 and 5.1b.2, a.5) has a larger dispersion when the $GABA_B$ receptors are not blocked. To quantify the variability of the cycle and of the durations of the Up and Down states we computed their coefficients of variation. For the two networks displayed in fig. 5.1, the CV values were: 0.29 (0.34), 0.22 (0.25) and 0.20 (0.25) for the Down state, the Up state and the whole cycle duration respectively in the typical (atypical) network in the control condition and 0.15 (0.15), 0.10(0.20) and 0.13 (0.15) when the $GABA_B$ receptors are

blocked. These values showed a substantial decrease in variability following $GABA_B$ receptors blockade in both networks, especially for the duration of the Down states. Panels 3 and 6 in figs. 5.1a and 5.1b illustrate the correlograms of the spike trains for the control and the $GABA_B$ blocked conditions.

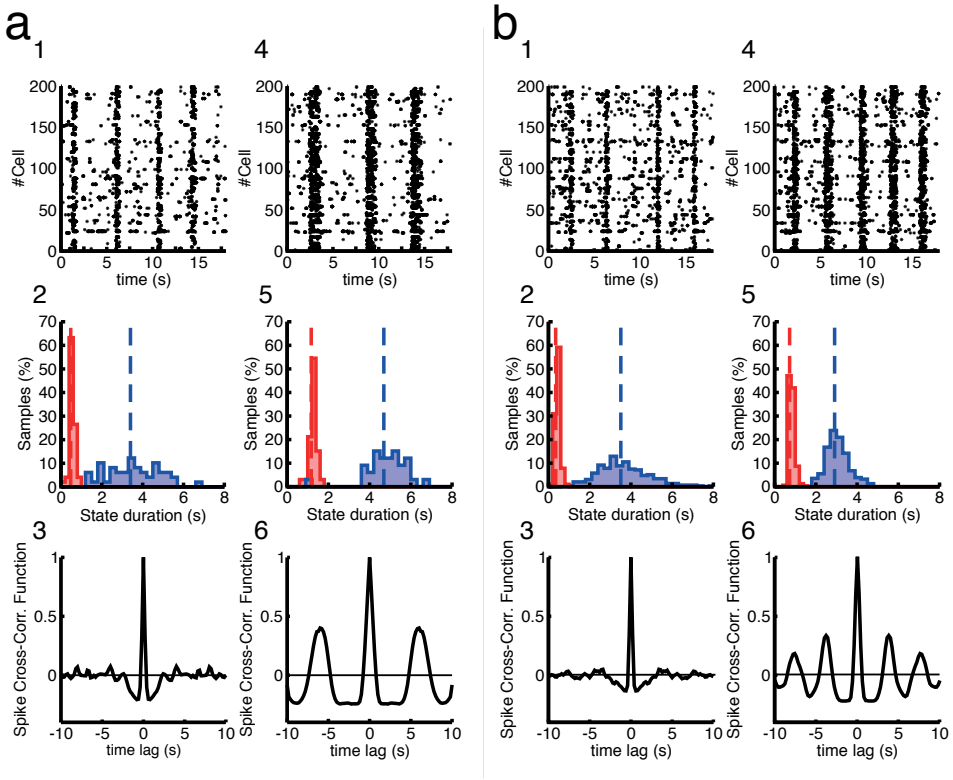

Figure 5.1: **a) Properties of the slow oscillation in a typical network.** Plots on the left refer to the control condition and on the right to the slice with blocked $GABA_B$ receptors. Panels (1, 4) Rastergrams. Panels (2, 5) Histograms of the duration of the Up (red) and Down (blue) states. Dashed lines correspond to their mean value: Mean durations of Up (Down) states are 0.45s (3.42s) in (2) and 1.17s (4.69s) in (5). Panels (3, 6) Spike-train correlation functions averaged over 100 pairs of neurons. Note how the oscillation becomes more regular in the blocked condition. **b) Properties of the slow oscillation in an atypical network.** Conventions are as in fig. 5.1a. Mean durations of Up (Down) states are 0.36s (3.51s) in (2) and 0.73s (2.91s) in (5).

5.3.3 Explaining the regulation of variability by $GABA_B$ receptors

In the experimental results we found that the decrease in the variability of the duration of Down states and cycles occurred for both typical and atypical networks,

while the decrease in Up state duration variability only occurred in typical networks. To investigate the factors responsible for the variability of the Down states duration in our model we looked at the traces of the synaptic and adaptation currents (fig. 5.2) for the two networks described in fig. 5.1.

Let us first see why when the $GABA_B$ receptors are blocked the oscillation is rather regular. Fluctuations of the excitation occur either from synaptic or external noise. Since in the blocked condition the inhibition is fast ($GABA_A$-mediated), it can track these fluctuations easily (Renart et al. [2010]) so that they do not propagate through the network unless a large population of excitatory neurons becomes active. Thus, the dynamics consists in a gradual increase of the excitation that starts during the Down state and grows until an Up state is generated (figs. 5.2b and 5.2d). At this point the fast inhibition follows this large change in the excitation but it cannot suppress it. During Up states the adaptation current progressively increases and produces the end of the Up state. Since the characteristic time of the adaptation conductance is large and spiking is rare during the Down state this current decays smoothly and slowly. These mechanisms give rise to a rather regular sequence of cycles. This is illustrated in fig. 5.2 with the temporal traces of the synaptic and adaptation currents computed with the model (panel b is for the same typical network shown in fig. 5.1a and panel d refers to the atypical network in fig. 5.1b). When the $GABA_B$ receptors are not blocked they produce two main effects. First, the total inhibitory current increases. A consequence of this change is the shortening of the duration of the Up states (fig. 5.1 and figs. 5.2a,c). The second effect is the loss of regularity. The experimental observation shows that when the $GABA_B$ receptors are not blocked Down states can be either longer or shorter than in the blocked condition, the second case being the most typical. Fig. 5.1a corresponds to a simulated network with properties similar to a typical network while fig. 5.1b shows an example of an atypical network. In the two networks the variability is higher in the control condition but it has to be explained differently because the mean duration of their Down states is related differently to the corresponding networks with blocked $GABA_B$ receptors.

For the atypical network (fig. 5.1b) a comparison of the temporal trace of the currents for the control and the blocked networks obtained with simulations (shown in fig. 5.2c and d) indicates that some Up states are suppressed in the control condition. This enlarges the mean duration of the Down states (fig. 5.1b) and increases their variability (from CV=0.15 to 0.34). For the network corresponding to the typical case (fig. 5.1a) the temporal traces of the currents (shown in fig. 5.2a and b) indicate that, in contrast

to the atypical case, new Up states with respect to the blocked condition appear. This also introduces a similar change in the variability of the duration of the Down states (CV increases from 0.15 to 0.29). To explain this different behavior, let us focus on the way the two networks were constructed. They differ in the value of only two parameters. First, in the typical network the NMDA unitary conductance is 40% larger than in the atypical one. To isolate the effect of a larger NMDA conductance on the duration of the Down states let us consider a network identical to the atypical one (fig. 5.1b) but with the NMDA unitary conductances increased by 40%. The distributions of Down state durations appear in figs. 5.3a (control) and 5.3b (blocked $GABA_B$). The stronger excitatory recurrent inputs produce a reduction of the duration of Down states in both the control and the blocked conditions. This can be seen by comparing the mean duration of Down states for the modified network (full vertical lines) with the corresponding mean duration for the original atypical network (dashed vertical lines). However, one important difference arises. In the control condition the shortening of the duration of the Down states is about 68% while in the blocked condition it is only about 33%. Notice that this difference makes the original atypical network (fig. 5.1b) become typical, in the sense that now the duration of Down states is longer when $GABA_B$ receptors are blocked.

Why this differential shortening of Down states? The explanation can be found in fig. 5.3c. Here we show the cross-correlation function between the excitatory and inhibitory currents during the Down states for the atypical network in fig. 5.1b. In the blocked condition (dashed line), the tracking of excitatory currents by inhibitory ones is almost instantaneous (the peak is located at 1.0 ± 1.0 ms). A consequence of this is that inhibitory inputs can follow excitatory ones until they are strong enough to cause the network to arrive to an Up state. However, in the control condition the slow dynamics of the $GABA_B$ receptors makes the tracking of the excitation by inhibition difficult. This fact is reflected by the peak of the cross-correlation function at 46.0 ± 1.0 ms as can be seen in fig. 5.3c (full line). This lag is 86.0 ± 1.0 ms if only the $GABA_B$ component of the inhibition is considered (dashed-dotted line). Since the tracking mechanism is less efficient in the control condition, the shortening of Down states duration when increasing the value of NMDA unitary conductances is much more pronounced than in the blocked condition.

The two example networks displayed in fig. 5.1a,b have been selected such that they have approximately the same Down state duration in the control condition, which reflects the experimental observation that the difference between 'typical' and 'atypical'

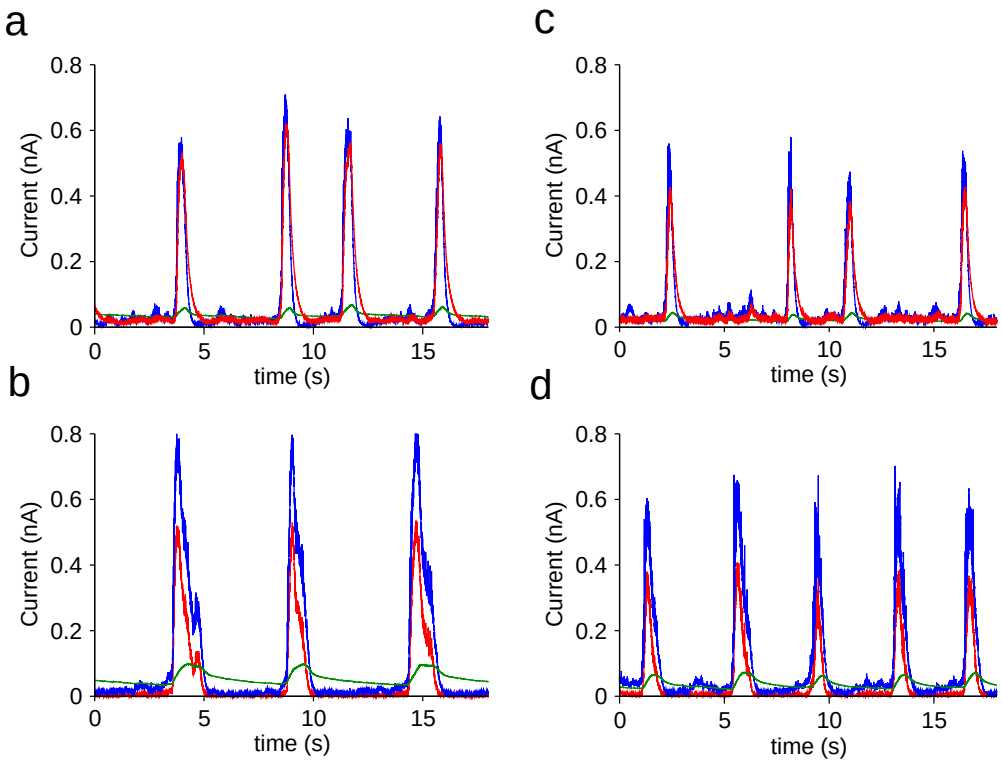

Figure 5.2: **Temporal traces of the synaptic and adaptation currents** Temporal traces of the population averaged currents for the typical network (left side) and the atypical one (right side). Panels (a) and (c) refer to the control slice and panels (b) and (d) to the slice with the $GABA_B$ receptors blocked. Notice the increased regularity in the blocked case. Blue lines: total excitatory (AMPA plus NMDA) current. Red lines: total inhibitory ($GABA_A$ plus $GABA_B$) current. Green lines: adaptation currents.

networks do not depend on the duration of cycles before blocking $GABA_B$ receptors. Although the network in fig. 5.3a,b is already a typical one, the mean duration of its Down states in the control condition is shorter than that of the atypical network in fig. 5.1b. To obtain the typical network in fig. 5.1a we have then taken the characteristic time of the adaptation conductance 80% larger than in the atypical network.

5.4 Discussion

The model reproduces some of the experimentally observed features in ferret's slices. To start with, the typical durations of Up and Down states are well matched (frequency <1 Hz). The model also predicts a decrease in the variability of the Down state and cycle durations and an enlargement of the duration of the Up states when

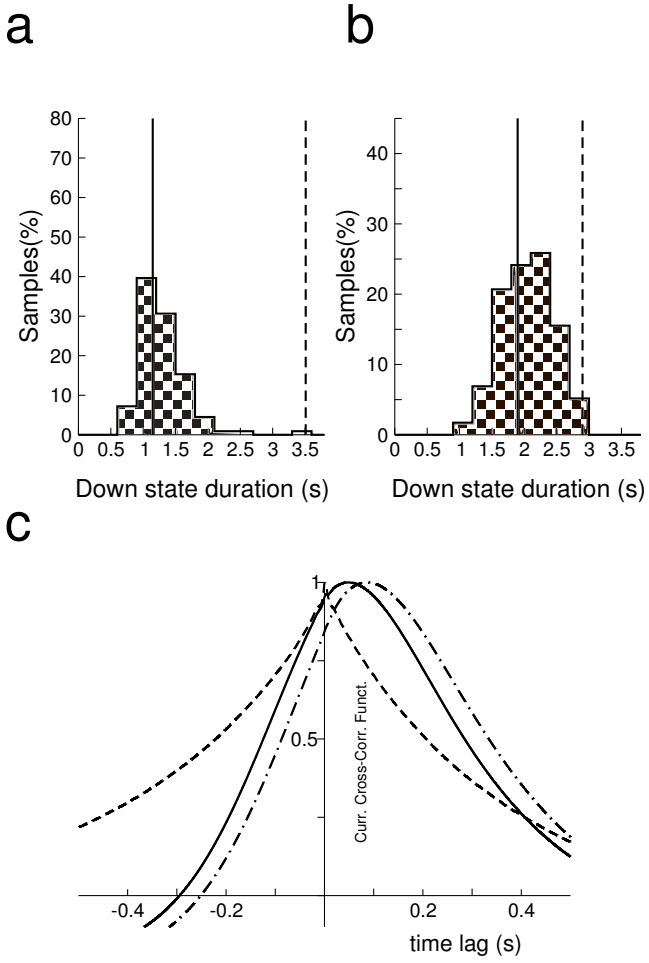

cu

Figure 5.3: **a) b) Influence of NMDA conductances in the duration of Down states. a)** Histograms of the duration of the Down states in a network with the same parameters as the atypical one but with NMDA unitary conductances increased 40% in the control condition. Average Down state duration (solid line) is 1.1s, 68% smaller than the original value, 3.51s (dashed line). **b)** Same as (a) but in the blocked condition. Average Down states duration (solid line): 1.8s, about 33% smaller than the original value, 2.91s (dashed line). **c) Correlation function between excitatory and inhibitory currents in the atypical network.** Full line: Correlation function between total excitatory and inhibitory currents in the control condition. Dashed line: same as before but in the $GABA_B$ blocked condition. Dashed-dotted line: Correlation function between total excitation and $GABA_B$ component of the inhibition.

$GABA_B$receptors are blocked as reported in the experiments. We also give a plausible explanation on how the relatively slow dynamics of $GABA_B$ receptors increase the variability of the duration of the Down states and determine the difference between the experimentally found typical and atypical networks. Tracking of excitatory activity has been reported to be an effective decorrelation mechanism in recurrent neurons (see [Renart et al., 2010] and the three previous chapters). Here we have described another

situation where the presence or absence of it seems to be relevant to understand the phenomenon.

Final conclusions

Asynchronous states in generic balanced networks of *densely* connected and *strongly* interacting neurons can be characterized independently of the neuron model. Balance equations that relate spike train auto- and cross-covariance functions were derived assuming vanishing cross-covariance functions of the total afferent currents to recurrent pairs and of the total current afferent to recurrent neurons and the activity of external ones. Population-averaged spike-count cross-covariances can be calculated from spike train cross-covariance functions and are, on average, $O(1/N)$, [1] in agreement with previous definitions of asynchronous states [Ginzburg and Sompolinsky, 1994]. The distribution of pairwise spike-count cross-covariances is wide, implying that they take positive and negative values with similar probabilities. In such states, however, the components of the currents afferent to pairs of neurons are correlated due to the large amount of common input. We have proved that for the asynchronous state to exist, it is a *necessary* and *sufficient* condition that the inhibitory activity precisely tracks the excitatory one.

To prove that an asynchronous state indeed exists in realistic networks, we focused on leaky-integrate-and-fire (LIF) neurons. We have used two different approaches. In chapter 3, we studied networks with fast synaptic kinetics for which the linear response approximation [Brunel and Hakim, 1999, Lindner and Schimansky-Geier, 2001] was appropriate. In chapter 4 we took into account the fact that when the number of incoming inputs to a neuron is large, the effective membrane time constant is small. This allows one to employ the adiabatic approximation [Moreno-Bote and Parga, 2004, 2006, 2010]. In both cases we found self-consistent equations for the spike train cross-covariance functions and solve them to leading order in N, finding *balance* equations that relate them to the auto-covariance functions.

Our simulations show that, in both cases and for biologically realistic network sizes,

[1] N is a parameter proportional to the number of neurons in the network

spike-count cross-covariances can be well predicted from the leading order solution. In the case of slow synaptic filters, the leading order solution reproduces also the whole spike train cross-covariance function for a network of inhibitory neurons with a realistic value of N. In the case of fast synaptic filters, the leading order solution reproduces the low frequency components of the spike train cross-covariance function for a finite value of N. The range of validity of this solution in the frequency space increases with N. An analytical study about the finite size solution shows that a fast time scale appears in this case that makes cross-covariance functions to be small and very concentrated in time. The same study allows us to find more accurate solutions for the spike train cross-covariance functions in networks with fast synaptic filters.

Auto-covariance functions of a macroscopic signal such as Multi-Unit Activity (MUA) in terms of auto-covariance functions of the neurons were also calculated. In principle, the described technique allows for the calculation of other macroscopic signals such as Local Field Potential (LFP) in networks with pyramidal cells. This is a working line that should be explored in the next future. Preliminary results are quite encouraging.

The example networks we have studied in detail are biologically relevant. In chapter 3 we focused on networks with excitatory and inhibitory neurons while in chapter 4 we studied networks with only inhibitory neurons. Networks of the first type are common in cerebral cortex while basal ganglia is an example of structures having only inhibitory neurons. Low cross-correlations of neuronal activity have been experimentally reported in the cortex [Renart et al., 2010, Graupner and Reyes, 2013, Ecker et al., 2010, Miura et al., 2012, Hansen et al., 2012, Middleton et al., 2012] and in basal ganglia [Magill et al., 2000, Nini et al., 1995, Raz et al., 2000, Bar-Gad et al., 2003].
To finish, in chapter 5 we studied slow oscillations with a computational model [Parga and Abbott, 2007]. We could reproduce some of the experimental features of ferrets' slices and explain the observed changes in the duration of the Up/Down cycles and the differences in their variability, when $GABA_B$ receptors were blocked. We found that the tracking (or the lack of it) of excitation by inhibition also plays here an important role.

Madrid, 9th May 2014.

Conclusiones finales

El estados asíncrono en redes balanceadas formadas por neuronas densamente conectadas y que interactúan fuertemente pueden ser caracterizados, en caso de que existan, independientemente del modelo de neurona. Hemos encontrado ecuaciones de balance que relacionan funciones de covarianza cruzada y auto-covarianza de trenes de espigas suponiendo que las corrientes aferentes totales que llegan a pares de neurons así como la actividad de neuronas externas y dichas corrientes no están correlacionadas. La covarianza del número de espigas emitidas por pares de neuronas se puede calcular a partir de las funciones de covarianza cruzada de los trenes de espigas y son, en media, $O(1/N)$, donde N es un parámetro proporcional al número de neuronas. Esto está de acuerdo con previas definiciones del estado asíncrono [Ginzburg and Sompolinsky, 1994]. La distribución de dichas covarianzas es ancha, lo que permite encontrar valores positivos y negativos para covarianzas de pares individuales con similar probabilidad. A pesar de que partimos de una caracterización del estado asíncrono en el que las corrientes totales (suma de contribución excitadora e inhibidora) que reciben pares de neuonas no están correlacionadas, las componentes de la corriente total están fuertemente correlacionadas debido al gran número de entradas comunes, lo que está de acuerdo con datos experimentales [Graupner and Reyes, 2013]. Hemos probado analíticamente que el seguimiento de la actividad instantánea excitadora llevado a cabo por la ihibición es condición necesaria y suficiente para que exista un estado asíncrono.

Para comprobar que el estado asíncrono existe en redes realistas nos hemos centrado en neuronas de integración y disparo. Hemos utilizado dos aproximaciones analíticas diferentes. En el capítulo 3, hemos estudiado redes con dinámica sináptica rápida para las cuales la teoría de respuesta lineal [Brunel and Hakim, 1999, Lindner and Schimansky-Geier, 2001] resultaba apropiada. En el capítulo 4 tuvimos en cuenta que en el cerebro las neuronas están sometidas a un gran bombardeo de imputs lo que implica que la constante de membrane es pequeña cuando se la compara con las constantes de tiempo sinápticas. Esto permite utilizar una aproximación adiabática [Moreno-Bote and Parga, 2004, 2006, 2010]. En ambos casos, encontramos ecuaciones

autoconsistentes para las funciones de covarianza cruzada de trenes de espigas y las resolvemos a orden dominante en N. Encontramos ecuaciones de *balance* que relacionan estas funciones con las auto-covarianzas de los trenes de espigas.

Nuestras simulaciones muestran que en ambos casos la covarianza del número de espigas emitidas por pares de neuronas se puede predecir bien a partir de la solución para el orden dominante. En el caso de filtros sinápticos lentos, esta solución, además, reproduce enteramente la función de covarianza cruzada de trenes de espigas para una red inhibidora con un tamaño realista de N. En el caso de filtros sinápticos rápidos, la soluci'on a orden dominante reproduce las componente de baja frecuencia de la función de covarianza cruzada de espigas para un valor de N finito. El rango de frecuencias para el cual la solución a orden dominante es una buena aproximación de las funciones de covarianza cruzada de trenes de espiga esta solución en el espacio de frecuencias aumenta cuando aumenta N. Un estudio anaítico nos permite comprobar que la aparición de una escala de tiempos rápida es la responsable de que las correlaciones además de pequeñas, estén concentradas en el tiempo. Este mismo estudio nos permite encontrar mejores aproximaciones analíticas para las funciones de covarianza cruzada de trenes de espigas en redes con este tipo de filtros.

Hemos calulado también funciones de auto-covarianza de señales macroscópicas como el Multi-Unit Activity (MUA) en términos de funciones de auto-covarianza de espigas. En principio, la técnica que describimos permitiría calcular las funciones de auto-covarianza y spectro de potencias de otras señales macroscópicas como el Local Field Potential en redes con neuronas piramidales. Esta es una línea de trabajo que se va a estudiar en un futuro próximo. Los resultados preliminares son muy esperanzadores.
Las redes que hemos estudiado como ejemplo y con mayor detalle son biológicamente relevantes. En el capítulo 3 nos concentramos en redes con neuronas excitadoras e inhibidoras mientras que en el capítulo 4 estudiamos redes con neuronas inhibidoras. Redes del primer tipo son comunes en la corteza cerebral mientras que los ganglios basales son un ejemplo de estructura formada únicamente por neuronas inhibidoras. En ambos casos, estudios experimentales [Renart et al., 2010, Graupner and Reyes, 2013, Ecker et al., 2010, Miura et al., 2012, Hansen et al., 2012, Middleton et al., 2012] (corteza) [Magill et al., 2000, Nini et al., 1995, Raz et al., 2000, Bar-Gad et al., 2003] (ganglios basales) han mostrado que las actividades de las neuronas pueden, en ciertas circunstancias, no estar correlacionadas.

Por último, en el capítulo 5 estudiamos oscilaciones lentas con un modelo computa-

cional. El modelo reproduce algunas características de rodajas de cerebro de hurón y explica los distintos cambios en la duración de los estados Up/Down y las diferencias en su variabilidad cuando se bloquean los receptores de $GABA_B$. Encontramos que el intervalo de tiempo con el que la inhibición sigue a la excitación también juega aquí un papel importante.

Madrid, 9th May 2014.

References

M. Abeles. *Corticonics: Neural Circuits of the Cerebral Cortex.* Cambridge University Press, 1991.

D. Amit and N. Brunel. Model of global spontaneous activity and local structured activity during delay periods in the cerebral cortex. *Cerebral Cortex*, 7:237–252, 1997a.

D. Amit and N. Brunel. Dynamics of a recurrent network of spiking neurons before and following learning. *Network: Comput. Neural Syst.*, 8:373–404, 1997b.

J. Anderson, I. Lampl, I. Reichova, M. Carandini, and D. Ferster. Stimulus dependence of two-state fluctuations of membrane potential in cat visual cortex. *Nat. Neurosci.*, 3(6):617–621, 2000a.

J. S. Anderson, M. Carandini, and D. Ferster. Orientation tuning of input conductance, excitation, and inhibition in cat primary visual cortex. *J. Neurophysiol.*, 84(2):909–926, 2000b.

B. B. Averbeck, P. E. Latham, and A. Pouget. Neural correlations, population coding and computation. *Nat. Rev. Neurosci.*, 7:358–366, 2006.

W. Bair, E. Zohary, and W. T. Newsome. Correlated firing in macaque visual area MT: time scales and relationship to behavior. *J. Neurosci*, 21(5):1676–1697, 2001.

I. Bar-Gad, G. Heimer, Y. Ritov, and H. Bergman. Functional correlations between neighboring neurons in the primate globus pallidus are weak or nonexistent. *J. Neurosci.*, 23:4012–4016, 2003.

M. Bazhenov, I. Timofeev, M. Steriade, and T. J. Sejnowski. Model of thalamocortical slow-wave sleep oscillations and transitions to activated states. *J. Neurosci.*, 22: 8691–8704, 2002.

A. Bernacchia and X.-J. Wang. Decorrelation by recurrent inhibition in heterogeneous neural circuits. *Neural Comput.*, 25(7):1732–1767, 2013.

O. Bernarder, R.J. Douglas, K.A.C. Martin, and C. Koch. Synaptic background activity influences spatiotemporal integration in single pyramidal cells. *Proc. Natl. Acad. Sci. USA*, 88:11569–11573, 1991.

L. J. Borg-Graham, C. Monier, and Y. Fregnac. Visual input evokes transient and strong shunting inhibition in visual cortical neurons. *Nature*, 393:369–373, 1998.

K.H. Britten, M.N. Shadlen, W.T. Newsome, and Movshon J.A. The analysis of visual motion: A comparison of neuronal and psychophysical performance. *J. Neurosci.*, 12:4745–4765, 1992.

N. Brunel and V. Hakim. Fast global oscillations in networks of integrate-and-fire neurons with low firing rates. *Neural Comput.*, 11(7):1621–1671, 1999.

N. Brunel and X.J. Wang. What determines the frequency of fast network oscillations with irregular neural discharges? I. Synaptic dynamics and excitation-inhibition balance. *J.Physiol.*, 90(1):415–430, 2003.

J. Cafaro and F. Rieke. Noise correlations improve response fidelity and stimulus encoding. *Nature*, 468(7326):964–967, 2010.

F. Carnevale, V. de Lafuente, R. Romo, and N. Parga. Uncertainty biases perceptual decision reports. *under revision*, 2012.

M. R. Cohen and A. Kohn. Measuring and interpreting neuronal correlations. *Nat. Neurosci.*, 14(7):811–819, 2011.

M.R. Cohen and J.H. Maunsell. Attention improves performance primarily by reducing interneuronal correlations. *Nat. Neurosci.*, 12:1594–1600, 2009.

A. Compte, C. Constantinidis, J. Tegner, S. Raghavachari, M. V. Chafee, P. S. Goldman-Rakic, and X.-J. Wang. Temporally irregular mnemonic persistent activity in prefrontal neurons of monkeys during a delayed response task. *J. Neurophysiol.*, 90(5):3441–3454, 2003.

C. Constantinidis and P.S. Goldman-Rakic. Correlated discharges among putative pyramidal neurons and interneurons in the primate prefrontal cortex. *J. Neurophysiol.*, 88(6):3487–3497, 2002.

A. Contreras, D.and Destexhe, T.J. Sejnowski, and M. Steriade. Control of spatiotemporal coherence of a thalamic oscillation by corticothalamic feedback. *Science*, 274: 771–774, 1996.

R. Cossart, D. Aronov, and R. Yuste. Attractor dynamics of network up states in the neocortex. *Nature*, 423:283–288, 2003.

V. Crunelli, T. I. Toth, D. W. Cope, K. Blethyn, and S. W. Hughes. The window t-type calcium current in brain dynamics of different behavioural states. *J. Physiol.*, 562:121–129, 2005.

J. de la Rocha, B. Doiron, E. S. Brown, K. Josic, and A. Reyes. Correlation between neural spike trains increases with firing rate. *Nature*, 448(7155):802–806, 2007.

J. Demas, S. J. Eglen, and R. OL Wong. Developmental loss of synchronous spontaneous activity in the mouse retina is independent of visual experience. *J. Neurosci.*, 23(7):2851–2860, 2003.

A. Destexhe, D. Contreras, and M. Steriade. Spatiotemporal analysis of local field potentials and unit discharges in cat cerebral cortex during natural wake and sleep states. *J. Neurosci.*, 19(11):4595–4608, 1999.

A. Destexhe, M. Rudolph, J.-M. Fellous, and T.J. Sejnowski. Fluctuating synaptic conductances recreate in vivo-like activity in neocortical neurons. *Neuroscience*, 107:13–24, 2001.

M. Diesmann, M.O. Gewaltig, and A. Aertsen. Stable propagation of synchronous spiking in cortical neural networks. *Nature*, 402:529–533, 1999.

J. D. Dorn and D. L. Ringach. Estimating membrane voltage correlations from extracellular spike trains. *J. Neurophysiol.*, 89(4):2271–2278, 2003.

A. J. Doupe, D. J. Perkel, A. Reiner, and E.A. Stern. Birdbrains could teach basal ganglia research a new song. *Trends Neurosci.*, 28(7):353–363, 2005.

A.S. Ecker, P. Berens, G.A. Keliris, M. Bethge, N.K. Logothetis, and A.S. Tolias. Decorrelated Neuronal Firing in Cortical Microcircuits. *Science*, 327(5965):584–587, 2010.

A.S. Ecker, P. Berens, R.J. Cotton, M. Subramaniyan, G.H. Denfield, C.R. Cadwell, S.M. Smirnakis, M. Bethge, and Tolias A.S. State dependence of noise correlations in macaque primary visual cortex. *Neuron*, 82(1):235–248, 2014.

N. Fourcaud and N. Brunel. Dynamics of the firing probability of noisy integrate-and-fire neurons. *Neural Comp.*, 14:2057–2110, 2002.

L. Gabernet, S. P. Jadhav, D. E. Feldman, M. Carandini, and M. Scanziani. Somatosensory Integration Controlled by Dynamic Thalamocortical Feed-Forward Inhibition. *Neuron*, 48(2):315–327, 2005.

T.J. Gawne and B.J. Richmond. How independent are the messages carried by adjacent inferior temporal cortical neurons? *J. Neurosci.*, 13:2758–2771, 1993.

I. Ginzburg and H. Sompolinsky. Theory of correlations in stochastic neural networks. *Phys. Rev. E*, 50:3171–3191, 1994.

HD Golledge, S Panzer, F Zheng, G Pola, JW Scannell, DV Giannikopoulos, RJ Mason, MJ Tovee, and MP Young. Correlations, feature-binding and population coding in primary visual cortex. *Neuroreport*, 14:1045–1050, 2003.

M. Graupner and A.D. Reyes. Synaptic input correlations leading to membrane potential decorrelation of spontaneous activity in cortex. *J. Neurosci.*, 33(38):15075–15085, 2013.

B.J. Hansen, M.I. Chelaru, and V. Dragoi. Correlated variability in laminar cortical circuits. *Neuron*, 76(3):590–602, 2012.

M. Helias, T. Tetzlaff, and M. Diesmann. Echoes in correlated neural systems. *New J. Phys.*, 15:023002, 2013.

M Helias, T Tetzlaff, and M Diesmann. The correlation structure of local neuronal networks intrinsically results from recurrent dynamics. *PLoS Comput. Biol.*, 10(: e1003428), 2014.

J.L. Herrero, M.A. Gieselmann, M. Sanayei, and A. Thiele. Attention induced variance and noise correlation reduction in macaque v1 is mediated by nmda receptors. *Neuron*, 78:729–739, 2013.

J. Hertz. Cross-correlations in high-conductance states of a model cortical network. *Neural Comput.*, 22(2):427–447, 2010.

O. Hikosaka, Y. Takikawa, and R. Kawagoe. Role of the basal ganglia in the control of purposive saccadic eye movements. *Physiological reviews*, 80(3):953–978, 2000.

J. A. Hirsch, J.M. Alonso, R. C. Reid, and L. M. Martinez. Synaptic integration in striate cortical simple cells. *J. Neurosci.*, 18(22):9517–9528, 1998.

Y. Igarashi, M. Oizumi, and M. Okada. Theory of correlation in a network with synaptic depression. *Physical Review E*, 85(1), 2012.

K.O. Johnson. Sensory discrimination: decision process. *J. Neurophysiol.*, 43:1771–1792, 1980.

L. C. Katz and C. J. Shatz. Synaptic activity and the construction of cortical circuits. *Science*, 274(5290):1133–1138, 1996.

R. R. Kimpo, F. E. Theunissen, and A. J. Doupe. Propagation of correlated activity through multiple stages of a neural circuit. *J. Neurosci.*, 23:5750–5761, 2003.

A. Kohn and M. A. Smith. Stimulus dependence of neuronal correlation in primary visual cortex of the macaque. *J. Neurosci*, 25(14):3661–3673, 2005.

T. Komiyama, T.R. Sato, D.H. O'Connor, Y.X. Zhang, D. Huber, B.M. Hooks, M. Gabitto, and K. Svoboda. Learning-related fine-scale specificity imaged in motor cortex circuits of behaving mice. *Nature*, 464:1182–1186, 2010.

B. Kriener, T. Tetzlaff, A. Aertsen, M. Diesmann, and S. Rotter. Correlations and population dynamics in cortical networks. *Neural Comput.*, 20:2185–2226, 2008.

A. Kuhn, A. Aertsen, and S. Rotter. Neuronal integration of synaptic input in the fluctuation-driven regime. *J. Neurosci.*, 24:2345–2356, 2004.

I. Lampl, I. Reichova, and D. Ferster. Synchronous membrane potential fluctuations in neurons of the cat visual cortex. *Neuron*, 22(2):361–374, 1999.

J.F. Léger, E. Stern, A. Aertsen, and D. Heck. Synaptic integration in rat frontal cortex shaped by network activity. *Neural Comput.*, 20:1–43, 2005.

B. Lindner and L. Schimansky-Geier. Transmission of noise coded versus additive signals through a neuronal ensemble. *Phys. Rev. Lett.*, 86:2934–2937, 2001.

B. Lindner, B. Doiron, and A. Longtin. Theory of oscillatory firing induced by spatially correlated noise and delayed inhibitory feedback. *Phys. Rev. E*, 72:061919, 2005.

A. Luczak, P. Barthó, S.L. Marguet, G. Buzáki, and K.D. Harris. Sequential structure of neocortical spontaneous activity in vivo. *Proc. Natl. Acad. Sci. USA*, (104):347–352, 2007.

P.J. Magill, J.P. Bolam, and M.D. Bevan. Relationship of activity in the subthalamic nucleus globus pallidus network to cortical electroencephalogram. *J. Neurosci.*, 20 (2):820–833, 2000.

B. Q. Mao, F. Hamzei-Sichani, D. Aronov, R. C. Fromke, and R. Yuste. Dynamics of spontaneous activity in neocortical slices. *Neuron*, 32:883–898, 2001.

A Mazzoni, S. Panzeri, N. K. Logothetis, and N. Brunel. Encoding of naturalistic stimuli by local field potential spectra in networks of excitatory and inhibitory neurons. *PLoS Comput. Biol.*, 4(12):e1000239, 2008.

D. A. McCormick, B. W. Connors, J. W. Lighthall, and D. A. Prince. Comparative electrophysiology of pyramidal and sparsely spiny stellate neurons of the neocortex. *J. Neurophysiol.*, 54(4):782–806, 1985.

O. Melamed, O. Barack, G. Silberberg, and M. Tsodyks H. Markram. Slow oscillations in neural networks with facilitating synapses. *J. Comput. Neurosci.*, 25:308–316, 2008.

R. Metherate and J. H. Ashe. Ionic flux contributions to neocortical slow waves and nucleus basalis- mediated activation: whole-cell recordings in vivo. *J. Neurosci.*, 13: 5312–5323, 1993.

J. W. Middleton, C. Omar, B. Doiron, and D. J. Simons. Neural correlation is stimulus modulated by feedforward inhibitory circuitry. *J. Neurosci.*, 32(2):506–518, 2012.

J.F. Mitchell, K.A. Sundberg, and J.H. Reynolds. Spatial attention decorrelates intrinsic activity fluctuations in macaque area v4. *Neuron*, 63:879–888, 2009.

K Miura, ZF Mainen, and N Uchida. Odor representations in olfactory cortex: Distributed rate coding and decorrelated population activity. *Neuron*, 74(6):1087–1098, 2012.

R. Moreno-Bote and N. Parga. Role of synapticfiltering on the firing response of simple model neurons. *Phys. Rev. Lett.*, 92(2):028102, 2004.

R. Moreno-Bote and N. Parga. Membrane potential and response properties of populations of cortical neurons in the high conductance state. *Phys. Rev. Lett.*, 94:088103, 2005.

R. Moreno-Bote and N. Parga. Auto- and crosscorrelograms for the spike response of leaky integrate-and-fire neurons with slow synapses. *Phys. Rev. Lett.*, 96:028101, 2006.

R. Moreno-Bote and N. Parga. Response of integrate-and-fire neurons to noisy inputs filtered by synapses with arbitrary timescales: Firing rate and correlations. *Neural Comp.*, 22(6):1528–1572, 2010.

K. Nakayama, H. Nishimaru, M. Iizuka, S. Ozaki, and N. Kudo. Rostrocaudal progression in the development of periodic spontaneous activity in fetal rat spinal motor circuits in vitro. *J. Neurophysiol.*, 81(5):2592–2595, 1999.

A Nini, A Feingold, H Slovin, and H Bergman. Neurons in the globus pallidus do not show correlated activity in the normal monkey, but phase-locked oscillations appear in the mptp model of parkinsonism. *J. Neurosci.*, 74(4):1800–1805, 1995.

H. Noda and W.R. Adey. Firing of neuron pairs in cat association cortex during sleep and wakefulness. *J. Neurophysiol.*, 33:672–684, 1970.

M. J. O'Donovan. The origin of spontaneous activity in developing networks of the vertebrate nervous system. *Current opinion in neurobiology*, 9(1):94–104, 1999.

M. Okun and I. Lampl. Instantaneous correlation of excitation and inhibition during ongoing and sensory-evoked activities. *Nat. Neurosci.*, 11:535–537, 2008.

M.V. Oram, M.W. Foldiak, D.I. Perrett, and F. Sengpiel. The 'Ideal Homunculus': decoding neural population signals. *Trends Neurosci.*, 21:259–265, 1998.

S. Ostojic. Two types of asynchronous activity in networks of excitatory and inhibitory spiking neurons. *Nature. Neurosci.*, 17(4):594–600, 2014.

S. Ostojic, N. Brunel, and V. Hakim. How connectivity, background activity and synaptic properties shape the cross-correlation between spike trains. *J. Neurosci.*, 29(33):10234–10253, 2009.

S. Panzeri, S.R. Schultz, A. Treves, and E.T. Rolls. Correlations and the encoding of information in the nervous system. *Proc. R. Soc. Lond. B*, 266:1001–1012, 1999.

D. Pare, E. Shink, H. Gaudreau, A. Destexhe, and E. Lang. Impact of spontaneous synaptic activity on the resting properties of cat neocortical pyramidal neurons in vivo. *J. Neurophysiol.*, 79(3):1450–1460, 1998.

N. Parga and L. F. Abbott. Network model of spontaneous activity exhibiting synchronous transitions between up and down states. *Frontiers in Neuroscience*, 1: 57–66, 2007.

V. Pernice, B. Staude, S. Cardanobile, and S. Rotter. How structure determines correlations in neuronal networks. *PLoS Comput. Biol.*, 7(5):e1002059, 2011.

A. Peyrache, K. Benchenane, M. Khamassi, I.W. Sidney, and F.P. Battaglia. Sequential reinstatement of neocortical activity during slow oscillations depends on cells global activity. *Front. Syst. Neurosci.*, 3(18), 2009.

F. Pouille and M. Scanziani. Enforcement of Temporal Fidelity in Pyramidal Cells by Somatic Feed-Forward Inhibition. *Science*, 293(5532):1159–1163, 2001.

J.F. Poulet and G.G. Petersen. Internal brain state regulates membrane potential synchrony in barrel cortex of behaving mice. *Nature*, 454:881–885, 2008.

M. E. Raichle and M. A. Mintun. Brain work and brain imaging. *Ann. Rev. Neurosci.*, 29(1):449–476, 2006.

A Raz, E Vaadia, and H Bergman. Firing patterns and correlations of spontaneous discharge of pallidal neurons in the normal and the tremulous 1-methyl-4-phenyl-1,2,3,6-tetrahydropyridine vervet model of parkinsonism. *J. Neurosci.*, 15(20(22)): 8559–8571, 2000.

A. Renart, R. Moreno Bote, X. J. Wang, and N. Parga. Mean-driven and fluctuation-driven persistent activity in recurrent networks. *Neural Comput.*, 19(1):1–46, 2007.

A Renart, J. de la Rocha, P. Bartho, L. Hollender, N. Parga, A. Reyes, and K.D. Harris. The asynchronous state in cortical circuits. *Science*, 327(5965):587–590, 2010.

A. Roxin, N. Brunel, D. Hansel, G. Mongillo, and C. vanVreeswijk. On the distribution of firing rates in networks of cortical neurons. *J. Neurosci*, 31(45):16217–16226, 2011.

S. Sadaghiani, R. Scheeringa, K. Lehongre, B. Morillon, A.-L. Giraud, and A. Kleinschmidt. Intrinsic connectivity networks, alpha oscillations, and tonic alertness: A simultaneous Electroencephalography/Functional magnetic resonance imaging study. *J. Neurosci.*, 30(30):10243–10250, 2010.

E. Salinas and T. J. Sejnowski. Impact of correlated synaptic input on output firing rate and variability in simple neuronal models. *J. Neurosci.*, 20:6193–6209, 2000.

M.V. Sanchez-Vives and D.A. McCormick. Cellular and network mechanisms of rhythmic recurrent activity in neocortex. *Nat. Neurosci.*, 3:1027–1034, 2000.

MV Sanchez-Vives, M Perez-Zabalza, J Manrique, R Reig, M Winograd, and N Parga. Gabab modulation of emergent cortical rhythms: an experimental and computational study. *Annual Meeting of the Society for Neuroscience, Neuroscience 2010. Abstract 545.1 (San Diego, 13-17 November 2010)*, 2010.

J. K. Seamans, L. Nogueira, and A. Lavin. Synaptic basis of persistent activity in prefrontal cortex in vivo and in organ-otypic cultures. *Cereb. Cortex*, 13:1242–1250, 2003.

M.N. Shadlen and W.T. Newsome. Noise, neural codes and cortical organization. *Curr. Opin. Neurobiol.*, 4:569–579, 1994.

M.N. Shadlen and W.T. Newsome. The variable discharge of cortical neurons: Implications for connectivity, computation, and information coding. *J. Neurosci.*, 18(10): 3870–3896, 1998.

A. J. Smith, S. Owens, and I. D. Forsythe. Characterisation of inhibitory and excitatory postsynaptic currents of the rat medial superior olive. *J. Physiol*, 529(3):681–698, 2000.

M.A. Smith and A. Kohn. Spatial and temporal scales of neuronal correlation in primary visual cortex. *J. Neurosci*, 28(48):12591–12603, 2008.

W.R. Softy and C. Koch. The highly irregular firing of cortical cells is inconsistent with temporal integration of random epsps. *J. Neurosci.*, 13(1):334–350, 1993.

M Steriade, DA McCormick, and TJ Sejnowski. Thalamocortical oscillations in the sleeping and aroused brain. *Science*, (262):679–685, 1993a.

M. Steriade, A. Nunez, and F. Amzica. A novel slow (¡1hz) oscillation of neocortical neurons in vivo: depolarizing and hyperpolarizing components. *J. Neurosci.*, 13: 3252–3265, 1993b.

M. Steriade, A Nunez, and F Amzica. Intracellular analysis of relations between the slow (¡1hz) neocortical oscillation and other sleep rhythms of the electroencephalogram. *J. Neurosci.*, 13:3252–3265, 1993c.

E.A. Stern, A.E. Kincaid, and C.J. Wilson. Spontaneous subthreshold membrane potential fluctuations and action potential variability of rat corticostriatal and striatal neurons in vivo. *J. Neurophysiol.*, 77(4):1697–1715, 1997.

T. Tetzlaff, S. Rotter, E. Stark, M. Abeles, A. Aertsen, and M. Diesmann. Dependence of neuronal correlations on filter characteristics and marginal spike train statistics. *Neural Comput.*, 20(9):2133–2184, 2008.

T. Tetzlaff, M. Helias, G.T. Einevoll, and M. Diesmann. Decorrelation of neural-network activity by inhibitory feedback. *PLoS Comput. Biol.*, 8(8), 2012.

I. Timofeev, F. Grenier, M. Bazhenov, and M. Steriade T.J. Sejnowski. Origin of slow cortical oscillations in deafferented cortical slabs. *Cerebral Cortex*, 10:1185–1199, 2000.

T. Toyoizumi, K.R. Rad, and L Paninski. Mean-field approximations for coupled populations of generalized linear model spiking neurons with markov refractoriness. *Neural Comput.*, 21(5):1203–1243, 2008.

J. Trousdale, Y. Hu, E. Shea-Brown, and K. Josić. Impact of network structure and cellular response on spike time correlations. *PLoS Comput. Biol.*, 8(3):e1002408, 2012.

C. van Vreeswijk and H. Sompolinsky. Chaos in neuronal networks with balanced excitatory and inhibitory activity. *Science*, (274):1724–1726, 1996.

C. van Vreeswijk and H. Sompolinsky. Chaotic balanced state in a model of cortical circuits. *Neural Comput.*, 10(6):1321–1371, 1998.

TP Vogels and LF Abbott. Signal propagation and logic gating in networks of integrate-and-fire neurons. *J. Neurosci.*, 25(46):10786–10795, 2005.

M. Wehr and A. M. Zador. Balanced inhibition underlies tuning and sharpens spike timing in auditory cortex. *Nature*, 426(6965):442–446, 2003.

T. Wichmann and M.R. DeLong. Functional and pathophysiological models of the basal ganglia. *Curr. Opin. Neurobiol.*, 6:751–758, 1996.

C.J. Wilson and Y. Kawaguchi. The origins of two-state spontaneous membrane potential fluctuations of neostriatal spiny neurons. *J. Neurosci.*, 16:2397–2410, 1996.

R. O. L. Wong and D. M. Oakley. Changing patterns of spontaneous bursting activity of on and off retinal ganglion cells during development. *Neuron*, 16(6):1087–1095, 1996.

W. T. Wong, J. R. Sanes, and R. O.L. Wong. Developmentally regulated spontaneous activity in the embryonic chick retina. *J. Neurosci.*, 18(21).

E. Zohary, M.N. Shadlen, and W.T. Newsome. Correlated neuronal discharge rate and its implications for psychophysical performance. *Nature*, 370:140–143, 1994.